



*University of Mississippi
School of Engineering
Post Office Box 1848
University, MS 38677*

October 4, 2002

Harry Lee James
Bridge Engineer, Bridge Division
Mississippi Department of Transportation
401 N. W. Street
Jackson, MS 39201

Re: Final Report for Seismic Vulnerability Work Assignment
MDOT Project Number: SP-9999-00(27) 101411/011000 [79-999-00-027-11 PE]

Dear Mr. James:

Please find enclosed six copies of the subject final report, entitled "Seismic Vulnerability of Existing Bridge Substructures Supporting the I-55 Undercrossing at MS-302 (Goodman Road)," for your review and approval. Please feel free to contact me at 662-915-5370 (Voice), 662-915-5523 (Fax), or cvchris@olemiss.edu (Email), if you have any questions or concerns. It has been my pleasure to work with Bridge Division on this assignment, and I appreciate the support and guidance you have provided at each stage.

Sincerely,

Dr. Chris Mullen
Associate Professor of Civil Engineering, UM
Director, CCEP

Cc: Patrick Brown UM Office of Research (cover letter)
Dr. Tom White Director, MSU Mississippi Transportation Institute (cover letter)

***SEISMIC VULNERABILITY OF EXISTING HIGHWAY BRIDGE
SUBSTRUCTURES SUPPORTING THE I-55 UNDERCROSSING AT
MS302 (GOODMAN ROAD)***

Final Report

to

**Mississippi Department of Transportation
Bridge Division**

**MDOT Project Number: SP-9999-00(27) 101411/011000
[79-999-00-027-11 PE]**

BY

**Dr. Chris L. Mullen, P. E.
Associate Professor, Department of Civil Engineering
Director, Center for Community Earthquake Preparedness
University of Mississippi**

October 1, 2002

EXECUTIVE SUMMARY

As part of a work assignment issued by the Mississippi Department of Transportation, Bridge Division, the following report has been prepared to document results of an investigation of seismic vulnerability of the primary structural elements supporting the deck of the existing I-55 Undercrossing at MS-302 (Goodman Road). In order to assess the complex nature of the response to seismic excitation, a multi-level analysis has been performed, including: 1) a two-dimensional pushover analysis of a typical bent, 2) an eigenvalue and linear response spectrum analysis of a three-dimensional, fixed-base, finite element model of the four-span, concrete structural system, and 3) a three-dimensional, nonlinear, time history analysis of the soil-structure system including the embankments and the soil column to a depth of about 100 ft below the deck level.

The emphasis has been placed on the bending induced in the reinforced concrete bents and abutments that offer primary support for the roadway deck girders. In modeling the soil resistance around the piled footings, use has been made of soil borings performed at the site as well as geophysical data at the nearby Baptist Memorial Hospital-Desoto.

Damage states computed for sections in the plastic hinge regions of the columns and piles provide a basis for establishing vulnerability of the members. Dynamic bending moments and accelerations have been computed in the bridge models subject to site specific input time histories generated using a source spectral model supplied by the United States Geological Survey. Three simulations have been performed, using inputs representing source intensity levels of nominal Richter magnitude, $M=6, 7, \text{ and } 8$. The peak responses are compared to the damage states, and performance is evaluated for each intensity level.

Results of the computer simulations indicate that target performance criteria for the different intensities do not appear to be met in the strict sense. The primary substructures show moderate vulnerability, especially for the severe intensity event. Before investing in expensive retrofitting of these structural elements, however, it is recommended that

evaluation of other existing structures of critical importance be established first and a comprehensive approach taken to the region with highest hazard exposure.

One of the key aspects of the study was the execution of a field vibration test, which helped establish confidence in the realism of the finite element model. It is recommended that further testing with an augmented sensor array be done on this and other structures in the corridors that will serve as lifelines in the event of a moderate or severe earthquake event. Testing under forced vibration at higher load intensities should be performed to calibrate response of the nonlinear models and to obtain further insight to soil response and structure-foundation interaction. Permanent installation of response sensors should be considered or at least permanent mounting devices to enable quick installation of temporary arrays.

ACKNOWLEDGEMENTS

The author would like to thank the MDOT Bridge Division personnel for their financial support through the work assignment for this project under the Mississippi Transportation Institute research agreement. The Bridge Engineer, Mr. Harry Lee James, has provided guidance in selecting the bridge for study. Design engineer, Mr. Mike Cresap, assisted in obtaining copies of the soil reports and half-size as-built drawings and answered a number of questions about details of the original bridge design. Senior contracts engineer, Mr. Dan Miller, was generous in his monitoring of the project schedule. All of the above mentioned Bridge Division personnel provided useful feedback on the original scope and the final results of the work during presentations made in the Jackson design office.

The assistance of the MDOT District II maintenance personnel was also greatly appreciated. The field vibration study would not have been executed successfully without their help in establishing a safe working environment on the bridge.

The entire project could not have been completed without the dedicated and competent work by graduate research assistants in the Structural Mechanics and Earthquake Engineering program who participated in the project: Prabin Tuladhar, Bernard LeBlanc, Saroj Shrestha, and Tedeswi Tadealli.

Mr. Tuladhar constructed the preliminary finite element models that were used to plan the field vibration study. He performed both a Level 1 and Level 2 study using the preliminary models. For the latter, he additionally studied the use of linear springs for all restrained degrees of freedom. Results of his work may be found in his masters thesis. Prabin was chiefly responsible for the successful operation of the data acquisition and spectrum analyzer during the field study.

Mr. Bernard LeBlanc constructed all of the finite element models appearing in the final report and performed the Level 1 and Level 3 studies using these models. The successful completion of the latter was a significant accomplishment. Bernard was instrumental in the installation of successful operation of the accelerometers during the field study and performed the final system identification and mode shape visualization using the field data.

Mr. Shrestha participated in the field study providing assistance in all aspects of the work. Saroj also performed the analysis of random variation of the input on the response computed for the soil column and for the Level 2 model constructed by Mr. Tuladhar.

Mr. Tadealli prepared many of the graphics appearing in the figures in the final report. Tej worked with others in the Department of Geology and Geological Engineering to obtain GIS data useful to the representation of seismic hazards in north Mississippi.

LIST OF TABLES

Table 4.1	Moment-Curvature Capacities of the Sections
Table 5.1	Characteristic Modal Properties of the Level 2 Model
Table 5.2	Comparison of FE and Modal System Identification Analysis Results
Table 5.3	Seismic Source Parameters for SMSIM (Boore and Joyner, 1991)
Table 5.4	Spectral Amplification Function for SMSIM (Hwang et al., 1999)
Table 5.5	ProShake Predictions of Soil Column Response
Table 5.6	ABAQUS Prediction of Level 2 Model Response
Table 5.7	Statistics of Simulated Peak Accelerations, %g
Table 6.1	Drucker-Prager Model Parameters
Table 6.2	Characteristic Modal Properties of the Level 3 Model
Table 6.3	Peak Accelerations (%g) Input at the Base of the Level 3 Model
Table 6.4	Peak Accelerations (%g) Computed at Key Points on the Level 3 Model

LIST OF FIGURES

- Figure 1.1** Bridge selected for vulnerability study
- Figure 1.2** Seismic hazard exposure in north Mississippi
- Figure 1.3** Highway system in north Mississippi- Memphis and environs
- Figure 1.4** USGS acceleration coefficient contours (AASHTO LRFD, 1994)
- Figure 1.5** Proposed USGS hazard maps: (0.2 s / 1.0s) , (10% / 2%) in 50 yr
-
- Figure 4.1** Bent substructure stiffness degradation and capacity estimate
- Figure 4.2** Fiber models of typical bent cross-sections
- Figure 4.3** Fiber material response curves
- Figure 4.4** Section stiffness degradation and capacity estimates
- Figure 4.5** Bent plastic collapse mechanism under lateral inertial loading
-
- Figure 5.1** Level 2 analysis model: deck-substructure system- isometric view
- Figure 5.2** Characteristic modes of the Level 2 model
- Figure 5.3** Accelerometer array installation and vibration measurement
- Figure 5.4** Schematic four-channel array configuration
- Figure 5.5** Sample record as presented by SigLab VNA and viewed in the field
- Figure 5.6** Sample records as presented by STAR Modal and viewed in the lab
- Figure 5.7** Transducer array configuration to identify transverse modes
- Figure 5.8** Transducer array configurations
- Figure 5.9** Results of modal system identification
- Figure 5.10** ProShake soil column model for generation of site-specific ground motions
- Figure 5.11** Soil degradation curves
- Figure 5.12** Predicted soil column acceleration and shear strain time histories (M=6,7,8)
- Figure 5.13** Predicted soil column acceleration response spectra
-
- Figure 6.1** Level 3 analysis model: soil-structure system (isometric view and details)
- Figure 6.2** Level 3 analysis model: soil-structure system (plan and elevation views)
- Figure 6.3** Section stiffness degradation and capacity estimates: piles
- Figure 6.4** Condition of girder supports at time of field vibration test
- Figure 6.5** Characteristic modes of the Level 3 model
- Figure 6.6** Input component time histories (M=6,7,8)
- Figure 6.7** Response time histories at Bent 3 (M=6,7,8)
- Figure 6.8** Section hysteresis: top of column (M=6,7,8)

- Figure 6.9** Section hysteresis: top of abutment pile (M=6,7,8)
- Figure 6.10** Response time histories at Bent 3: drift ratio
- Figure 6.11** Response time histories at Bent 3: transverse shear
-
- Figure A.1** Bridge elevation showing primary substructure elements
- Figure A.2** Bridge plan showing primary substructure elements
- Figure A.3** Interior bent (typical): (elevation/section) views
- Figure A.4** Deck superstructure (typical): section views
- Figure A.5** Abutment details (typical)
- Figure A.6** Pile details (typical)
-
- Figure B.1** Soil profile composite from soil boring data
- Figure B.2** Boring logs

TABLE OF CONTENTS

Executive Summary	i
Acknowledgements	iii
List of Tables	v
List of Figures	vi
1. INTRODUCTION	1
<i>Background to Project Initiation</i>	1
<i>Selected Bridge, Site, and Seismic Hazard Exposure</i>	2
<i>Bridge Structure and Design Codes</i>	4
<i>Scope of Work</i>	6
<i>Organization of Final Report</i>	7
2. OBJECTIVES	8
3. SEISMIC VULNERABILITY ASSESSMENT PROCEDURE	9
<i>Level 1 Analysis</i>	9
<i>Level 2 Analysis</i>	10
<i>Generation of Site-Specific Motion</i>	12
<i>Level 3 Analysis</i>	12
4. LEVEL 1 ASSESSMENT	13
<i>Flexural Capacity</i>	14
<i>Shear Capacity</i>	17
5. LEVEL 2 ASSESSMENT	20
<i>Natural Modes and Frequencies</i>	21
<i>Field Vibration Measurements</i>	23
<i>Modal System Identification and Visualization</i>	26
<i>Development of Site-Specific Response Spectra</i>	31
<i>Response Spectrum Analysis</i>	36
<i>Effect of Random Nature of Loading on Response</i>	38
6. LEVEL 3 ASSESSMENT	41
<i>Background to Modeling Approach</i>	42
<i>Natural Modes and Frequencies</i>	45
<i>Response Simulations</i>	46
<i>Damage Measures</i>	49
7. SUMMARY AND CONCLUSIONS	54
8. RECOMMENDATIONS	58
References Cited	
Appendix A. As-Built Drawings	
Appendix B. Soil and Foundation Report	

1. INTRODUCTION

Background to Project Initiation

In the fall of 1998, a comprehensive seismic vulnerability study (Swann et al., 1999) was completed which was sponsored through a Hazard Mitigation Grant from the Federal Emergency Management Agency. The study considered the vulnerability of select facilities at the Oxford, MS, campus of the University of Mississippi (UM-Oxford). A final report was submitted to the Mississippi Emergency Management Agency (MEMA) in Jackson, MS. The findings of the study were primarily based on detailed three-dimensional (3D) finite element (FE) simulations of nonlinear damage response of the facility structural models. The models enabled detailed conclusions to be drawn regarding the seismic vulnerability of the facilities over a range of ground shaking intensity as well as preliminary recommendations for seismic retrofit and the expected benefits of such recommendations by analysis of modified models incorporating the recommendations.

One of these models was of an existing highway bridge with high embankments. Previous work (Mullen and Cakmak, 1997) by the principal investigator (PI) of the present project has indicated that damage response of short span bridges, particularly those subject to strong ground shaking, is strongly influenced by the motion of the embankments in relation to the lower foundation levels of the pier columns. The model of the UM-Oxford campus bridge included continuum-type finite element modeling of the soil down to about 100 ft (30 m) depth as well as nonlinear contact interaction elements that allowed coupling of motions between 1) the bridge superstructure, modeled using traditional structural element-type such as beams and shells, and 2) the embankment soil elements. In addition, radiation damping in the soil was modeled using special infinite elements at the artificially defined soil boundaries. A summary of the findings of the campus bridge analysis is included in (Mullen and Swann, 2001).

Benefits of retrofitting some of the vulnerable columns were demonstrated through computational simulations (Gopalakrishnan, 1999). In the retrofit analysis case, moment versus curvature relations were modified to allow for full development of the plastic

moment capacity of the columns, and the time history analysis was repeated with the strengthened columns.

On a number of occasions prior to the submittal of the final report to MEMA, the PI presented preliminary results of the FEMA and other related seismic projects to Mississippi Department of Transportation (MDOT) Bridge Division personnel in the central MDOT office at Jackson, MS. The first presentation was held on September 17, 1998, and was attended by Mr. Frank Massey, Bridge Engineer at the time. Proposals were made for several possible projects and computational support activities of possible interest to the Bridge Division. Availability of newly acquired vibration measurement equipment, potential use of 3D FE analysis in defining seismic retrofit needs, and possible selection of a candidate bridge structure in Mississippi were discussed.

Upon Mr. Massey's retirement from MDOT, a second presentation was made in Jackson during October, 1999, which was attended by Mr. Harry Lee James, the newly appointed Bridge Engineer. Draft sections from the MEMA report were presented, and the decision was made to proceed with a project proposal focusing on a candidate bridge in north Mississippi.

Selected Bridge, Site, and Seismic Hazard Exposure

Figure 1.1 shows photos taken at the beginning of the project of the bridge that MDOT Bridge Division personnel selected. Figure 1.2 identifies the site geographically based on data available from the Mississippi Automated Resource Information System (MARIS), a Geographic Information System (GIS) database authorized by the MS state legislature. The epicentral location of the intense 1811 recorded earthquake that occurred at the southern end of the New Madrid seismic zone (NMSZ) is plotted (red star on map showing the seven states adjacent to the NMSZ, which participate in the Central United States Earthquake Consortium (CUSEC), as well as a zoomed-in view showing the counties closest to the epicenter. The location of the bridge site on these maps (red circle on latter view and blue circle on view showing the three counties in MS which are closest to the epicenter) provides an indication of the proximity of the bridge to this epicentral

location and the reason for concern for this site. In the zoomed-in view showing the MS counties with highest seismic hazard exposure, the MARIS data for interstate, state, and county roads are overlain with data for the major rivers and lakes.

Also shown on the zoomed-in view of the three counties in MS is the adjacent site of the Baptist Memorial Hospital (BMH)-Desoto hospital (red double-cross). A seismic vulnerability study (Mullen et al., 1997) of this hospital building complex was performed by the PI as part of a project sponsored by the CUSEC. To provide data for modeling the hospital building subsurface geology, a geophysical investigation was performed which provided soil strength, density, and shear velocity data to depths over 100 ft. This data has been used to supplement standard penetration data for the bridge site in the geotechnical report (Wells, 1987), a copy of which was provided to the PI for the present study.

Overlain on the MARIS maps are contour lines for equal maximum 1.0 s spectral acceleration coefficients, which have been reconstructed from the 1997 edition of the National Earthquake Hazard Reduction Program (*NEHRP Recommended Provisions for Seismic Regulations for New Buildings and Other Structures* (FEMA 302, 1997)). Contours from an earlier edition of the NEHRP document are adopted in recent design specifications for the American Association of State Highway and Transportation Officials (AASHTO), as discussed further below.

Figure 1.3 is an excerpt of a recent MDOT map for the MS highway system, which shows that the selected intersection allows traffic from Interstate 55 (I-55) to access Goodman Road (MS-302). From the figure, it is seen that the intersection is a critical one, capable of providing post-earthquake recovery access for emergency response vehicles traveling to the BMH-Desoto hospital, a major regional facility with an emergency intensive-care surgical unit. In fact, the motivation for the CUSEC study mentioned above was the need to evaluate the potential use of the hospital facility as the primary backup for Memphis hospitals in the event of an intense rupture within the NMSZ. The figure also highlights the significant economic impact that might be expected because

Goodman Road is one of the major access routes to both a rapidly growing population of commuters from Southaven, MS, to Memphis, TN, and people traveling from throughout the mid-South region to casino and recreation facilities in Tunica, MS.

Bridge Structure and Design Codes

The bridge existing at the selected site is a conventional four-span concrete structure. Figure A.1 shows the basic layout of the structural system according to the as-built design drawings supplied to the PI by MDOT Bridge Division personnel. According to the drawings, it was originally constructed in 1988 and had been designed to satisfy the *AASHTO Standard Specifications for Highway Bridges* (Standard Specifications, 1996).

The design specifications in effect at the time were adopted by AASHTO in 1983. In these specifications, the importance of seismic response analysis was minimal for this site. More recent specifications (Standard Specifications, 1996) increased the importance of seismic analysis but required only static equivalent representations of the loading for this site. According to the alternative *AASHTO LRFD Bridge Design Specifications* (AASHTO LRFD, 1994), however, which are based on Load and Resistance Factor Design (LRFD) methodology, the current functioning of the intersection as described above indicates that the design of a new bridge at the site must incorporate more rigorous methods of dynamic analysis in the seismic analysis.

Both the standard and LRFD specifications locate the bridge site in the same seismic hazard category. The hazard category is distinguished based on an acceleration coefficient defined in the specification. Figure 1.4 shows contour maps of the acceleration coefficient appearing in the 1994 AASHTO LRFD specifications, which were adopted from maps generated by the United States Geological Survey (USGS) for the 1988 edition of the NEHRP recommended provisions.

The 1994 AASHTO LRFD specifications demand that, for the relevant hazard category, a dynamic spectral analysis be performed because of the classification of the bridge as *Critical*. A *Critical* Bridge is one that must “remain open to emergency vehicles and for

security/defense purposes after a large earthquake, e.g. a 2,500-year return period event.” The Critical Multi-Span Bridge is the highest class requiring analysis by the Multimode Spectral Method.

In the time since the 1988 USGS maps were generated, research studies have been performed leading to significant new knowledge and a need to generate new maps. Of major importance are paleo-lithographic field investigations performed by a number of seismologists in the region that have led to discovery of physical evidence confirming a recurrence interval of approximately 400 to 500 years for earthquakes large enough to induce liquefaction of sand layers, which is caused by increased pore water pressure during intense seismic shaking.

Also important is a major USGS hazard-mapping project that has recently been completed in the Memphis area, which has clarified the subsurface geologic morphology and has provided new data on shear wave velocities near the surface. Reflecting both the paleo-lithographic and regional morphology data, a new national map (Figure 1.5) has been developed by the USGS and posted on their web site for comments.

If adopted as is likely, the hazard classification for the bridge site will likely increase. Under the expected higher hazard classification, an elastic or inelastic time history analysis will be required.

Scope of Work

After a number of draft proposals were submitted during the spring and summer of 1999, a final scope of work was agreed upon, and a contract was approved dated August 16, 1999. Since MDOT-sponsored retrofit work to date had focused solely on safeguarding decks against failure due to insufficient seat width, it was decided that the proposed study would focus on identifying vulnerability of primary substructure elements (Figure A.2), specifically, the pier bents, footings, and piles, to seismic shaking induced flexural and shear actions.

The final approved scope of work (Seismic vulnerability work assignment, 1999) incorporated an extension of the methodology used in the FEMA campus facility study for vulnerability evaluation. The methodology involves multilevel analyses to provide an effective way of conducting a performance-based assessment. A consensus performance-based seismic evaluation methodology is not yet available in the United States for existing highway bridges. FEMA, however, has published such guidelines for rehabilitation of existing buildings (FEMA 273, 1997). The building guidelines incorporate varying performance expectations depending on intensity of seismic shaking and needs of the facility owner. Criteria for evaluation of performance vary with the analysis procedure used. Procedures specifically addressed by FEMA 273 are: 1) Linear Static (LSP), 2) Nonlinear Static (NSP), 3) Linear Dynamic (LDP), and 4) Nonlinear Dynamic (NDP). In the FEMA methodology only one of these analysis procedures is used for assessing a given structure.

Organization of Final Report

Based on the experience gained in the FEMA campus study, the PI has defined a three-level procedure that includes elements of all but the LSP and attempts to maximize the insight from and reliability of results gained at each level while minimizing the computational effort. The next two sections describe the objectives (Section 2) and details of the procedure adopted in this study (Section 3), as agreed upon in the approved scope of work (Seismic vulnerability work assignment, 1999). Subsequent sections (Sections 4-6) discuss the various modeling efforts, associated field tests, and findings associated with each analysis level. The final sections present conclusions of the study (Section 7) and recommendations (Section 8) based on these conclusions.

2. OBJECTIVES

The study aims to assess a number of individual objectives based on the results of each separate level of analysis, namely, to determine:

1. The ultimate lateral force capacity and stiffness of the bents treated in isolation (Level 1)
2. The modal vibration response characteristics of the bridge system through computational modeling and field measurements, with special emphasis on the behavior of the bents and abutments (Level 2 and Level 3)
3. The ability of the bridge substructures to satisfy requirements of recent AASHTO design specifications (Level 2)
4. The ability of the substructure elements to perform satisfactorily over a range of input ground motion intensities. A range of performance criteria is identified as appropriate at each intensity level. (Level 3)

3. SEISMIC VULNERABILITY ASSESSMENT PROCEDURE

A three-level assessment procedure has been implemented in this project in order to meet the stated objectives. Each higher level incorporates a different type and an increasing amount of computational effort. A brief description of each is provided below to providing the intended relationship to the individual objectives.

Level 1 Analysis

Level 1 is basically a NSP. The major difference here is that only a substructure representing one of the two-column pier bents is analyzed. The objectives are to establish the computable measures of damage at the material, cross-section, element, and substructure levels. The basic approach used in the FEMA campus study has been adopted for this purpose. First, a fiber analysis is performed to compute three key flexural damage limit states for the cross-sections of the cap beam and columns in the bent, namely:

1. Moment and curvature at which extreme unconfined concrete fibers first crack on the tension side of the neutral axis
2. Moment and curvature at which extreme fibers in the longitudinal steel reinforcement first yield on the tension side of the neutral axis
3. Peak moment and curvature at which extreme confined fibers crush and degrade on the compression side of the neutral axis

The cross-section response is also used to determine key flexural damage limit states in the columns and in the bent frame subsystem. A pushover analysis is performed with vertical loads maintained constant at the value of the dead load reactions at each bearing position on the cap beam. Horizontal loads are then increased monotonically, and damage is accounted for in the response computation.

While the occurrence of cracking and yielding in each member is monitored computationally throughout the loading process, the most important result here is the ultimate in-plane flexural capacity for the bent frame subsystem. For reference, an approximate fully plastic analysis of the type recommended in the current AASHTO

standard specifications is also performed using the results of the cross-section analysis.

Finally, the shear capacity of the column is estimated using the design method proposed by the University of California at San Diego (Seible et al., 1995). This procedure is adopted, because it has been successfully used in the seismic retrofit evaluation of numerous highway bridge columns in California and is easily extended to include design of column wrap solutions for retrofitting, should this be required here. This method is similar to that in the LRFD Specifications for prestressed concrete members in which the shear force resistance contributions of the concrete, the transverse steel reinforcement, and the axial force are summed to obtain the total capacity.

Level 2 Analysis

Level 2 is basically a LDP. As stated in the previous section, the current AASHTO LRFD Specifications require use of the Multimode Spectral Method, a type of LDP, for this bridge. The first step in such a procedure is an eigenvalue analysis to determine the natural frequencies and mode shapes of the linear-elastic 3D system, in its original condition prior to seismic loading. The mode shapes and relative ordering of the frequencies provide insight not only to the mass and stiffness distribution but also the influence of boundary conditions.

Current practice does not require specific consideration of the foundation stiffness or the embankment mass and stiffness in the model to be used in the LDP, but the PI's experience is that these aspects are extremely important in the estimating damage to substructure elements. The foundations, however, are not considered for the Level 2 analysis, since this has been done in the more accurate Level 3 analysis.

The eigenvalue analysis has focused on modes involving net translation or rotation of the bridge deck. These modes are typically associated with having the most damage potential for the columns of the bents. They are found from the analysis both by visual checking of most shape plots and by seeking the modes which have the highest modal participation factors and effective mass in each of the six global degrees-of-freedom.

The eigenvalue analysis results are affected by all the assumptions of material properties, FE selection, and boundary condition definition. To provide confidence in the appropriateness of the modeling assumptions, field vibration tests were performed once a preliminary fixed base model had been completed. An array of four accelerometers was temporarily installed on the bents in several configurations aimed at capturing the characteristic modes involving net translation or rotation of the bridge deck. The time-dependent response at each accelerometer position was recorded simultaneously under ambient truck and automobile traffic loading events.

Modal analysis was then performed using polynomial regression analysis of amplitude peaks in frequency response functions computed from the measured time histories. Such analysis is valid when the response of the system is linear. The modal analysis identifies both frequencies and mode shapes for a simple classical modes model having at least as many degrees-of-freedom as there are measurement points. Graphical animation of the modal coordinates at the corresponding modal frequencies helps to visualize the identified mode shapes. Consistencies observed between the eigenvalue solution and the modal system identified by modal analysis of the measured time histories provides confirmation that the FE model corresponds well to the actual system, at least at strain levels associated with the ambient vibration.

The second step in the Level 2 analysis is to perform response spectrum predictions of response to either the design spectrum in the AASHTO LRFD *Design Specifications* or a site-specific input spectrum allowed the code. Both types of spectra have been considered here, but the former does not permit distinction between different intensities, since the Specifications only consider a single return period. Results will, therefore, only be reported for the site-specific spectrum which was derived as discussed below.

Generation of Site-Specific Input Motion

While a number of methods are available to generate site-specific spectra, the one used here is one promoted by the Mid-America Earthquake (MAE) Center, a research

consortium funded primarily by the National Science Foundation (NSF). Upon asking the MAE Center staff which person was responsible for developing such spectra and synthetic time histories characteristic of the New Madrid seismic zone, the PI was told to contact Professor Howard Hwang at the Center for Earthquake Research and Information (CERI) at the University of Memphis, one of the member institutions of the MAE Center consortium. Dr. Hwang recommended that a probabilistic, source-spectrum, random-vibrations model incorporated in the Fortran computer software, SMSIM, be used. The software was obtained by the PI directly from Dr. David Boore at the USGS office in Menlo Park, California.

Level 3 Analysis

The highest level is the Level 3, which is a NDP. In the Level 3 analysis, the full complexities of the problem are addressed. The governing equations of motion are solved including nonlinear aspects of the system, both geometric and material. Soil-structure interaction may be included with explicit modeling of the soil system to some depth and distance from the foundations of the structure. This provides the most realistic assessment but is computationally intensive and numerical solution of the equations of motion can be difficult or impossible. The work here has been guided by past studies the PI has performed as will be discussed later.

4. LEVEL 1 ASSESSMENT

Each of the six intermediate bent frames, comprised of two main columns, cap beam, and footing (see Figure A.3), is considered an essential substructure for safety against collapse of the roadway above (Goodman Road) onto the roadway below (I-55). In the absence of seismic loads, the capacity of each frame is controlled primarily by the vertical demand of the roadway deck, with secondary dependence on lateral loads from wind and braking loads. Seismic loading primarily increases the longitudinal and transverse lateral demands, but the vertical ones can be significantly increased as well. For very large earthquakes, tension can actually be induced in the bearings.

Preliminary insight into seismic vulnerability is obtained by considering a typical bent in

isolation subject only to the dead loads from the girder bearings and to a lateral load that increases monotonically until damage and ultimately collapse occurs. Figure 4.1 shows the ABAQUS model (Hibbitt et al., 1998) developed to represent the substructure and loading from a mechanics point of view and the predicted load versus deflection response, which is seen to be nonlinear.

A detailed discussion of the model and results is found in a master's thesis conducted under the supervision of the PI (LeBlanc, 2001). This model is a slight revision of a similar model and analysis conducted earlier by a previous masters student (Tuladhar, 2000). The revisions reflect the approach in meshing the column validated in the PI's dissertation (Mullen and Cakmak, 1997), whereby the column clear height is divided into multiple elements, with at least one in the plastic hinge formation zone and at least one in the mid-region where response is expected to remain elastic.

As seen in the top of Figure 4.1, top and bottom hinge zones have been introduced, each of length $1/6$ of the clear height, L , taken as 20 ft for the purposes of the Level 2 analysis. The mid-region has been split into two elements to provide nodal response output at the mid-height. The two-node, 3D beam element in ABAQUS, Type B33, has been used, which uses three Gauss integration points along the length to integrate the stiffness of each element.

In order to capture the nonlinear aspect of the response, it is necessary to model the damage that occurs in the various constituent materials (material nonlinearity) as well as the interaction of the axial force in the columns on the bending moments (geometric nonlinearity or P-Delta effect). Flexure-related material nonlinearity was represented in this study using the moment-curvature relation input as paired data into the ABAQUS beam element (Hibbitt et al., 1998). These curves are used to monitor the section damage at each of the three integration points in each element, so that proper tracking of the spread of plasticity, and associated change in element stiffness, may take place within the hinge elements during each increment of loading.

Flexural Capacity

A cross-section fiber model was used to generate the moment-curvature data points in each bending direction for each beam and column element in the substructure. BIAX, a specialized research-oriented program (Wallace, 1992) having such a model, was used in this study. The BIAX program allows subdivision of the cross-section into small rectangular regions and use of accepted uniaxial stress versus strain relations for concrete and steel material. The PI believes, based on his own experience, that this program enables an acceptable approximation of the cross-sectional properties for reinforced concrete members.

Figure 4.2 shows the gross concrete sections and steel reinforcement layout for a typical column, Section X-X, and cap beam (between the columns), Section A-A. The top of the figure shows the as-built drawing (also see Figure A1.2), and directly beneath these are shown the schematic representation of the corresponding BIAX models. Note that each model was defined such that a typical concrete fiber occupies an area of about 2 in². These fine subdivisions of the gross section area are not shown for clarity but their relative size can be inferred from the stair-step edges of the trapezoidal column section.

The BIAX model predicts the response of the composite cross-section by defining uniaxial stress-strain relations for each fiber area, whether steel or concrete. The relations selected for this analysis are shown in Figure 4.3. The concrete area is divided into two regions:

1. Confined concrete within the transverse reinforcement (Figure 4.2)
2. Unconfined concrete outside this reinforcement.

In reality, the degree of confinement is highly variable depending on the rigidity of the reinforcement, which is in turn affected by the detailing of the cross-ties and the bar hooks. The assumed relations clearly give a tremendous strength and toughness benefit to the confinement of the concrete.

Nonlinear moment-curvature relations predicted by BIAX for monotonically increasing

moment holding a constant axial force equal to the dead load reaction are shown in Figure 4.4. These are obtained by incrementing the deformation (rotation), resolving the strain at the fiber location based on plane sections remaining plane, and then summing up the stress contributions of each fiber to the total force and moment on the cross-section based on the assumed stress-strain relation.

By tracking the tensile stress in the unconfined concrete fibers, it is possible to precisely determine three critical moment levels corresponding to distinct damage states for each cross-section:

1. M_{CR} - cracking, defined as complete loss of tensile strength, occurs in one or more fibers
2. M_Y - yielding, defined as yielding of the tensile steel, occurs in one or more fibers
3. M_U - ultimate, defined as effective inability to increase the moment with increasing rotation

The above critical states were used to define the moment-curvature input curves for the 3D beam-column elements in the ABAQUS bent model shown at the top of Figure 4.1. Solving the incremental equations of equilibrium using displacement-based finite element analysis procedures, ABAQUS computed the nodal displacements, reaction forces, and internal member forces (axial forces, shears, and bending moments) throughout the bent.

Table 4.1 Moment-Curvature Capacities of the Sections

Local Bending Axis	Cracking		Yield	
	Curvature (rad/ft)	Moment (kip-ft)	Curvature (rad/ft)	Moment (kip-ft)
1-Axis				
Column	2.85 E-05	658	3.22 E-04	12376
Cap-beam	2.92 E-04	4170	5.89 E-04	7935
Intermediate pile	5.98 E-05	2558	5.03 E-04	3544
Abutment pile	7.10 E-05	916.8	1.82 E-04	1667
2-Axis				
Column	1.13 E-05	1220	8.70 E-04	6640
Cap-beam	1.82 E-04	1284	7.10 E-04	4794
Intermediate pile	5.98 E-05	2558	5.03 E-04	3544
Abutment pile	7.10 E-05	916.8	1.82 E-04	1667

A normalized load-deformation curve representing these results is given at the bottom of Figure 4.1. The total horizontal load, P , applied at the cap beam level has been expressed as a ratio with respect to the approximate asymptote of 2000 k, at which value a mechanism may be assumed to develop leading to total collapse. The deformation has been expressed as the drift ratio, d , defined here as the relative displacement between the top and bottom of the columns, δ , divided by the column height, L . This measure of

column damage is analogous to the interstory drift ratio used in building codes.

Figure 4.5 shows schematically the condition of a collapse mechanism in which a fully-plastic moment has been developed at the base of each column and at the interior connections of the cap beam to the columns. Equating external work to the internal energy absorbed in rotation of the four plastic hinges in the mechanism (i.e. neglecting elastic deformation and heat energy), the following simple relation is established:

$$P * \Delta = 2 * (M_p^{\text{Column}} + M_p^{\text{Capbeam}}) * \Delta$$

Using the chord length definition, $L = \Delta / \theta$, this reduces to:

$$P = 2 * (M_p^{\text{Column}} + M_p^{\text{Capbeam}}) / L'$$

The plastic moments may be approximated from Figure 4.4, and the chord length from Figure A.3:

$$M_p^{\text{Column}} = 20000 \text{ k-ft} \quad M_p^{\text{Capbeam}} = 10,000 \text{ k-ft} \quad L' = 20 + (5.5/2) = 22.75 \text{ ft}$$

This gives an estimate of the pushover capacity as:

$$P = 2 * (30000) / (22.75) = 2640 \text{ k}$$

The approximate capacity is seen to be 32 percent larger than the approximate asymptotic limit, $P=2000 \text{ k}$, computed using ABAQUS, which accounts for distributed plasticity over the height of the columns and over the length of the cap beams. The mechanism limit analysis, on the other hand, lumps the plasticity effects at discrete hinge locations.

Shear Capacity

The pushover analysis above has been strictly concerned with the flexural capacity.

These columns have a height-to-width ratio, $L/W = 20/6 = 3.33$ (or less if the trapezoidal shape is considered), implying that shear deformation is significant. Also, the transverse (horizontal) reinforcement is only No. 5 bars with spacing, $s = 12 \text{ in}$. This spacing is considered inadequate in many cases and was deemed to be the cause of a number of failures of circular bridge columns in California.

Procedures developed by University of California at San Diego researchers (Seible et al., 1995) for evaluating retrofit needs of bridge columns are applied to this case. The total capacity of the column is considered the sum of the contributions of:

1. The effective concrete area on the cross-section
2. The horizontal shear reinforcement across a single inclined crack over one spacing
3. The axial load compression strut that extends over the entire height of the column

For a rectangular section, the three contributions are estimated as (refer to App. C):

$$\begin{aligned}
 1) \text{ Concrete:} \quad V_c &= k * \sqrt{f'_c} * A_e && (0.5 < k < 3) \\
 2) \text{ Steel} \quad V_s &= (n * A_h * f_{hy} * D' * \cot ?) / s && (\text{rectangular section}) \\
 3) \text{ Axial Force:} \quad V_p &= (D - c) / L && (\text{for double bending})
 \end{aligned}$$

where

- k = shear strength reduction factor that depends on column ductility ratio
- f'_c = unconfined compressive strength of the concrete (psi)
- A_g = gross concrete section area (in²)
- A_e = effective concrete shear transfer area, taken as $A_e = 0.8 * A_g$ (in²)
- D = gross concrete section dimension parallel to loading direction (in)
- cc = concrete cover to center of bar (in)
- n = number of legs of transverse reinforcement in the direction of loading
- A_h = area of transverse reinforcement bar (in²)
- f_{yh} = tensile yield strength of transverse reinforcement bar (psi)
- d_h = diameter of horizontal reinforcement bar (in)
- D' = confined core length parallel to loading direction (in), taken as $D - 2 * cc - d_h$
- $?$ = shear crack inclination to column axis (deg)
- s = horizontal bar spacing (in)
- c = depth of equivalent rectangular compression block (in)

For the present case:

$$\begin{aligned}
 1) V_c &= 3 * \sqrt{4500} * (0.8 * 4 * 6 * 144) && (\text{neglecting triangle areas in } A_g) \\
 2) V_s &= (2 * 0.31 * 60000 * (72 - 2 * 2 - 0.625) * \cot 30) / 12 && (\# 5 \text{ bars @ } 12 \text{ in}) \\
 3) V_p &= (10 * 68) * (72 - 2) / (20 * 12) && (\text{see Fig. 4.1 b for bearing DL}) \\
 V_{TOT} &= 556 + 362 + 198 = 1116 \text{ k}
 \end{aligned}$$

Assuming equal distribution of shear forces to each column, the total lateral load capacity of the bent is thus estimated as, $P = 2*(1116) = 2232$ k, for drift ratios up to $d = 2*d_Y$, or a displacement ductility ratio, $\mu_\gamma = 2$. From Fig. 4.1c, the drift ratio at first yield, $d_Y = 0.005$. According to the UCSD shear design approach, this capacity reduces linearly with further increase in μ_γ to $P = (2232)/3 = 744$ k, up to $\mu_\gamma = 4$. A slower linear reduction is then expected to $P = (744)/2 = 372$ k, at a $\mu_\gamma = 8$, after which this residual value is maintained until longitudinal and/or transverse bar fracture or buckling occurs.

Clearly, a shear failure preceding formation of a flexural collapse mechanism is a possibility, at least at drift ratios in excess of twice the yield value.

5. LEVEL 2 ASSESSMENT

The ABAQUS 3D FE model that was constructed to perform the Level 2 analysis is shown in Figure 5.1. The Level 2 model was developed by Prabin Tuladhar in the fall of 1999 for use in planning the field vibration measurements performed in the summer of 2000. After the field study, the model was used to evaluate the effect of foundation stiffness using linear springs with properties determined using the method prescribed in FEMA 273 and to perform preliminary Level 2 response spectrum analysis.

As discussed in the Level 1 analysis, the column mesh was refined after Tuladhar's preliminary work for the purposes of adapting his Level 2 model to the Level 3 analysis. Adjustments were made to the clear heights of the columns in each interior bent to more adequately reflect the as-built drawings. The clear heights were, respectively: { 20'-6 11/16", 17'-8 11/16", and 18'-2 7/16" } for Phase I Bents {2, 3, 4}, and { 21'-8 1/4", 18'-10 1/4", and 19'-4" } for Phase II Bents {2, 3, 4}, see Figure A.3.

All results in this section correspond to analysis of the refined model, with eigenvalue analysis of the refined model performed by Bernard LeBlanc (LeBlanc, 2001) and response spectrum analysis performed by Saroj Shrestha. All three students participated in the field vibration study discussed below.

All dimensions and construction details are based on the as-built drawings, for example see Figures A.3 (Bent) and A.4 (Deck). Since the emphasis has been placed on the behavior of the substructures, the mesh design has been dictated by the need to capture natural modes and frequencies (mass and stiffness properties) accurately, not to predict stresses accurately.

Consistent with the Level 2 analysis methodology, all material properties are modeled as linear elastic. All 6 degrees-of-freedom (DOF) have been restrained at the bottom of each column, but only vertical displacement has been restrained at the abutment end of each girder. Because the properties are assumed linear and, because the cubic shape functions for the 3D ABAQUS element used are exact for linear response, only one element is

needed. This was the approach used by Tuladhar’s Level 2 model to represent the clear height of each column, i.e. the length between the rigid elements (see top of Figure 4.1).

The difference in elevation between nodes of plate elements used to model the slab and the neutral axes of the girders sharing these common nodes is accounted for using a special offset option in the beam element section definition. This allows for the proper stiffness of the composite slab-girder deck system. Construction joints and girder bearings have not been explicitly modeled, however. These features introduce highly nonlinear behavior and associated numerical difficulties, which cannot be treated in a linear analysis.

The treatment of the system as essentially a fixed base system without the explicit modeling of the soil basically decouples the Phase I and Phase II models, which are separated at the deck and bent levels. For convenience, the Level 2 analysis nonetheless includes both models simultaneously, rather than separately for visual clarity. Should the transverse motion exceed the 1-inch gap between bents, pounding could actually occur. This scenario, however, is unlikely, because as the Level 1 model shows (Fig. 4.1c), this would require that a plastic collapse mechanism form.

Natural Modes and Frequencies

Static self-weight analyses were performed using the revised Level 2 model to obtain the deformed geometry under gravity forces. Eigenvalue analyses were then performed using the gravity loaded configuration. Table 5.1 summarizes the characteristic modes and the participation factors computed by ABAQUS.

Table 5.1 Characteristic Modal Properties of the Level 2 Model

Mode	No.	Frequency (Hz)	Description
A	1	1.29	Vertical translation of the end spans of the deck
B	17	2.96	Rotation of the deck in counter clockwise direction
C	18	3.63	N-S translation of deck (lateral direction)
D	34	5.19	E-W translation of the deck (longitudinal direction)

Mode	Participation Factors					
	X Translation	Y Translation	Z Translation	X Rotation	Y Rotation	Z Rotation
A	-0.0878	-0.0142	0.0430	-0.0861	-204.	4.41
B	0.00922	0.398	-0.0197	-7.73	0.117	-199.
C	0.266	1.62	0.00280	-36.2	3.50	11.6
D	-1.35	0.110	-0.00417	-1.18	-43.1	69.9

These modes were selected as characteristic because their mode shapes, depicted in plan and isometric views in Figure 5.2, correspond to net movement of the center of gravity of the system in one of the global axes, as represented by the large participation factors highlighted in Table 5.1. Such net movement is usually what drives damage of the substructures, if energy in the loading is sufficient to excite that mode.

Clearly, numerous other modes were calculated, but these others are usually higher mode representations of the vertical characteristic mode or so-called breathing modes, which don't lead to any significant net movement. Damage of the latter modes usually will be localized to specific elements, in particular the deck, which is not the focus of this study.

These characteristic modes represent the natural tendencies of the fixed base system, without regard to any particular loading. The damage response to a particular seismic event will in large measure be determined by the amount of energy that the event contains at the frequency corresponding to one of these characteristic modes. The dominant frequency of seismic events tends toward lower frequencies as the magnitude increases. In this case, a very large magnitude event (perhaps, $M > 6.5$) would be required to have a dominant frequency at the fundamental mode (Mode A), but a moderate event could easily have a dominant frequency near Modes B, C, or D.

Field Vibration Measurements

The Level 2 analysis model was constructed considering only the as-built drawings supplied by MDOT Bridge Division and engineering principles, including both elementary mechanics and finite element practice. A field vibration measurement task was planned for comparison with the Level 2 analysis and was executed in the summer of 2000. This task was an ambitious and novel undertaking in the context of MDOT facilities and practice. The work and findings have been well received by researchers at three international conferences (Mullen et al., 2000, Mullen et al, 2001, and Leblanc and Mullen, 2001).

The scope of the field vibration measurements was limited by the four channels available in the data acquisition system owned by the PI prior to the project award. As part of the contract agreement, four new uniaxial accelerometers, one triaxial accelerometer, a 12-lb instrumented hammer, and associated cables were purchased (Figure 5.3). After detailed discussions with the selected vendor's technical representative, a configuration for an adaptable system, especially designed to perform well under the difficult site conditions, was established (Figure 5.4).

The uniaxial seismic accelerometers are rugged and heavy, each weighing almost 1 lb (4.448 N). The triaxial accelerometer is lightweight and has a cable that splits into three separate cables (Figure 5.3, inset). Each of the accelerometers possesses a high sensitivity in the 2 Hz-1 kHz frequency range, according to the manufacturer's specifications (PCB Piezotronics). Note that the lowest computed frequency is about 1.3 Hz.

The uniaxial accelerometers have a short threaded insert that enables installation by screwing into the concrete to ensure an acceptable coupling between structure and transducer. This seemingly minor feature contributed to the most time-consuming and dangerous aspect of the field work, namely:

1. Access to the transducer location, by ladder if elevated but below the deck level
2. Pre-drilling starter holes for the threaded part of the transducer, including providing power to an electric drill- a car battery and adapter cables were used in

this case. Drilling the holes and screwing the accelerometers into the holes by hand was especially difficult from the ladder positions.

To ensure reliable signals, heavy duty co-axial cables in lengths of 250 ft each were used to collect the signals into a four-channel signal conditioner unit before continuing the remaining distance to a four-channel SigLab 20-22/42 (DSPT, 1998) data acquisition unit, Figure 5.4. The abutment-to-abutment deck length is 340 ft, so four additional 250 ft cables connected the signal conditioner and data acquisition units for maximum flexibility. A sheltered space was established in the I55 shoulder between the two pier columns of the west most span to avoid possible hazards from errant vehicles. Continuous power to the data acquisition unit was supplied by the battery of our van, which incidentally was proved sufficient to transport all equipment and personnel for the field study. This fact demonstrates the highly mobile aspect of the final system design.

The typical test scenario consisted of:

1. Meet District II maintenance personnel, who would use MDOT vehicles (see Figure 5.3) to place cones at edge of lane nearest to shoulder of lane where transducers would be placed.
2. Unroll cables to selected positions for transducer installation.
3. Predrill holes, with ladder setup if necessary, and install transducers.
4. Hook up cables to transducers, and test connectivity to signal conditioner.
5. Setup data acquisition unit position, boot laptop, test unit operability, initialize Virtual Network Analyzer software through Matlab platform.
6. Using walkie-talkie communication between transducer location and Siglab unit, confirm operability of each transducer.
7. Set storage locations on laptop, initialize trigger settings, await trigger, record vibrations, close data files on laptop.
8. Remobilize transducer array for new configuration as needed and repeat Steps 2-7, assuming use of same shoulder.
9. Roll up cables and demobilize all equipment.
10. MDOT personnel remove cones and all vehicles leave site.

Figure 5.5 shows a typical response measurement obtained using the above procedure and the typical double window format of the Siglab VNA. The display corresponds to the array configuration shown in Figure 5.4, and the individual traces correspond to the three transducers designated as output, Y, locations. The input, X, location in this configuration is nominally the same as the instrumented hammer impact location (see Figure 5.3, last photo). The reason for this setup is related to the modal extraction software, which is discussed below.

The top window in Figure 5.5 shows a plot of the real-valued amplitude (magnitude) of the complex-valued frequency response or transfer function (FRF or XFER) versus frequency, in Hertz. The FRF or XFER is dimensionless in this case and is defined as the real amplitude of the complex ratio, $H(i\omega)=Y(i\omega)/X(i\omega)$, where $Y(i\omega)$ is the complex Fourier transform of the output time history, $y(t)$ and $X(i\omega)$ is the complex Fourier

transform of the input time history, $x(t)$.

The bottom window in Figure 5.5 shows the time histories of each of the output transducers, $y(t)$, and the input, $x(t)$. The manufacturer calibration sheet indicates that 10 V corresponds to 1 g of acceleration for these transducers. Thus, the peak acceleration shown is about $0.3 \text{ V} / (10 \text{ V/g}) = 0.03 \text{ g}$. This peak value, however, corresponds to the red trace, which is clearly dominated by very high frequency energy, so the amplitude at the frequencies near the characteristic modes of interest to this study is seen to be very low, perhaps as low as 0.003 g or less.

Modal System Identification and Visualization

Identifying modal system properties using field vibration measurements proved to be difficult because of the relatively low energy level at frequencies near the characteristic modes anticipated by the FE model. This can be seen most clearly by looking at the analysis of the data performed offsite in the office after the measurements were taken. Figure 5.6 shows the FRF plots as seen using the modal system identification software (Spectral Dynamics, 1994) made available to the project by Dr. Raju Mantena, Associate Professor of Mechanical Engineering at the University of Mississippi.

To process the FRF data stored in a binary file by the SigLab VNA, the file was first converted to a neutral (software independent) text file in the Uniform File Format (UFF). The STAR Modal software reads this format and may be used to interactively display and zoom in on the data as shown. Note that the predominant energy, indicated by highest peaks, is about 1 kHz and 2 kHz.

Considerable zooming is required to observe the peaks in the range, 1-20 Hz, seen in the top window of Figure 5.5. These same peaks are barely observable in the bottom window of Figure 5.6, which is already a zoomed in view of the full range view in the top window of Figure 5.6. This difficulty in observation highlights the importance of having a reliable finite element model in advance of the field test to guide the search.

While the peaks of the FRF are visible with the SigLab VNA, it is not clear from the FRF alone that the measured response is associated with any modes anticipated by the finite element model or consistent with likely response behavior. The STAR Modal software takes the measured data the extra step by computing and graphically animating mode shapes of postulated classical mode models based on curve fitting of the FRF curves over a user-specified range of frequencies, presumably containing a select peak or small number of peaks. The theory upon which the curve fitting yields the necessary parameters of the classical modes model is described in the STAR Modal user's manual.

The field tests were performed in a single input-multiple output (SI-MO) manner, with three outputs typically measured simultaneously. A polynomial curve fitting procedure was selected in STAR Modal that uses all three of the outputs to estimate the best fit. This method of operation is especially efficient and introduces reliability to the data through the simultaneous nature of the measurements. For a laboratory-sized specimen, modal system identification is typically performed in a SI-SO manner, keeping the output location the same and varying the input location.

The input in such laboratory cases is usually an impact hammer with an accelerometer mounted in the head. This was the intent in the design of the field vibration study, and a large instrumented hammer with 12 lb head capable of delivering 5000 lb of force was purchased and used in the field (see Figure 5.3, last photo). A major difficulty that was soon encountered, however, was that the hammer proved insufficient to excite the very stiff and massive bridge structure. In fact, early attempts to excite the bridge lead to breakage of the instrumented portion inside the hammer head. The head was replaced after the first site visit, which proved to be purely exploratory, yielding no useful data. During the next visit, the repaired hammer was used not to excite the system but rather to provide a reference input needed in the SI-MO algorithm used by STAR Modal to identify the modal system properties and mode shapes.

In reality, excitation was provided by ambient truck traffic that over a period of time would typically excite the embankment soil, which would then activate bridge motion of

sufficient energy to trigger the transducers. A variety of vehicle types was encountered, with just a few shown for reference in Figure 5.3. Because the FRF approach in effect eliminates the effect of the particular input, the computed mode shapes were not affected by the variety of vehicles present on the bridge at any given moment. The important fact was that these vehicles eventually generated enough energy in the bridge system to develop significant peaks in the FRF's at the selected transducer locations.

Three SI-MO array configurations were successfully implemented during the site visits. The first array is shown schematically in Figure 5.7 with reference to the FE model. Setup for this array was extremely time-consuming, because it required that three uniaxial accelerometers be installed at the north face of the cap beams of each major interior bent. Each transducer installation required a ladder, portable power for use of the drill, and crossing of I-55 traffic to reach the bent pier. At the deck level, movement was easier, but cables had to be run over the full 340 ft of the roadway and, at each bent transducer location, the cable had to be delivered over the curb to the person on the ladder at the pier cap level. Once hook-up of the cables had been completed, verification of the signals proceeded by walkie-talkie (see photos in Figure 5.3).

For this first array, the transducers at the three pier caps were treated as outputs. Bents 2, 3, and 4 were labeled locations 41, 42, and 43 respectively (see photos in Figure 5.3). A fourth transducer was initially installed at the base of the curb midway between the bent 2 and 3 positions on the deck. The latter position was labeled 34. Because the impact hammer proved of little use as an input, the fourth transducer served as the reference input, viewing the deck as an input location for the vehicle-generated vibration of the bents. The placement midway between bents was intended to maximize the energy input in the transverse direction. This arrangement helped in identifying frequency peaks in the range of interest (after considerable zooming, as mentioned earlier), ultimately confirming that the procedure could be performed successfully in the field.

The algorithm used in the STAR Modal software, however, requires that the input transducer be located at a driving point having essentially the same location as one of the

output transducers. For this reason, the results of the final system identification for this arrangement of the output transducers actually corresponds to the arrangement shown in the top of Figure 5.8, where X is located at the base of the curb above the north face of bent 3.

A second array, which is a subtle variation on the first, was used to capture the effect of deck-embankment interaction on the transverse modes. The transducer at the bent 3 pier cap was removed and placed at one of the abutments (see Figure 5.3 photo, position labeled 32). The transducer on the deck was removed and placed at the opposite abutment. Because it was desired to measure outputs at both abutments and both intermediate bents, the driving point technique could not be applied and a STAR Modal analysis could not be performed for this case.

Subsequent to performing the STAR Modal analysis, however, newer software called ME'scopeVES (Vibrant Technology, Inc.) was made available by Dr. Mantena. This software uses an alternative algorithm, which does not require that the driving point be at the same position as one of the outputs. Thus, ME'scopeVES analysis was performed for this second array (LeBlanc and Mullen, 2001).

The third array is shown schematically at the top of Figure 5.4 and bottom of Figure 5.8. This configuration was restricted to the Bent 2-Phase II pier, and the uniaxial transducers were oriented to capture longitudinal modes. The driving point method was for the purposes of the STAR Modal analysis.

The results of the modal system identification are best viewed as real time animations of the modal responses at the identified frequencies. For the purposes of this report, snapshots of each array have been taken at the apparent maximum modal response positions and displayed relative to the initial undeformed configuration in Figure 5.9. The shapes are clearly consistent with the mode shapes predicted by the Level 2 Model at frequencies remarkably close as seen in Table 5.2.

Referring back to Table 5.1, Figure 5.2, and Figure 5.5, it is noticed that no identification was possible for either Mode A, which has a very low frequency of 1.3 Hz, or for Mode C, which involves net transverse movement of all three bents. Mode B, on the other hand involves mostly a rotation of the deck about a vertical axis through the center of gravity of the system, and Mode D, involves a net longitudinal movement of all three bents.

Table 5.2 Comparison of FE and Modal System Identification Analysis Results

Mode	Level 2 Model (Hz.)	STARModal (Hz.)	% Difference
Transverse (B)	2.96	2.99	1
Longitudinal (D)	5.19	5.24	9

Considering that truck traffic was essentially generating all the motions during the vibration testing, the above findings are not surprising. From the viewpoint of examining damage to the substructure, Mode A is not especially a concern, except during a very large event that could induce large enough vertical inertial forces in the deck to damage the foundations. It is presumed that the deck and piers have adequate resistance to such vertical responses.

Mode C, however, is of primary concern to damage in the columns associated with large transverse inertial forces of the type considered in the Level 1 analysis. This fact was recognized during the vibration testing, and a mechanism for exciting this mode by lightly impacting the curbs with MDOT maintenance vehicles was proposed to MDOT's personnel at the site. The decision was made at the time, however, that the proposed procedure could not be implemented without closing at least one lane of traffic, which was deemed unacceptable by District II managers.

Development of Site-Specific Response Spectra

A response spectrum analysis may be performed either conservatively, using the design spectrum specified in the code or more realistically using a site-specific spectra with due

consideration for the random nature of the loading. In this study, the relation between response to design spectral loading and site-specific spectral loading has been examined by Tuladhar for the intensity case of $M=7.5$, using his model. The effect of intensity and random variation has been examined by Shrestha for intensity cases $M=6, 7, \text{ and } 8$, with 10 Monte Carlo simulations for each intensity.

A suite of Fortran driver subroutines, collectively called SMSIM were downloaded from Dr. David Boore of the USGS in Menlo Park, CA. Upon request, he also supplied a sample input file with source and attenuation parameters he recommends for analysis of the deep subsurface geology in the Central US with his program. These subroutines use a host of generic subroutines available in a text on numerical methods (Press et al., 1992) which were not supplied with the driver subroutines. In the summer of 2000, the necessary routines were written and independently verified by the PI using examples in the referenced text. Monte Carlo simulations were then developed for the bridge site using the recommended seismic source parameters, listed in Table 5.3, and the spectral amplification function listed in Table 5.4, which has been used by Hwang (Hwang et al. 1999) for Memphis area rock at geologic depths.

A commercial software package, ProShake (EduPro Systems, 1999), was purchased for the project and used to perform a 1D shear wave propagation analysis through the soil column model shown in Figure 5.10. The solution algorithm incorporates a nonlinear shear modulus versus shear strain degradation constitutive relation. A graphical-user interface allows for ease of specification of input motions and model parameters as well as interactive computation and display of both time history and response spectrum amplitudes at each layer specified in the soil column. It should be noted that the soil column is assumed to be a composite of flat layers that are infinite in the horizontal direction.

The soil profile used for this study is plotted in Figure 5.10. The soil shear wave velocity and density data are based on a geophysical test done at the BMH-Desoto hospital (Mullen et al., 1997) site on the northeast corner of the I55-MS302 intersection only

several hundred yards from the bridge site. The layer depths have been adjusted to be compatible with the soil report for the bridge and to enable output locations at the both the level of the column footing and the level of the top of embankment. The default soil degradation curves for the soil types have been used for the study and are plotted for reference in Figure 5.11.

Table 5.3 Seismic Source Parameters for SMSIM (Boore and Joyner, 1991)

Parameter	Value
Magnitude (M)	6, 7, 8
Epicenter distance (R)	100 km
Partition vector	0.71
Shear wave velocity at source	3.5 km/sec
Crustal density	2.7 g/cm ³
Stress parameter	150 bars
Radiation coefficient	0.55
Quality factor	680 $f^{0.36}$
Kappa	0.0084 sec
High frequency cutoff	100 Hz
Strong motion duration	1/ f_c +0.05r
Window shape	Exponential

Table 5.4 Spectral Amplification Function for SMSIM (Hwang et al., 1999)

Frequency (Hz)	Amplification Function
0.10	1.00
0.13	1.19
0.21	1.34
0.32	1.76
0.34	1.81
0.41	1.89
0.53	1.97
1.25	2.02
2.73	2.02
5.85	2.02
8.20	2.02
13.66	2.02
15.76	2.02
18.63	2.03
24.11	2.02

The vulnerability assessment of the University of Mississippi campus, which was conducted by the PI for MEMA, revealed that, in Lafayette County at least, most of the site amplification of bedrock motion occurs within the last 100 to 200 feet of soil (Stewart, 1997). For the purposes of spectral analysis, therefore, the SMSIM generated

motions could be applied with little loss of dynamic response resolution to a model of a shallow soil column below the ground surface.

Figure 5.12 shows computed SMSIM acceleration time histories (Level 5), associated ProShake acceleration response time histories at the footing level (Level 2), and ProShake strain response time histories in the thick layer (Layer 4) just below the gravel layer, for the range of intensities, $M = 6, 7,$ and 8 . Each top figure shows the amplification in terms of acceleration, by comparison of output (Layer 2) to input (Layer 5), while Table 5.5 summarizes peak values of response and an amplification ratio defined as the peak acceleration (largest absolute value) of the output time history divided by the peak acceleration of the input time history.

Figure 5.13 shows evidence of amplification in the amplitudes of the computed response spectra. Maximum amplification ratios in the spectra are similar to those in the time histories summarized in Table 5.5. Ratios are in the range, 1.6-2.0, regardless of source intensity. The peak accelerations at the stiff soil level, Layer 5, are in the range, 4-24 percent, whereas the soil column amplifies these to the range, 8-37 percent.

As intensity increases, a noticeable shift occurs in the dominant period of input and output spectra, with the shift tending toward higher periods, or lower frequencies, in all cases. The shift is more pronounced in the output spectra. The reason for this lies in the strain histories observed in Figure 5.12. As the intensity increases, the shear strain in the soil column increases in the range, 0.7-5.0. From Figure 5.11, such peak shear strains imply that ProShake predicts the shear modulus will decrease roughly 15, 40, and 50 percent of the virgin or low strain value, for intensity, $M= 6, 7,$ and 8 , respectively. The damping ratio will increase roughly from 1 to 4, 7, and 10 percent, respectively. Depending on the depth of penetration of such reductions in the top layers of soil, such degradation in the shear modulus and increase in damping will significantly reduce the natural frequency of the soil column and alter the overall dynamic response characteristics of the soil and the soil-structure system.

For the $M = 6$ case, the output peak occurs at a period of about 0.5 s where there is no peak in the input. This period also may be predicted to be the fundamental natural period of the entire soil column considered as a single layer, based on the following relation in Hwang and Lee, 1990, using an average shear wave velocity computed from an equivalent time of travel through all the layers individually.

$$T = 4 * \left(\frac{H}{V} \right) = 0.509 \text{ s} \quad (f = 1/T = 1.96 \text{ Hz}) \quad \text{where } V = \frac{H}{\left(\sum \frac{H_i}{V_i} \right)} = 847 \text{ ft/s}$$

Table 5.5 ProShake Predictions of Soil Column Response

M	PGA, % g (Top of Layer 5)	PGA, %g (Top of Layer 2)	Amplification Ratio	Max. Shear Strain (Top of Layer 4)
6	4.29	8.32	1.94	0.0068
7	12.6	25.0	1.97	0.0297
8	24.0	36.9	1.56	0.0508

Response Spectrum Analysis

The Layer 2 ProShake response spectra were used as input to ABAQUS response spectrum analyses of the Level 2 model shown in Figure 5.1. A limitation of the ABAQUS analysis procedure is that the same input spectrum must be applied at all supports, i.e. all restrained degrees of freedom, regardless of elevation. This prevents the more accurate specification of the Layer 1 output spectrum as the input to the supports at each abutment. The previous work by the PI, Mullen and Cakmak, 1997, has indicated that, in a time history analysis, neglecting the difference between motions at the footing and abutment levels may lead to predictions of little or no damage, when this is in fact the case. However, in a response spectrum analysis, it is not clear that this will be the case.

Unlike a time history analysis, a response spectrum analysis only provides estimates of peak response to the excitation defined by the input response spectrum. The time of the peak cannot be determined and relative responses at different points in the system, e.g. drift ratios, cannot be established. Further, response spectrum analysis is premised on the validity of mode superposition, which is strictly speaking invalid in the case of a damaging event.

In a response spectrum analysis, peak amplitudes of response are determined directly by summing contributions from user-selected modes at frequencies of interest. It is presumed that an eigenvalue analysis has been performed to establish these frequencies. Since the response spectrum ordinates represent maximum responses of SDOF systems at given frequencies, summing of these amplitudes over a reduced discrete set of frequencies yields too conservative an estimate to use in practice. The conventional practice of summing using the Complete Quadratic Combination (CQC) method, which purports to estimate a more reasonable value, has been adopted for this analysis.

The 1994 AASHTO LRFD Design Specifications recommend that at least 12 frequencies be included in the summation when applying the Multimode Spectral Method. If interpreted literally, this would not allow inclusion of Characteristic Modes B, C, or D listed in Table 5.1. The first 35 modes have, therefore, been used to allow for inclusion of all four of these modes.

Results for the three base case intensities, $M = 6, 7, \text{ and } 8$, are summarized in Table 5.6, which gives the peak moments in each of the Phase I exterior columns, which were the ones with the highest values in all cases, except for two instances at the top of the Phase I Bent 4 interior column where slightly higher moments were predicted. For completeness, Table 5.6 lists results for top and bottom plastic hinge regions and bending about both strong (transverse deck movement) and weak (longitudinal deck movement) axes.

**Table 5.6 ABAQUS Predictions of Level 2 Model Response
(Moments in Plastic Hinge Regions of Phase I Columns, k-ft)**

M	Top of Column		Base of Column	
	Strong Axis	Weak Axis	Strong Axis	Weak Axis
Bent 2				
6	492	539	810	2232
7	1617	2474	2680	4513
8	1836	3134	3031	6181
Bent 3	Strong Axis	Weak Axis	Strong Axis	Weak Axis
6	448	534	826	2680
7	1561	1666	2900	5598
8	1719	1908	3183	7502
Bent 4	Strong Axis	Weak Axis	Strong Axis	Weak Axis
6	606	613	1080	2680
7	2076	2377	3807	5652
8	2280	3898	4168	7397

Comparison of these results with the column section capacities in Table 4.1 indicates that the Level 2 analysis predicts that:

1. For M=6, the peak bending moment demand exceeds the cracking moment capacity at the base of the column in both strong and weak directions.
2. For M=7, the peak bending moment demand exceeds the cracking moment capacity but is less than the yield moment capacity at potential plastic hinge locations in both strong and weak directions.
3. For M=8, the peak bending moment demand exceeds the yield moment capacity at the base of the column in the weak axis only.

Effect of Random Nature of Loading on Response

The base case results presented above in Table 5.6 do not allow for the random nature of the predicted loading, which is inherently built into the design contour maps used for determining the peak ground acceleration coefficient to be used at a selected site (assumed on bedrock). To give some assessment of this variability, 10 simulations were

performed at the 3 different intensity levels, using the same parameters as in Tables 5.3 and 5.4, and the maximum values in either the time history run or the response spectrum output were recorded.

Table 5.7 summarizes the basic statistics of these peak acceleration computed for each set of 10 simulations, including the 1) mean, \mathbf{m}_A ; 2) standard deviation, \mathbf{s}_A ; 3) one standard deviation band, $\mathbf{m}_A \pm \mathbf{s}_A$; and 4) coefficient of variation (COV), $(\mathbf{s} / \mathbf{m})_A$. Results at three reference positions in the soil-structure system are considered: 1) base of the soil column (Layer 5) as predicted by SMSIM, 2) footing level (top of Layer 2) as predicted by ProShake, and 3) middle of Phase I cap beam as predicted by ABAQUS using response spectrum analysis of the Level 2 model.

The results in Table 5.7 indicate that, in all cases, 1) the standard deviation of the peak acceleration is less than 4 percent of g, and 2) the COV is less than 25 percent, indicating mild variability. The impact on the cap beam response is even milder, with standard deviation less than 1 percent of g and COV less than 10 percent.

The detail view of Figure 1.4 shows that a design acceleration coefficient, $A = 0.18$ g, would be appropriate for the bridge site, based on the 1994 LRFD (1988 USGS) maps. This design value corresponds to a specific target return period and incorporates both the source intensity for the target return period and the inherent variability. Comparing this to the one standard deviation bands in Table 5.6 of the SMSIM predictions, it might be considered that the maps correspond to the upper limit of the band for an $M = 7$ event.

Table 5.7 Statistics of Simulated Peak Accelerations, % g

M	SMSIM (Layer 5)		ProShake (Layer 2)		ABAQUS (Cap Beam)	
	m_A	s_A	m_A	s_A	m_A	s_A
6	4.4	0.5	10.2	2.6	14.7	1.2
7	13.2	2.5	22.4	2.8	24.9	1.1
8	28.1	3.4	33.3	3.2	30.6	1.1
	$m_A \pm s_A$	$\left(\frac{s}{m}\right)_A$	$m_A \pm s_A$	$\left(\frac{s}{m}\right)_A$	$m_A \pm s_A$	$\left(\frac{s}{m}\right)_A$
6	4-5	0.11	8-13	0.25	14-16	0.08
7	11-16	0.19	20-25	0.13	24-26	0.04
8	25-32	0.12	30-37	0.10	30-32	0.04

6. LEVEL 3 ASSESSMENT

The ABAQUS 3D FE model that was constructed to perform the Level 3 analysis is shown in isometric views in Figure 6.1 and plan and elevation views in Figure 6.2. The deck and girders in the superstructure are identical to those shown in Figure 5.1 for the Level 2 model. All bent elements have been modeled for nonlinear response in the manner described for the Level 1 model. Special treatment has been given to the modeling of the foundations for the columns of the interior bents, and explicit modeling of the abutments has been introduced. In addition, explicit modeling of the soil-foundation interaction has been introduced through the use of:

1. 3D continuum elements with nonlinear 3D constitutive laws
2. 3D infinite elements, which account for the damping associated with radiation of wave energy away from the structure and prevent the reflection of waves from an artificial restrained boundary of the FE model.

A detailed representation of the mesh around each footing is given in Figure 6.1, which has various detail views that identify specific aspects of the modeling of the:

1. Soil-footing connection
2. Bent footing and pile foundations
3. Abutment-deck connection
4. Column-footing connection

Dimensions have been determined with reference to the as-built drawings, see Figures A.2 (foundation layout), A.3 (footing), A.5 (abutment), and A.6 (piles).

Figure 6.2 shows the mesh design for the surrounding soil down to the depth indicated in the ProShake model (see Figure 5.10), consistent with both the information in the geotechnical report, see Figures B.1 (soil profile, including embankment) and B.2 (boring logs), and the geophysical investigation for the nearby hospital, see Mullen et al., 1997.

Background to Modeling Approach

Consistent with the objectives stated in Section 2 of the report, the emphasis in the Level 3 modeling approach has been placed on the behavior of the substructures. With this in

mind, the mesh has been designed to accurately capture natural modes and frequencies (mass and stiffness properties), not stresses necessarily. The methodology used in the Level 3 analysis is in fact the culmination of research developed by the PI over a number of years, which is briefly summarized below to provide a context for the discussion of results.

In Mullen and Cakmak, 1997, the importance of explicit modeling of embankment mass and stiffness was demonstrated using a relatively simple interaction model in which these properties were lumped to account for dynamic interaction between the embankment soil and the superstructure model, in this case considering only transverse shear wave motions. The study showed that the pier column damage highly sensitive to the presence or absence of such interaction, even in a limited manner.

The lumped approach was not seen as desirable as a general approach, however. Subsequent work by the PI extended the approach by explicit modeling of the subsurface and embankment soil using a coarse mesh of 3D linear continuum elements and infinite elements. To enable the interaction, constraint equations were used to tie the column translational DOF to those of the soil elements. The practical application of this approach was demonstrated in seismic vulnerability evaluations of a hospital building complex, see Mullen et al., 1997, and for a highway bridge with high embankments, see Mullen and Swann, 2001.

The use of constraint equations which effectively pinned all columns at their base was again not thought to be an optimal approach, and the effect of nonlinear response of the soil was not incorporated in the prior studies. A doctoral dissertation under the PI's advisement has been completed at UM recently by I. M. K. Ismail (Ismail, 2000). This work has demonstrated the feasibility of using a number of enhancements, including:

1. Use of 3D constitutive laws in ABAQUS for all soil continuum elements
2. Explicit modeling of the column-footing connection using a combination of plate and continuum elements to transfer the rotational DOF from the column to the footing

3. Use of a refined mesh in the soil adjacent to the footing to capture local damage around the footing and associated changes in the distribution of the internal forces over the height of the column
4. Estimation of the appropriate length scale needed to accurately model the dynamic properties of the embankment soil.

These enhancements were applied to a hypothetical 3-story office building whose columns were supported on spread footings. The simulations of damage to earthquake events, generated in the same manner as was done for this study, lead to some interesting conclusions. Most surprising was the fact that an erroneous assessment would be made of the safety of the building in a severe event if the local damage of the soil around the footings were neglected, even with all of other modeling enhancements listed above were included.

The Level 3 analysis, which further extends the above approach to the case of a structure with shallow pile foundations, has therefore adopted all of the enhancements listed above, including the nonlinear response of the soil throughout the entire model. Because of the localization of strain around the foundation elements, this potentially dramatic increase in problem complexity did not in fact increase the computation time significantly.

The piles were modeled as 3D nonlinear beam elements with node translational DOF compatibility at each layer of the soil elements. The typical pile section details and computed moment-curvature key points are shown in Figure 6.3 and listed in Table 4.1. The response curve was computed in a similar manner as for the Level 1 analysis, however, the computer program, IDARC2D (Kunnath et al., 1994) was used. Previous work by the PI has shown that IDARC2D and BIAX give results which are acceptably close for regular shapes. Whereas BIAX is more flexible in defining complex shapes like the columns, IDARC2D is simpler to use.

A decision had to be made how to model the various connections in the model, especially the girders at their bearing supports. The assumption here has been to assume rigid

connections between the girders and the bearings, which will tend to increase the forces transmitted to the supports (either bent cap or abutment). In the case of the abutment connections, observations at the time of the field vibration tests (Figure 6.4) indicate that certain bearings are not functioning properly.

The Drucker-Prager model in ABAQUS was used with the associated flow rule to characterize the nonlinear behavior of the soil layers. The key properties for the model are the slope of the yield surface (β) in stress invariant space, and the yield stress, s_y , in compression. Values selected for the different layers in the model are listed in Table 6.1.

Table 6.1 Drucker-Prager Model Parameters

Soil Layer (see Figure 5.10)	b (deg)	s_y (ksf)
1, 2	36	3.8
3	45	8.8
4	44	14.3

Natural Modes and Frequencies

A static self-weight analysis was performed using the Level 3 model to obtain the deformed geometry and stresses in the soil under gravity forces acting only on the bridge elements. The stresses in the soil due to the soil weight itself have been neglected. In the region of the footing, this turns out to be negligible in comparison to the bridge weight.

Eigenvalue analyses were then performed for the gravity loaded configuration as defined above. Table 6.2 summarizes the modes computed by ABAQUS most closely relating to the characteristic modes of the fixed base model. The corresponding mode shapes are depicted in the plan and isometric views given in Figure 6.5.

The process of identifying the characteristic modes for the Level 3 model proved to be far more difficult than that for the Level 2 model because of the many additional DOF and

resulting modes associated with the soil. The participation factors do not provide an effective basis for detection, because the mass of the soil exceeds that of the structure, so net movement of the system may involve local features of the soil rather than global movement of the structure.

Table 6.2 Characteristic Modal Properties of the Level 3 Model

Mode	No.	Frequency (Hz)	Description
A	1	1.51	Vertical translation of the end spans of the deck
B	17	3.11	Rotation of the deck in counter clockwise direction
C	18	3.81	N-S translation of deck (lateral direction)
D	34	5.46	E-W translation of the deck (longitudinal direction)

The frequencies of the Level 3 model are somewhat higher than those of the Level 2 model. At first this seems unexpected, because inclusion of soil as a deformable component of the system would tend to soften it relative to the fixed base conditions. The main difference here, however, is that the girders in the Level 2 model were free to move in the horizontal plane (essentially rollers in both directions), whereas the girders have a rigid connection to the abutment in the Level 3 model.

The reality is somewhere in between as confirmed by the field vibration tests. Figure 5.9 shows that for the two modes corresponding to rotational and longitudinal movement of the deck, that the modal frequencies are consistent with either model, but that the mode shapes and their animations indicate a clear effect of foundation flexibility.

Response Simulations

The SMSIM generated time histories for the three events of intensity, M=6, 7, and 8, displayed as the Layer 5 (red) traces in Figure 5.12, were resolved into longitudinal (1-axis) and transverse (2-axis) components assuming an epicenter in Marked Tree, Arkansas. The seismic waves are thus assumed to propagate to the site from the northwest at 30 deg counterclockwise from north. According to seismological

convention, vertical motion has been assumed to be 2/3 of the resultant SMSIM motion. Figure 6.6 shows the component time histories for the M=6, 7, and 8 events used as input to the Level 3 model. Peak values of acceleration are summarized in Table 6.3

Table 6.3 Peak Accelerations (% g) Input at the Base of the Level 3 Model

M	SMSIM	1-Axis	2-Axis	3-Axis
6	4.29	2.15	3.72	2.86
7	12.6	6.32	10.9	8.42
8	23.7	11.9	20.5	15.8

The three component acceleration time histories were applied to the bottom-most nodes of the ABAQUS model, and time history solutions were computed for each intensity level using the implicit integration scheme in ABAQUS Standard, version 5.8. The implicit integration scheme solves the incremental equations of equilibrium to within small tolerances on the residual or unbalanced global forces and moments. A number of special features were selected to control the solution algorithm and ensure that convergence was achieved, including:

1. The global stiffness matrix was reformed only once every four iterations
2. A correction was applied to prevent numerical errors leading to a drift or mean offset in the displacement solution
3. Data was written to the hard drive only once every three time steps
4. While the program uses a variable time-stepping algorithm, a maximum time step of 0.01 s was set.

Each run required over a week of continuous computation time. Fortunately, the runs were able to proceed without time sharing on Sweetgum, the Silicon Graphics, Inc., Origin 2000 64-processor supercomputer operated by the Mississippi Center for Supercomputing Research (MCSR), located on the UM campus. The project generated over 200 GBytes of output data files, nearly filling up the available permanent storage on the machine. The run was broken into phases called RESTART's, each generating a portion of the time history results, so that data could be post-processed in ABAQUS Post, using files of more manageable size. Once post-processed, the original RESTART files had to be deleted to make space available for other runs. Unfortunately, the deletion of these files makes impossible the retrieval at a later date of any other data from the runs without re-running the entire job.

The data that was post-processed and stored, and is therefore retrievable, includes:

1. Acceleration and displacement time histories at key points selected along the longitudinal centerline of the bridge (between Phase I and Phase II)
2. Moment-curvature hysteresis at the integration points in the plastic hinge regions nearest the top or bottom of each column and in the piles nearest the abutment cap beam
3. Moment contour plots for the bent elements at times of peak response
4. Stress contour plots beneath the footings at times of peak response

To enable a profile of amplification with increasing elevation, the following points were selected for post-processing of acceleration and displacement time histories:

1. Top of Soil Layer 4 (base of gravel layer) at center of model
2. Top of Soil Layer 3 (top of gravel level) at center of model
3. Footing of north column of each Phase I bent
4. Top of column of each Phase I bent
5. Deck at Bent 3
6. Abutments

Damage Measures

A measure of damage which characterizes the intensity of maximum inertial forces developed at key points is the peak response acceleration, which may also be expressed in terms of the amplification with respect to the corresponding peak of the input motion.

Figure 6.7 shows the horizontal acceleration component time histories at three of the key points listed above to give an indication of the effects of the wave propagation upward from the base. The vertical acceleration time histories are not shown, representing damage potential mostly for the deck which is not the primary concern here. The peak horizontal accelerations visible in these time histories are summarized in Table 6.4. For reference, peak vertical accelerations are also listed.

Table 6.4 Peak Accelerations (% g) Computed at Key Points on the Level 3 Model

M	1-Axis			2-Axis			3-Axis		
	Footing	Top of Column	Deck	Footing	Top of Column	Deck	Footing	Top of Column	Deck
6	12.8	17.4	24.8	30.5	44.1	54.3	16.1	15.8	56.3
7	49.9	38.1	59.6	53.6	125	109	55.7	53.6	157
8	38.7	66.7	85.4	72.9	187	127	112	94.3	370

It is the experience of the PI that peak acceleration, while generally correlated with damage, is a poor predictor of specific damage that might occur. For the objectives stated for the project in Section 2, focus has been placed on damage measures that are indicative of consequences of the damage in terms of a spectrum of needs, including:

1. Costly repair of members (e.g. flexure or shear cracking of concrete in the plastic hinge zone)
2. Loss of operability (e. g. by damage to abutment soil material on the embankment preventing access)
3. Complete bridge replacement (e.g. by severe damage distributed throughout the bents)
4. Life safety (e.g formation of a bent collapse mechanism)

The moment-curvature response in the plastic hinge locations of columns and piles has been selected as the best measure of assessing vulnerabilities for the bridge with respect to the above consequences. In particular, the achievement of key damage states in the critical sections provides a rational basis for distinguishing these vulnerabilities. Unlike the case in the Level 1 analysis, the loading is dynamic and cyclic, so the occurrence of the section damage must be viewed in terms of the cyclic loading as represented by the moment-curvature hysteresis rather than the simple backbone curve under monotonic increasing loading.

Figure 6.8 shows the simulated hysteresis curves for the column section nearest the bottom of the north column of the Phase I bridge. Results are plotted at each bent for each intensity level. The axis label refers not to the local bending axis (e.g., see Figure 4.2), but rather the implied motion in the direction of the listed global axis. This has been done to emphasize the relative importance of each input component motion, which in this

case is dominated by the north (transverse or global 2-axis) component.

The hysteresis plots are dimensionless, with both moment and curvature normalized by the appropriate yield moment or yield curvature for the section (see Table 4.1). It is at the yield key point that ductile response and energy absorption becomes significant. The ability of the connections to maintain integrity beyond this level that is most important in moderate to severe intensities. Such integrity has been assumed available until either a collapse mechanism (flexure) or shear failure occurs as predicted in the Level 1 analysis.

Figure 6.8 indicates that, for the time histories considered (Figure 6.6), the Level 3 analysis predicts that, in the bottom plastic hinge region of the reference column of each interior bent:

1. For $M=6$, the peak bending moment exceeds the cracking moment in the strong direction (global 2-axis), whereas no cracking (linear) response appears to develop in the weak direction (global 1-axis).
2. For $M=7$, the peak bending moment exceeds the yield moment in the strong direction (global 2-axis) but the curvature does not exceed the yield curvature (ductility ratio, $\mu < 1$). No cracking (linear) response appears to develop in the weak direction (global 1-axis), however.
3. For $M=8$, the peak bending moment exceeds the yield moment in the strong direction (global 2-axis) and a curvature ductility ratio, $\mu = 2.6$, is achieved when the computation failed to converge. Despite this, no cracking appears to develop in the weak direction (global 1-axis).

Figure 6.9 indicates that, for the time histories considered (Figure 6.6), the Level 3 analysis predicts that, in the top section of the abutment piles:

1. For $M=6$, no cracking is observed in either direction.
2. For $M=7$, the peak moment approaches the yield moment for the bending axis associated with motion in the longitudinal direction (global 1-axis), and cracking occurs in the transverse direction (global 2-axis).
3. For $M=8$, the peak moment exceeds the yield moment for the bending axis for

associated with motion in the longitudinal direction (global 1-axis), and a curvature ductility ratio, $\mu = 2.2$, is achieved when the computation failed to converge. Cracking occurs in the transverse direction (global 2-axis) and a curvature ductility ratio, $\mu = 1.2$, is achieved when the computation failed to converge.

The NEHRP recommended provisions for buildings (FEMA 302, 1997) recognize story drift as a distinct design criterion in recognition of the relationship of this measure of structural performance to damage levels in the columns. Previous work under the direction of the PI (Gopalakrishnan, 1999, and Mullen and Swann, 2001) has shown that the critical values of the analogous measure, drift ratio, may be different for highway bridge piers than those prescribed in the building codes. The Level 1 analysis provides the basis for establishing the relationship between drift ration and column damage.

Figure 4.1 shows that, for these columns, the standard allowable value of 0.01 for critical buildings is in fact a measure of severe damage for the bents. After this value, very little additional load capacity is achievable without significant deformation, which the actual system may not in fact be capable of delivering in a ductile fashion. Near the value of 0.005, however, first yield in at least one plastic hinge location is expected assuming the loading is monotonic.

Figure 6.10 shows the computed drift ratio time histories for Bent 3 for the three intensity levels, $M = 6, 7, 8$. The peak values for this bent indicate that, in comparison to the drift ratio values corresponding to critical damage states under monotonic loading (Figure 4.1):

1. For $M=6$, the 1st cracking level has just been exceeded.
2. For $M=7$, the 1st yield level has not been exceeded.
3. For $M=8$, the 1st yield level is approached.

While the observation for the $M=6$ case is consistent with the moment-curvature analysis (Figure 6.8), the observations for the more severe intensity cases are not. Clearly, one must allow for a difference in relative displacement-related damage response behavior

when comparing monotonic loading of an isolated bent whose base is fixed (Level 1 model) and cyclic loading of the full system with soil-structure interaction (Level 3 model).

The final damage measure to be considered in the vulnerability assessment is the peak shear in the column base. In this analysis, the shear force is not a direct output from the ABAQUS computation. In order to estimate this, lateral inertial and damping forces in the column itself are neglected, and the shear is computed as the difference in the top and bottom moments divided by the vertical distance between the two sections.

Figure 6.11 shows the estimated transverse shear time histories at the base of a select column in Bent 3. The column base shear force has been normalized with respect to half of the computed collapse bent (2 columns) flexure capacity, $V_u = 1926$ k, predicted for the Level 1 model. The peak values for this bent indicate that, in comparison to the load values corresponding to critical damage states under monotonic loading (Figure 4.1):

1. For $M=6$, a shear force 3 times greater than the 1st cracking force is experienced.
2. For $M=7$, a shear force 60 percent greater than the 1st yield force is experienced.
3. For $M=8$, a shear force 6 percent greater than the collapse force is experienced.

7. SUMMARY AND CONCLUSIONS

The existing concrete bridge that carries traffic on Goodman Road, Mississippi state highway, MS-302, over the interstate highway, I-55, has been given a detailed structural integrity evaluation to assess vulnerability of the substructure elements to damage caused by ground motions expected during a future earthquake with epicenter on the southern end of the New Madrid fault system.

To provide a rational basis for the assessment, engineering principles and software have been used to develop a number of predictive models for the response of the bridge to events generated using available geological techniques and software. Three levels of increasing model complexity have been selected to give a range of perceptions as to the expected performance.

The Level 1 model considers the nonlinear moment versus curvature response of typical beam, column, and pile sections and the resulting nonlinear force versus displacement of a typical fixed base bent substructure under pseudo-static lateral loading at the bearing positions as might be associated with an inertial force induced in the massive deck by accelerations at the fixed base. The predicted response of the sections provides critical damage states that can be related through the fiber model on which they are based to material damage conditions, specifically, cracking in the concrete and yielding of the steel reinforcement. The predicted response of the fixed base bent under static monotonic loading provides the basis for estimating the ultimate collapse load and the corresponding base shear of the bent substructure as a whole and for relating intermediate load values with critical section and material damage states. Critical damage states for the Level 1 model provide a useful basis for comparison with the predictions from the higher level dynamic analyses.

The Level 2 model considers the linear dynamic characteristics of the fixed base structural system including the entire deck and all five bents and the response computed using a multimode response spectrum (frequency domain) approach, which represents current conventional design practice. The linear dynamic characteristics are consistent

with the performance during ambient traffic, and a field vibration test was performed to establish the ability of the model to adequately predict these characteristics. Site specific input motions are required for the response spectrum analysis. Once the available software and soil data are obtained, this step is completed with relatively little computational expense. It is useful, therefore, to perform sensitivity analyses of the effects of random variations of the input motion on the predicted response both in the soil column and in the structure. In this study, ten input motions have been simulated at three intensity levels to obtain mean and variance statistics for key response parameters.

The Level 3 model considers the nonlinear dynamic response computed using a direct integration simulation (time domain) approach, the preferred method in many research investigations. In the latter model, the influence of the soil behavior on the damage in the substructures may be included. Unlike the Level 2 model, the analysis provides a complete picture of the nonlinear, dynamic response including relative displacement (drift), acceleration, moment, and shear time histories as well as moment versus curvature hysteresis curves for any select location in the model. For reference, peak values of the response may be compared with the critical states predicted in the Level 1 analysis as well as corresponding predictions from the Level 2 analysis.

A performance-based approach to vulnerability assessment has been considered, whereby target acceptance criteria for damage response are allowed to vary with intensity of the seismic event. Three intensity levels, $M=6, 7,$ and $8,$ have been considered covering moderate to severe damage cases. The target criteria used in this evaluation have been chosen based on three critical material damage states under flexure, having verified that flexure governs over shear failure in the columns:

1. 1st cracking of the concrete outer fibers under tensile stresses induced during bending
2. 1st yielding of the longitudinal steel reinforcement under tensile stresses induced during bending, which usually is followed soon after by crushing of the concrete under compressive stresses on the opposite face
3. Collapse of the bent substructure or pile as indicated by plastic hinge formation in

sufficient locations to cause global instability and evidence of large deformations that may place high demands on the connection as well as the sections, which may not have sufficient detailing to maintain structural integrity

The Level 1 section analysis results are summarized in Table 4.1 and the bent analysis results are plotted in Figure 4.1.

The Level 2 linear fixed base dynamic characteristics are summarized in Table 5.1 and Figure 5.2. Corresponding data from the field vibration test are summarized in Table 5.2 and Figure 5.9. Conditions of the test are presented in Figures 5.3 through 5.8. Site specific responses of the soil column and Level 2 model are summarized in Tables 5.5 and 5.6, respectively. Statistics of the input motions and responses are summarized in Table 5.7.

The Level 3 linear dynamic characteristics accounting for the more realistic soil and foundation conditions are summarized in Table 6.2 and Figure 6.5. Peak accelerations at different elevations are summarized in Table 6.4. Acceleration time histories are shown in Figure 6.7. These are supplemented by section hysteresis curves in Figures 6.8 and 6.9, drift ratio time histories in Figure 6.10, and transverse shear time histories in Figure 6.11.

Specific observations of performance at each intensity level are summarized at the end of Sections 4, 5, and 6, for Levels 1, 2, and 3, respectively. From these observations, the following overall conclusions are drawn:

1. The flexure capacity of the bent substructures governs over the shear capacity, and the flexure capacity computed by nonlinear static analysis procedures, which accounts for distributed plasticity, is 24 percent less than that estimated by conventional plastic methods of analysis, implying that the latter is significantly unconservative and will lead to corresponding errors if used in design.
2. For $M=6$, the performance of the substructures is considered just unacceptable based on either Level 2 or Level 3 analysis, indicating a slight vulnerability for

this level.

3. For $M=7$, the performance of the substructures is considered acceptable based on the Level 2 deterministic analysis but possibly only marginally acceptable based on the analysis of variability of results. The Level 3 deterministic analysis, however, predicts that the performance is unacceptable in the bent substructures in the transverse direction of the bridge, despite the relatively large column section dimensions in that direction. The piles appear to perform adequately based on either analysis.
4. For $M=8$, the performance of both the bent and pile substructures is unacceptable, depending on the ability of the plastic zone regions and connections to provide considerable ductility under cyclic loading conditions without collapse, based on the Level 3 deterministic analysis. The Level 2 analysis does not provide data on the collapse limit state which is governed by displacement ductility rather than simple formation of plastic hinges and a collapse mechanism.

8. RECOMMENDATIONS

It is recommended that the multi-level approach adopted in this study be further pursued based on the relative benefits and limitations of each level, as indicated by the results of this study. Specifically:

1. The Level 1 analysis provides data which gives a quick but accurate estimate of basic capacities of the key structural components under static monotonic loading, which may in fact be poorly estimated by hand calculations and which require very expensive tests to establish experimentally. The nonlinear section and substructure analyses provide important data needed for identification of intermediate limit states needed in performance-based design. Specific models useful to MDOT Bridge Division for preliminary design, final design, and future evaluations could be developed by the PI, and training for such analysis could be provided the PI to MDOT personnel, with little investment in time or computer resources.
2. The Level 2 analysis provides a reasonable estimate of the natural frequencies and mode shapes of the system, which are useful for guiding field vibration tests. The ease of computation makes it best suited to quick assessment of alternative designs and of the effect of random variations in the loading. The modeling procedure has too many deficiencies in its treatment of input seismic loading, damage response, and incorporation of foundation details, however. Prediction of performance is, therefore, not recommended using this procedure.
3. Field vibration testing compatible with the Level 2 analysis provides the only confirmation of the validity of the 3D predictive models. The attempt in this study was exploratory in nature and achieved good results for a limited number of modes relative to the damage assessment. The benefits of such testing have not been fully explored and are potentially unbounded. It is clear from this first trial, however, that immediate improvements in the system identification process may be obtained by using a more comprehensive accelerometer array. The speed and automation of the process would be greatly enhanced by the use of:

- a) permanently mounted or embedded sensors
- b) permanently embedded mounts (e.g. metal plates) for sensors to expedite field installation of a temporary array of sensors, at sufficient locations to enable characterization of the responses of interest using a variety of small arrays.

The nature and cost of implementing such measures should be coordinated with other projects currently being undertaken by the USGS and FHWA Turner-Fairbanks Research Center. The PI is well positioned to coordinate or act as liaison for such interactions.

4. The Level 3 analysis provides the best estimate of performance and is the only one of the three suitable for a reliable performance-based assessment. It is currently, however, computationally intensive. The procedures for modeling nonlinear soil response and foundation interfaces requires further validation which the ambient field vibration tests cannot provide because of the low level of loading. Tests at higher loading levels are recommended to aid in this validation process, but these tests will generally require lane closure. Advantage should be taken of testing that may be performed on bridge structures that are scheduled for maintenance, repair, or decommissioning.

The performance-based approach adopted in this study has been premised on damage limit states that relate to material, section, and substructure response characteristics having a basis in engineering analysis. The selection of appropriate limit states has been made on the presumption of a reasonable correlation with operational considerations. The latter is ultimately the responsibility of the owners with due consideration of many factors not considered in this analysis. It is, therefore, recommended that MDOT invest in appropriate research, testing, and operations review to improve these correlations and establish its own position on their relevance to MDOT facilities. Building design codes have already made the initial move toward performance-based design and many practitioners have already begun adoption of a version of this called displacement-based design.

The simulated responses computed using the Level 3 model indicate that vulnerabilities exist for the bridge substructures considered in the study with respect to the selected target limit states at each intensity level examined. In summary:

1. The columns of the interior bents appear marginally vulnerable to cracking during an M=6 event. The piles of the end bents do not appear to have such vulnerability, however.
2. The columns of the interior bents appear moderately vulnerable to yielding and the piles moderately vulnerable to yielding during M=7 and M=8 events.
3. The columns and piles appear severely vulnerable to yielding, and if large ductility ratios are not sustainable with the existing connection details, collapse of the interior bents and possible inoperability of the abutments.

Before committing the significant investment needed to address these vulnerabilities, it is recommended that MDOT examine a number of bridge substructures in other facilities that have a similar hazard exposure. This will enable MDOT to further implement the procedures used in this study to a variety of situations, from which some further perspective might be obtained. It will also enable a more comprehensive plan to be developed to address the vulnerabilities along a number of important corridors which will serve as lifelines for north Mississippi in the event of a moderate to severe earthquake event.

REFERENCES CITED

- “AASHTO LRFD bridge design specifications,” 1st edition, American Association of State Highway and Transportation Officials, 1994.
- DSP Technology, Inc., “SigLab version 3.0 user guide,” Fremont, CA, 1998.
- EduPro Civil Systems, Inc., “ProShake- ground response analysis program, version 1.1 users manual,” Redmond, Washington.
- Gopalakrishnan, J., “Analysis of seismic vulnerability and comparison of retrofit options for a skewed bridge on the University of Mississippi campus,” masters thesis submitted in partial fulfillment of the degree Master of Science in Engineering Science, Department of Civil Engineering, University of Mississippi, 1999.
- Hibbitt, Karlsson and Sorensen, “ABAQUS/Standard users manual- version 5.8,” Providence, Rhode Island, 1998.

- Hwang, H. H. M., and Lee, C. S., "Site-specific response spectra for Memphis Sheahan pumping station," Center for Earthquake Research and Information, Memphis State University, *Technical Report NCEER-90-0007*, May, 1990.
- Hwang, H., Pezeshk, S., Lin, Y.-W., He, J., and Chiu, J.-M., "Generation of synthetic ground motion," Center for Earthquake Research and Information and Department of Civil Engineering, University of Memphis, *Technical Report MAEC Project No. RR-2*, May, 1999 (draft).
- Ismail, I. M. K., and Mullen, C. L., "Computational simulation procedure for soil structure interaction modeling in building seismic damage response," 4th International Conference on Recent Advances in Geotechnical Earthquake Engineering and Soil Dynamics, San Diego, CA, March 26-31, 2001
- LeBlanc, B., "Seismic evaluation of an existing RC highway bridge substructure using three-dimensional computational simulations and modal analysis of ambient vibration data," masters thesis submitted in partial fulfillment of the degree Master of Science in Engineering Science, Department of Civil Engineering, University of Mississippi, August, 2001.
- Leblanc, B., and Mullen, C., "Characterization of abutment-deck interaction using 3D FEM and field vibration measurements for an existing highway bridge in north Mississippi," 2nd International Symposium on Maintenance and Rehabilitation of Pavements and Technological Control, Auburn, AL, July 29-August 1, 2001
- Mullen, C., and Cakmak, A., "NCEER/FHWA Highway Project 106 Tasks E-7.1.1 and E-7.1.2: Vulnerability assessment- structure fragility," Final Report to Federal Highway Administration, Department of Civil Engineering and Operations Research, Princeton University, *Technical Report NCEER-97-0017*, December, 1997.
- Mullen, C., Hackett, R., and Swann, C., "Structural seismic vulnerability evaluation of Baptist Memorial Hospital-Desoto," Final Report to Central United States Earthquake Consortium, Department of Civil Engineering and Mississippi Mineral Resources Institute, University of Mississippi, November, 1997.
- Mullen, C., and Swann, C., "Seismic response interaction between subsurface geology and selected facilities at the University of Mississippi," *Engineering Geology*, **62** (1-3), 2001, 223-250.
- Mullen, C., Tuladhar, P., "Performance-based evaluation of bridge substructure in north Mississippi using nonlinear FEM and field vibration measurements" ASME International Mechanical Engineering Congress and Exposition (IMECE 2000), Orlando, FL, November 9, 2000
- Mullen, C. L., Tuladhar, P., Leblanc, B., and Shrestha, S.
 "3D seismic damage simulations for an existing bridge substructure using nonlinear FEM calibrated with modal NDT," Structural Engineering, Mechanics, and Computation (SEMC 2001), Cape Town, South Africa, April 2-4, 2001
- "NEHRP guidelines for the seismic rehabilitation of buildings," *FEMA Publication 273*, Federal Emergency Management Agency, October, 1997.
- "NEHRP recommended provisions for seismic regulations for new buildings and other structure," *FEMA 302*, Federal Emergency Management Agency, 1997.
- PCB Piezotronics, Inc., "General operating guide for use with piezoelectric ICP accelerometers."
- Press, W. H., Teukolsky, S. A., Vetterling, W. T., and Flannery, B. P., *Numerical recipes in Fortran: The art of scientific computing*, and companion, "Example book [Fortran]," 2nd edition, Cambridge University Press, 1992.

Seible, F., Priestley, N., and Innamorato, D., "Earthquake retrofit of bridge columns with continuous carbon fiber jackets-Volume II, Design guidelines," *Report No. ACTT-95/08*, Structural Engineering Department, University of California-San Diego, August, 1995.

"Seismic vulnerability work assignment," Master Agreement: Research and Technology Development, Project No. SP-9999-00(027) 101411/011000 [79-9999-00-027-11 PE], Bridge Division, Mississippi Department of Transportation, August 16, 1999.

Spectral Dynamics, Inc., "STAR System users guide," San Jose, CA, November, 1994.

"Standard specifications for highway bridges," 16th edition, American Association of State Highway and Transportation Officials, 1996.

Stewart, R. K., "Soil effects on earthquake ground motions at the University of Mississippi- a preliminary analysis," masters thesis submitted in partial fulfillment of the degree Master of Science in Engineering Science, Department of Geology and Geological Engineering, University of Mississippi, 1996.

Swann, C., Mullen, C., Hackett, R., Stewart, R., and Lutken, C., "Evaluation of earthquake effects on selected structures and utilities at the University of Mississippi: A mitigation model for universities," Final Report to Mississippi Emergency Management Agency, October, 1999

Tuladhar, P., "Performance based seismic evaluation of an existing reinforced concrete highway bridge lifeline," masters thesis submitted in partial fulfillment of the degree Master of Science in Engineering Science, Department of Civil Engineering, University of Mississippi, 2000.

Vibrant Technology, Inc., "ME'scopeVES operating manual-version 3.0," September, 2001.

Wallace, J. W., "BIAX: A computer program for the analysis of reinforced concrete and reinforced masonry sections", *Report No. CU/CEE-92/4*, Department of Civil Engineering, Clarkson University, February, 1992.

Webb, D., "Soil & Foundation Report," *Report No. 87-17-7*, Soil Mechanics Division, Mississippi State Highway Department, 1987.



a. View from the south-looking toward Memphis



b. View from the north-looking toward Hernando

Figure 1.1 Bridge selected for vulnerability study



a. View from the west embankment-looking east



c. Top of deck showing gap at median-looking east



b. Deck system showing girder seating at abutment



d. Intermediate piers showing median gap-looking east

Figure 1.1 (cont'd) Bridge selected for vulnerability study- detail views

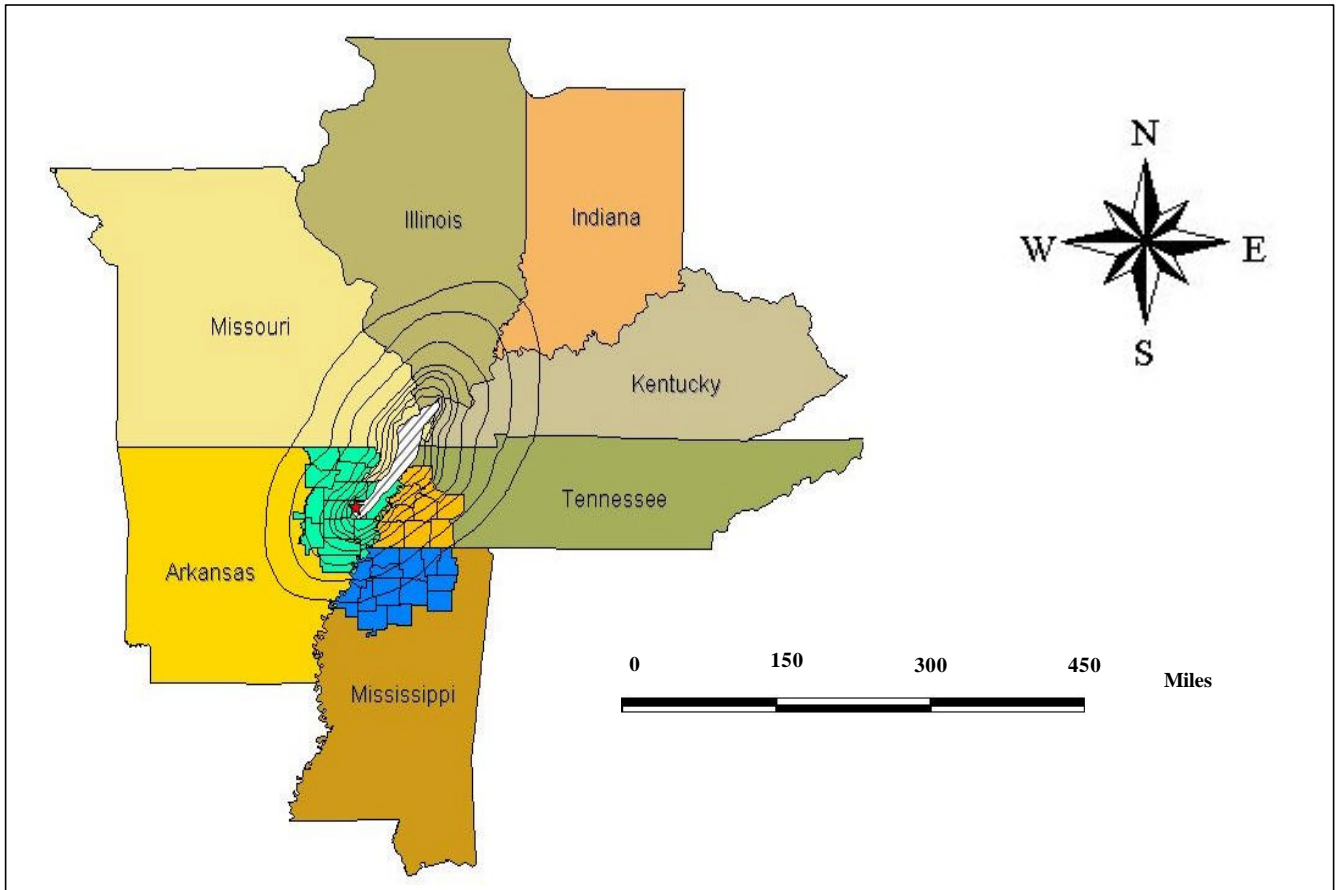


Figure 1.2 Seismic hazard exposure in north Mississippi- CUSEC states

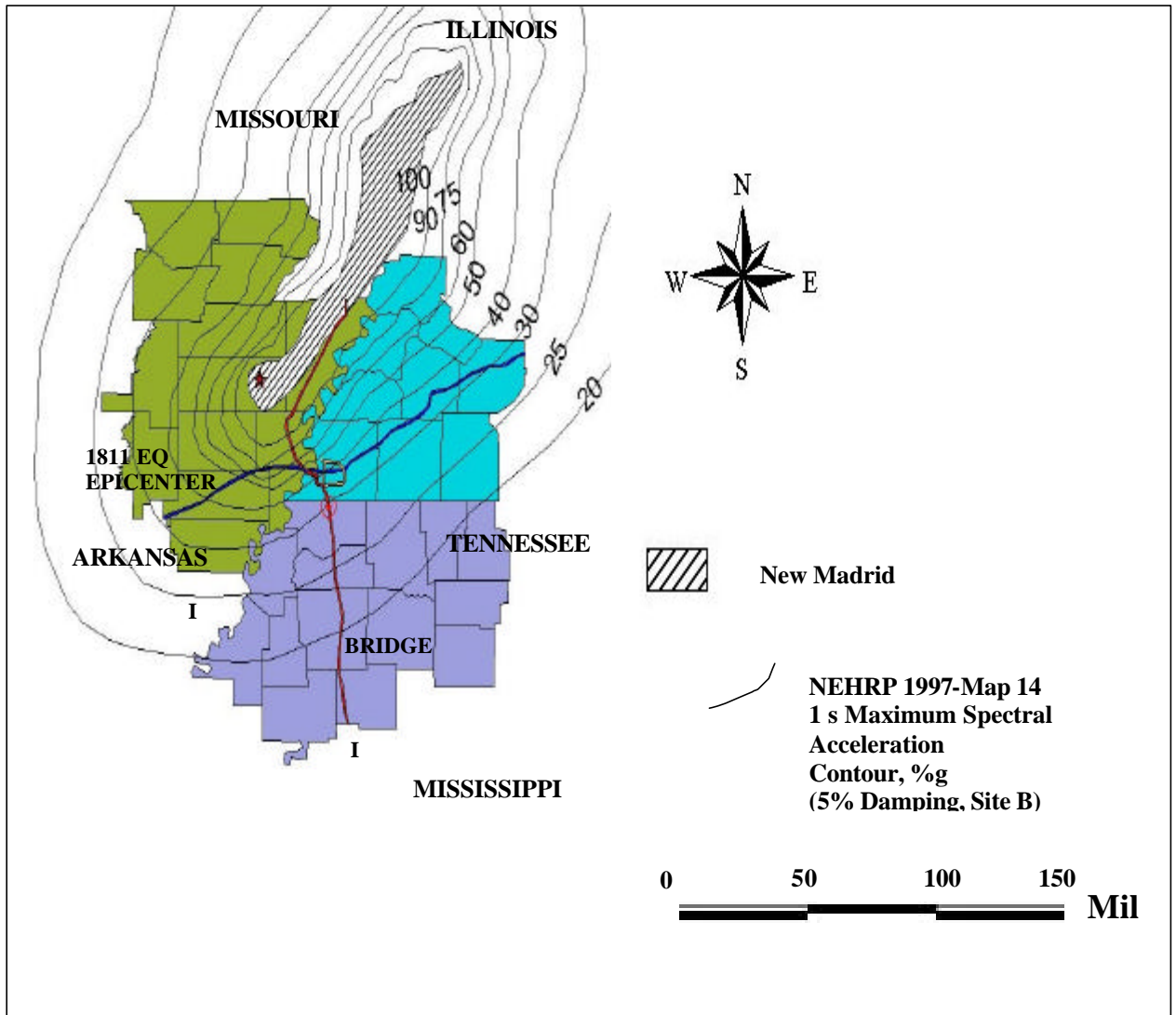


Figure 1.2 (cont'd) Seismic hazard exposure in north Mississippi- interstate highway lifelines

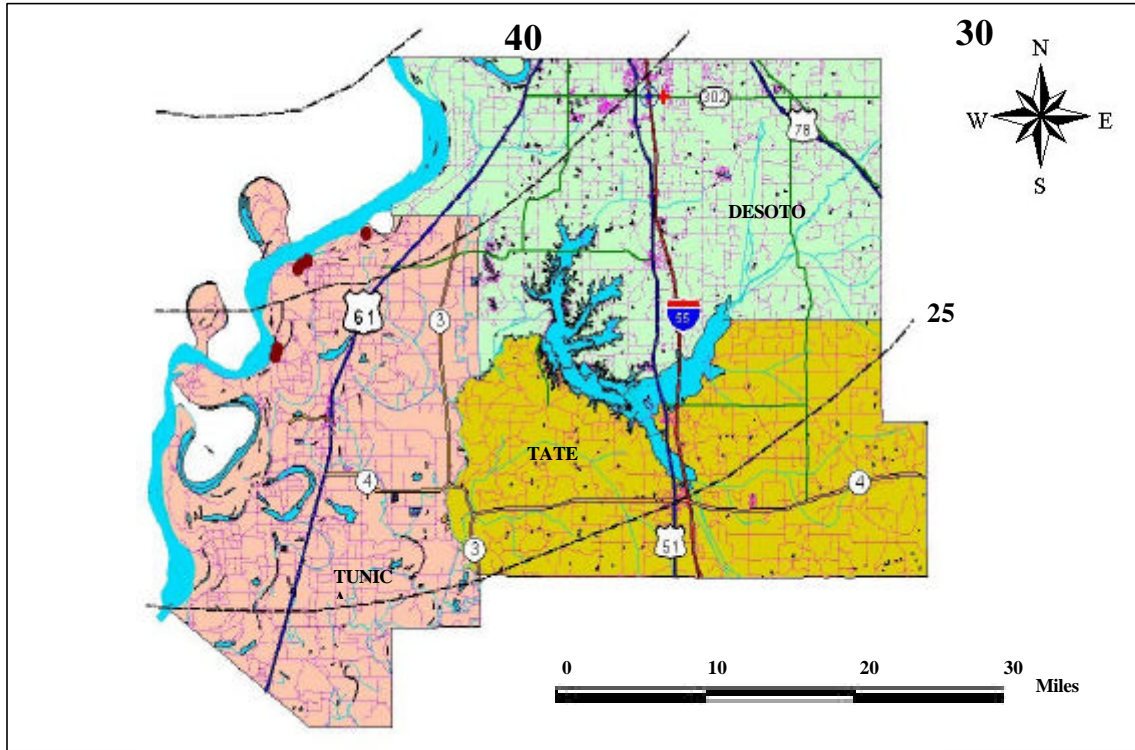
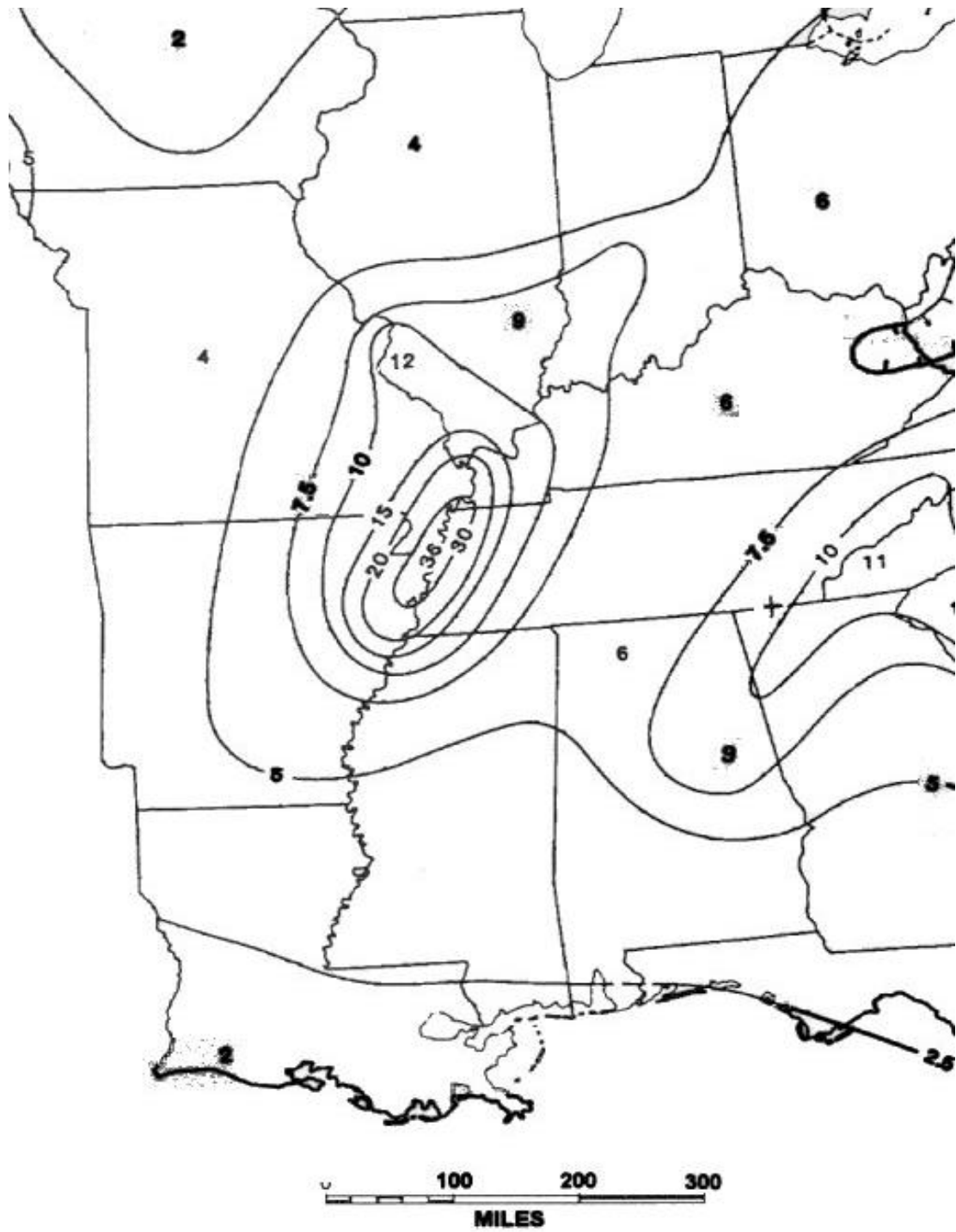


Figure 1.2 (cont'd) Seismic hazard exposure in north Mississippi- state highway lifelines

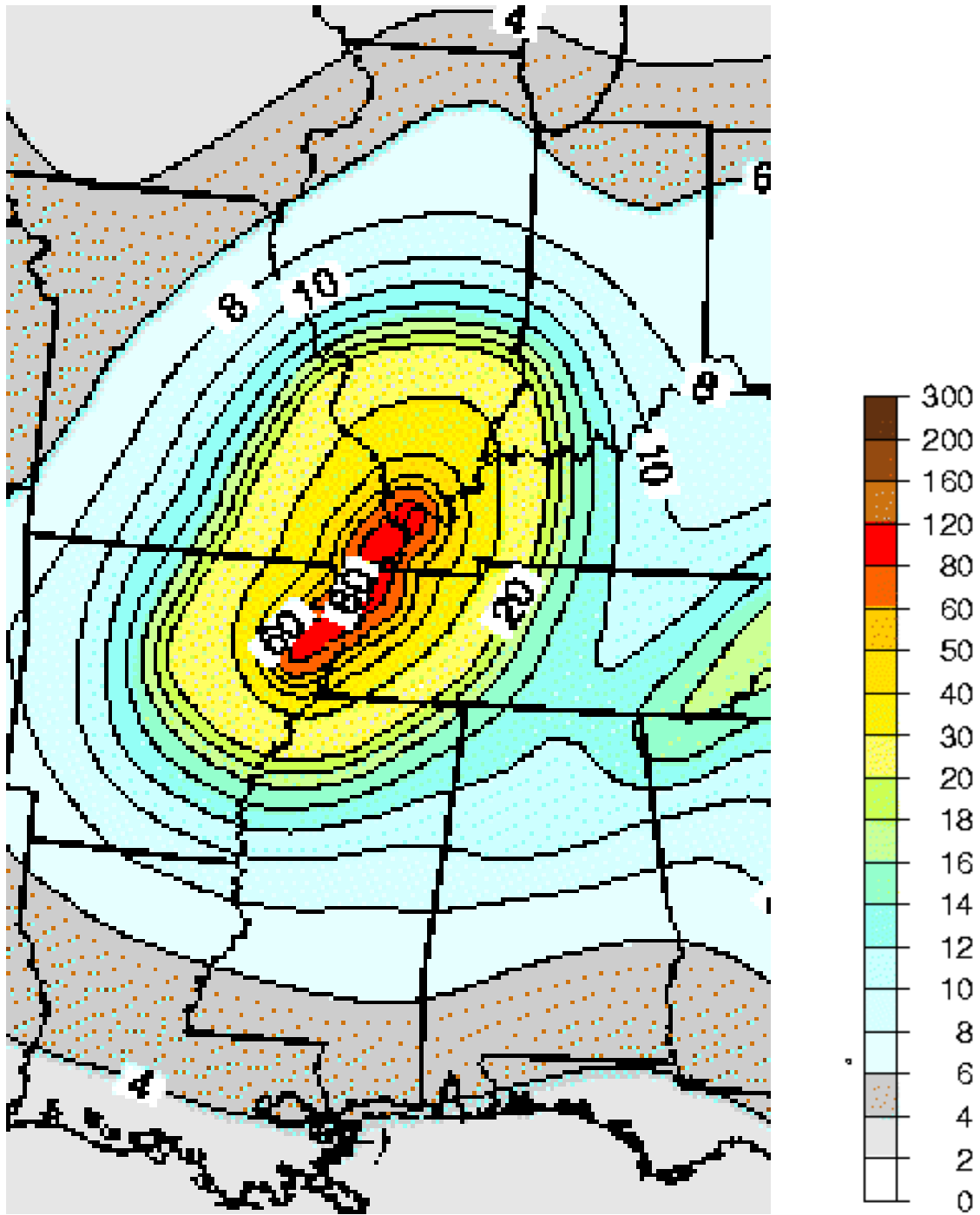


Figure 1.3 Highway system in north Mississippi- Memphis and environs



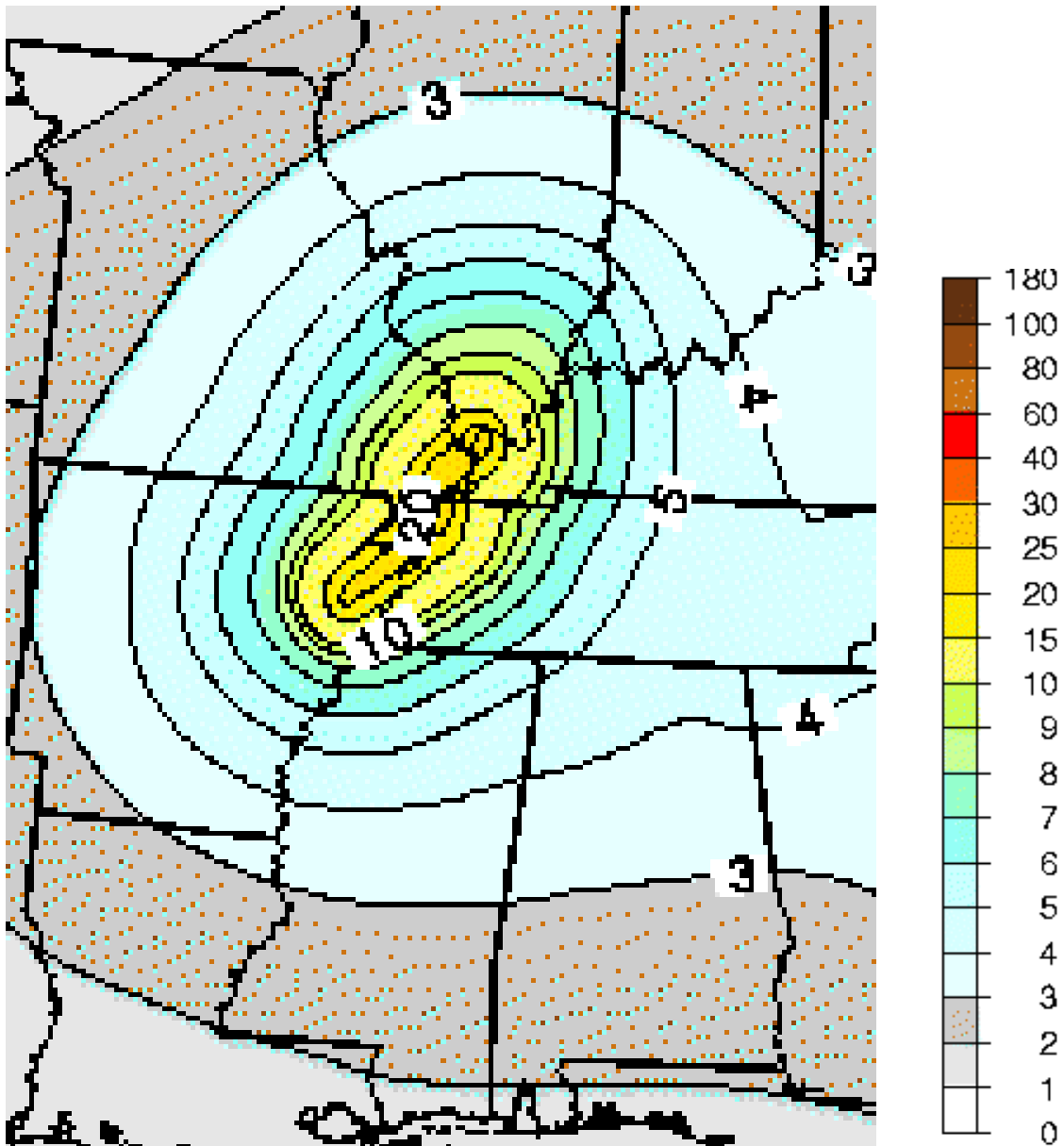
Prepared by the U.S. Geological Survey for the 1988 edition of NEHRP Recommended Provisions for the Development of Seismic Regulations for New Buildings

Figure 1.4 USGS acceleration coefficient contours (AASHTO LRFD, 1994)



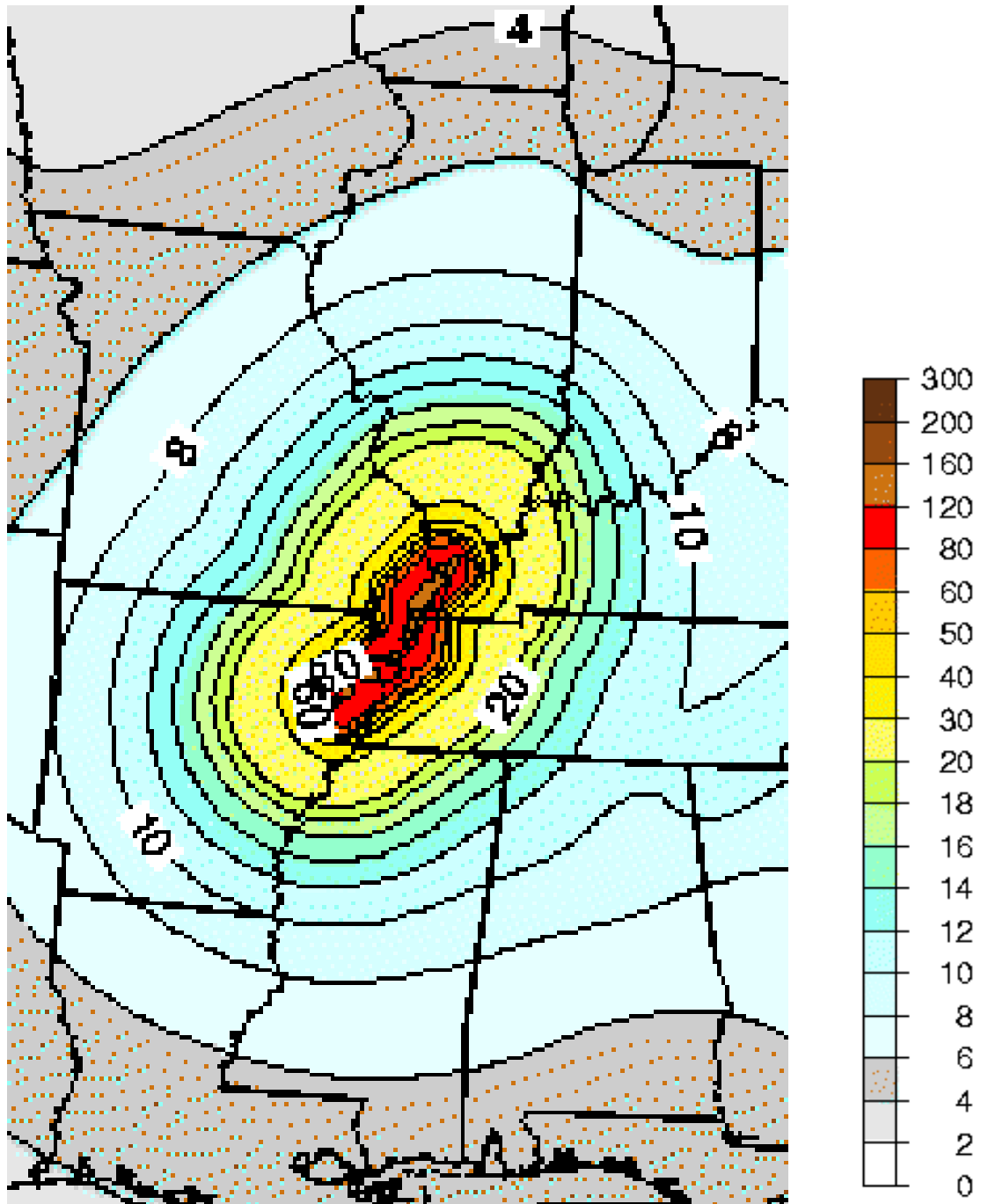
**0.2 sec SA (%g) with 10% Probability of Exceedance in 50 Years
Draft USGS Map, Jan. 2002**

Figure 1.5 Proposed USGS hazard maps: 0.2 s, 10% in 50 yr



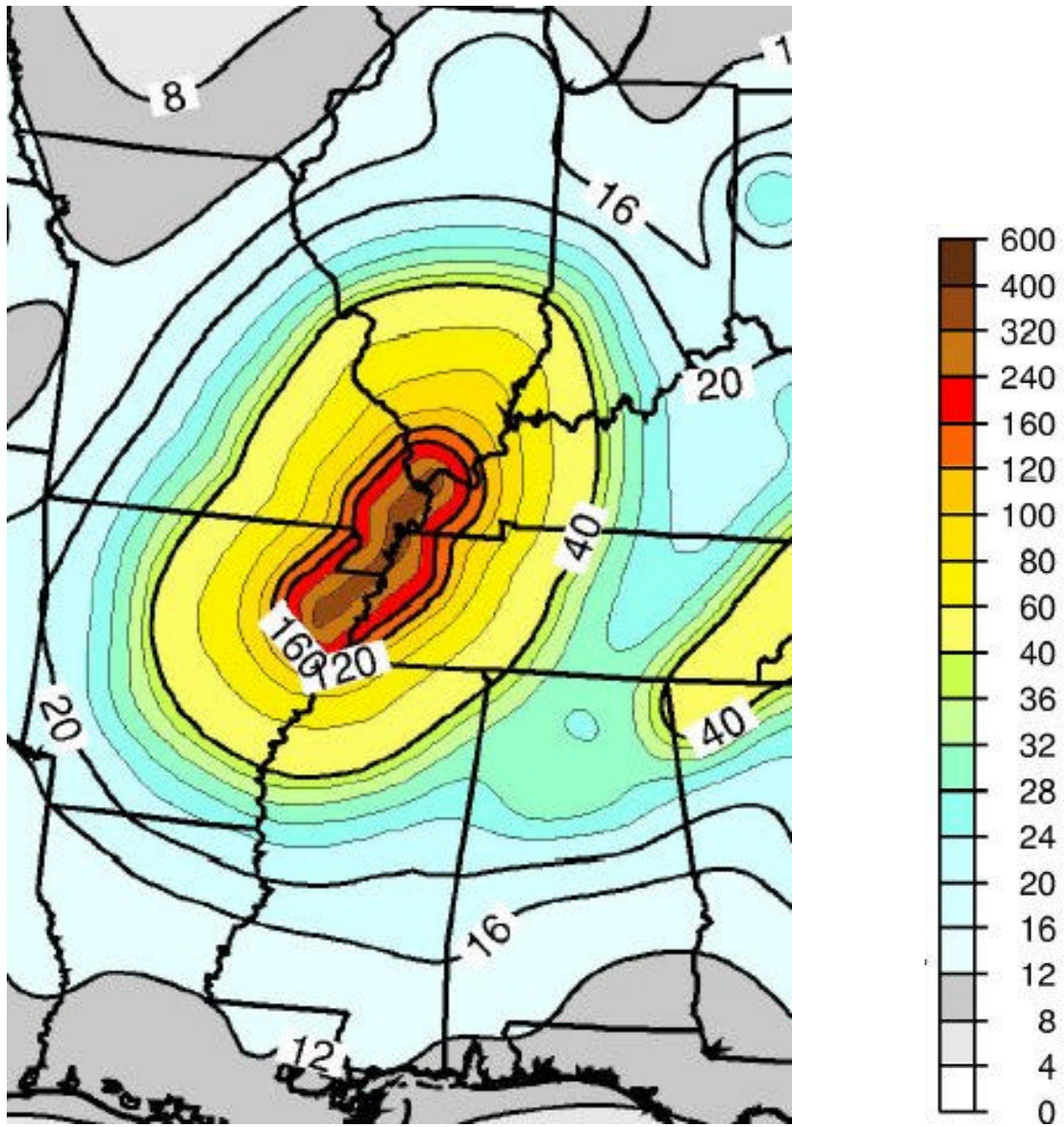
**1.0 sec SA (%g) with 10% Probability of Exceedance in 50 Years
Draft USGS Map, Jan. 2002**

Figure 1.5 (cont'd) Proposed USGS hazard maps: 1.0 s, 10% in 50 yr



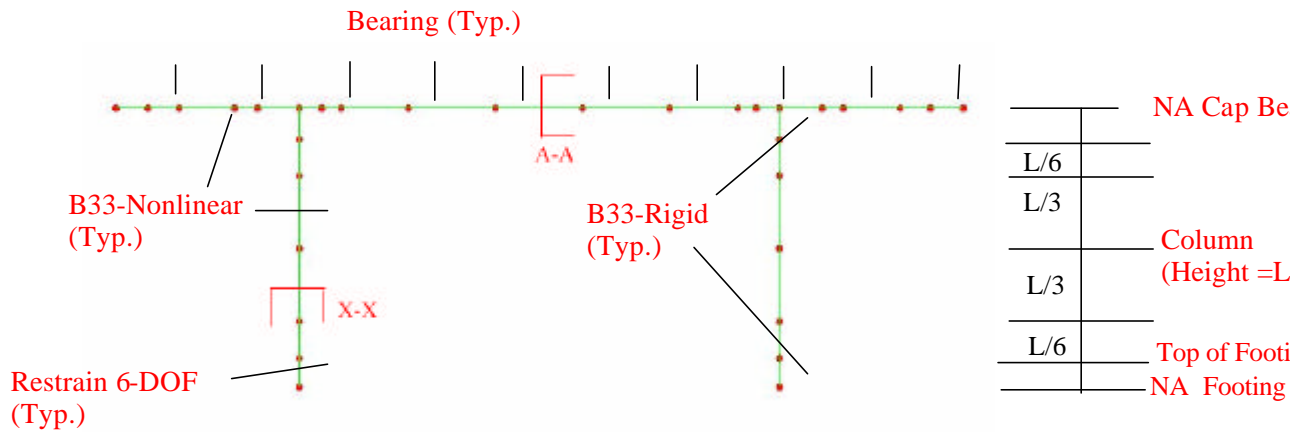
**1.0 sec SA (%g) with 2% Probability of Exceedance in 50 Years
Draft USGS Map, Jan. 2002**

Figure 1.5 (cont'd) Proposed USGS hazard maps: 1.0 s, 2 % in 50 yr

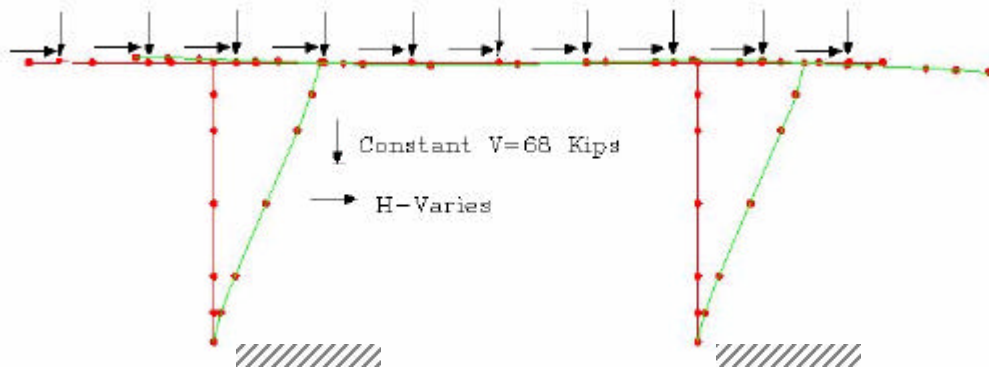


**0.2 sec SA (%g) with 2% Probability of Exceedance in 50 Years
Draft USGS Map, Jan. 2002**

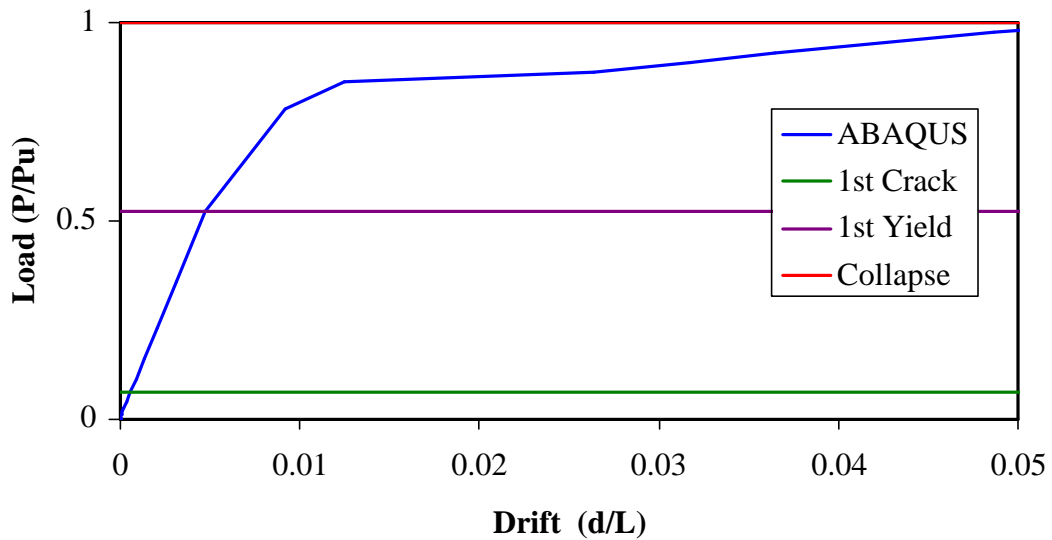
Figure 1.5 (cont'd) Proposed USGS hazard maps: 0.2 s, 2% in 50 yr



a. ABAQUS 2D Level 1 model

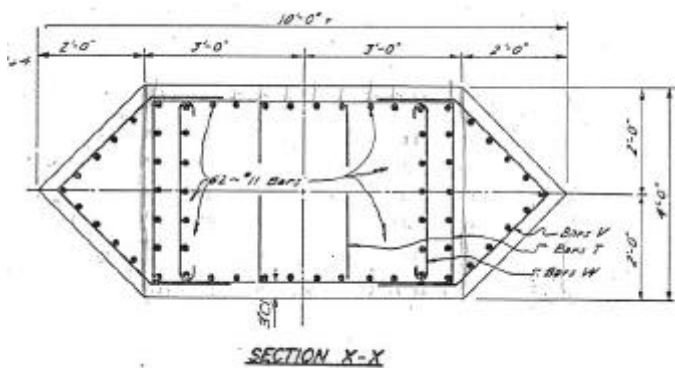


b. Load case and deformed shape

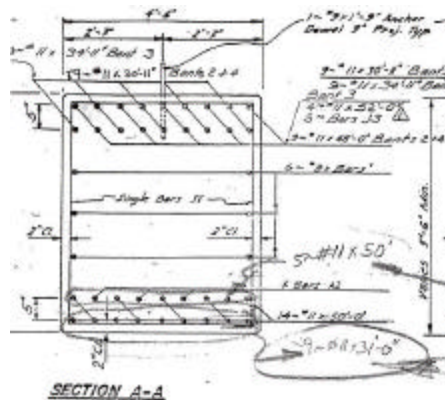


c. Force-deformation response curve

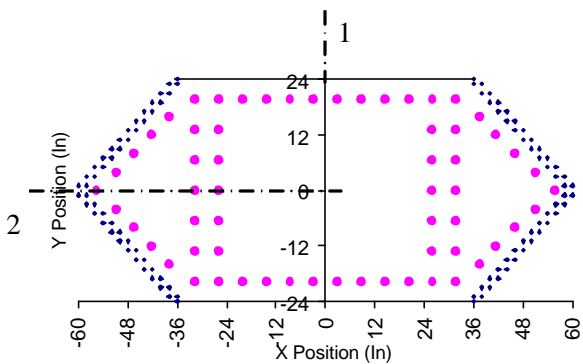
Figure 4.1 Bent substructure stiffness degradation and capacity estimate



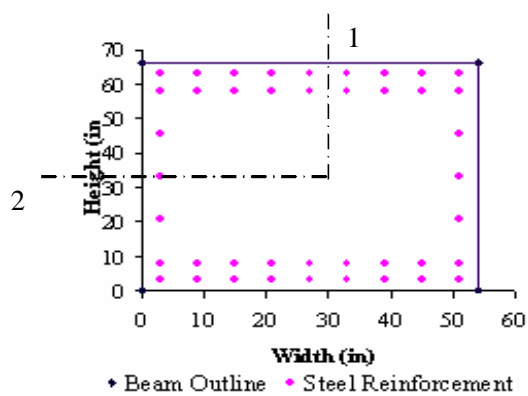
a. Column as-built drawing



b. Beam as-built drawing

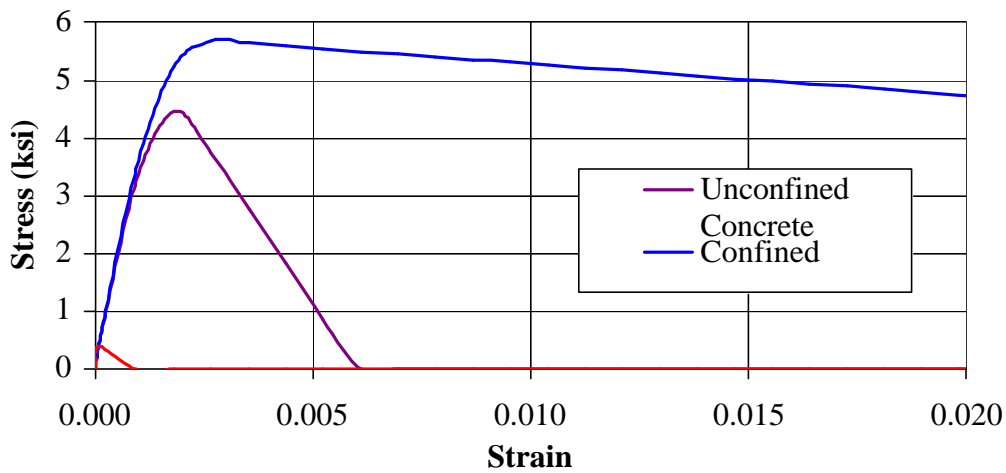


c. Column BIAx fiber model

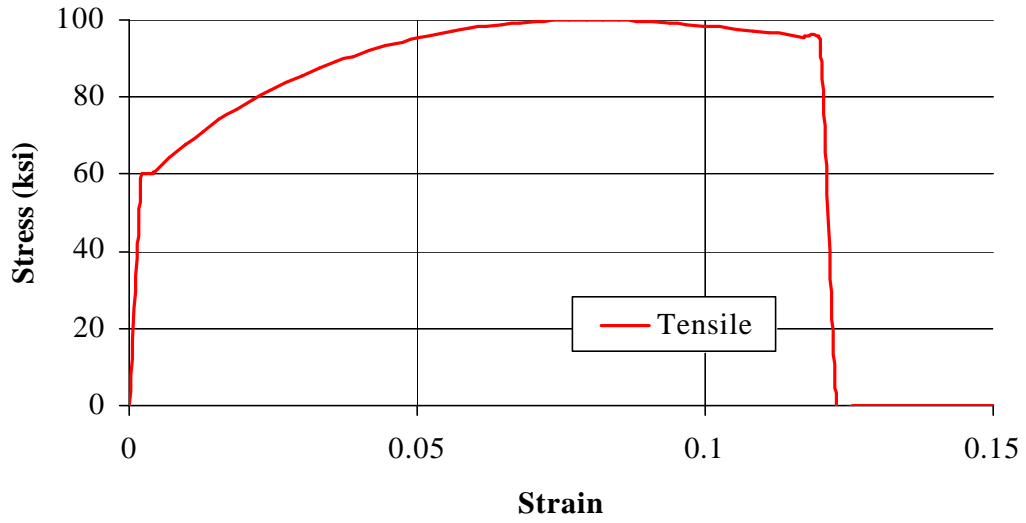


d. Beam BIAx fiber model

Figure 4.2 Fiber models of typical bent cross-sections

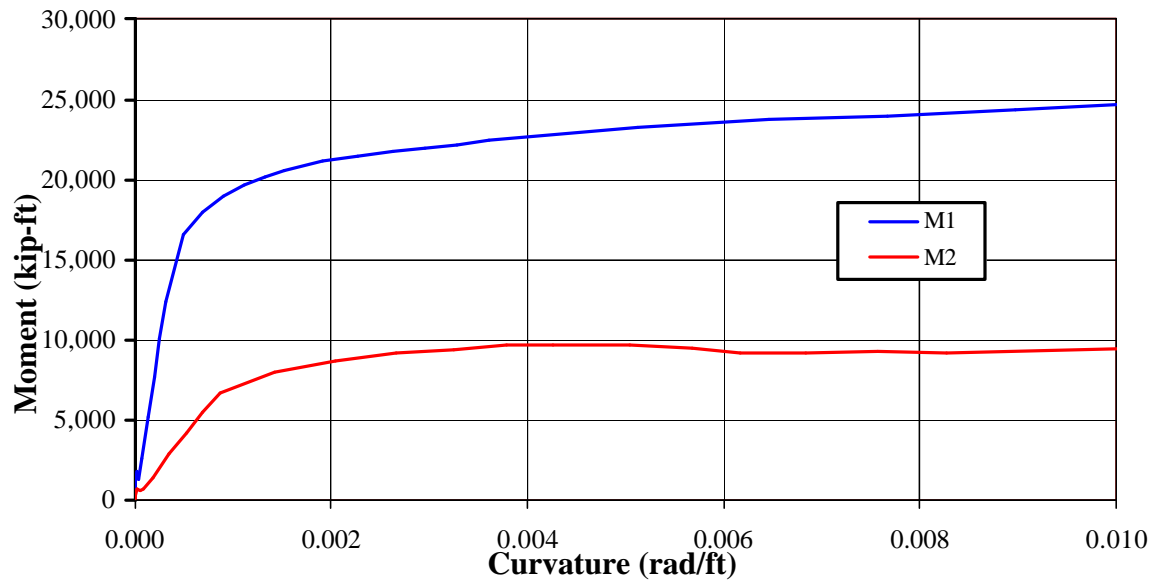


b. Concrete stress-strain relations

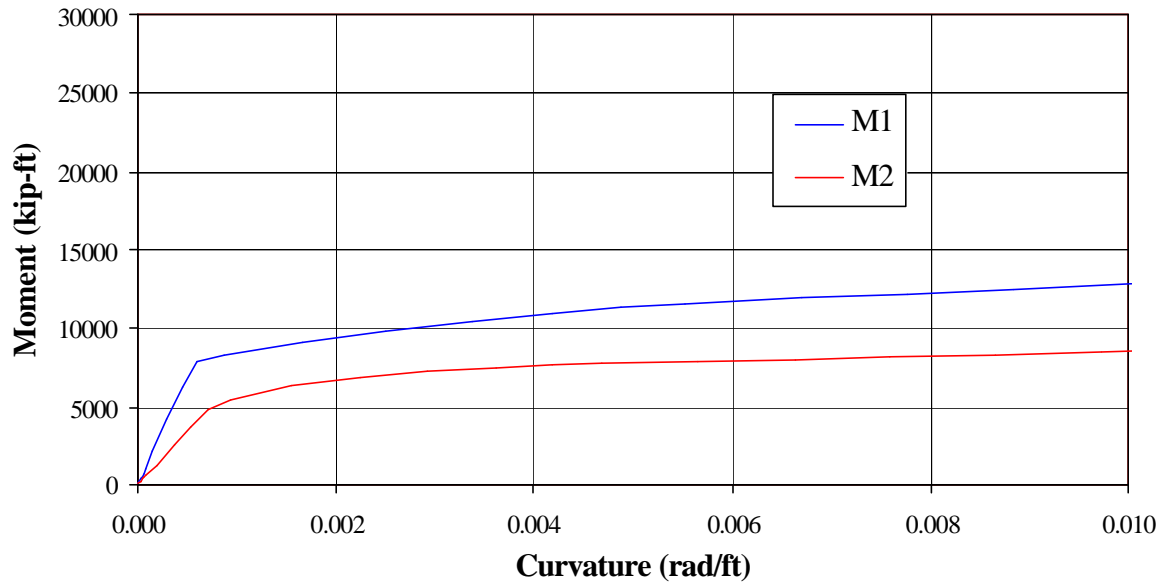


b. Steel stress-strain relation

Figure 4.3 Fiber material response curves



a. Column section X-X



b. Beam section A-A

Figure 4.4 Section stiffness degradation and capacity estimates

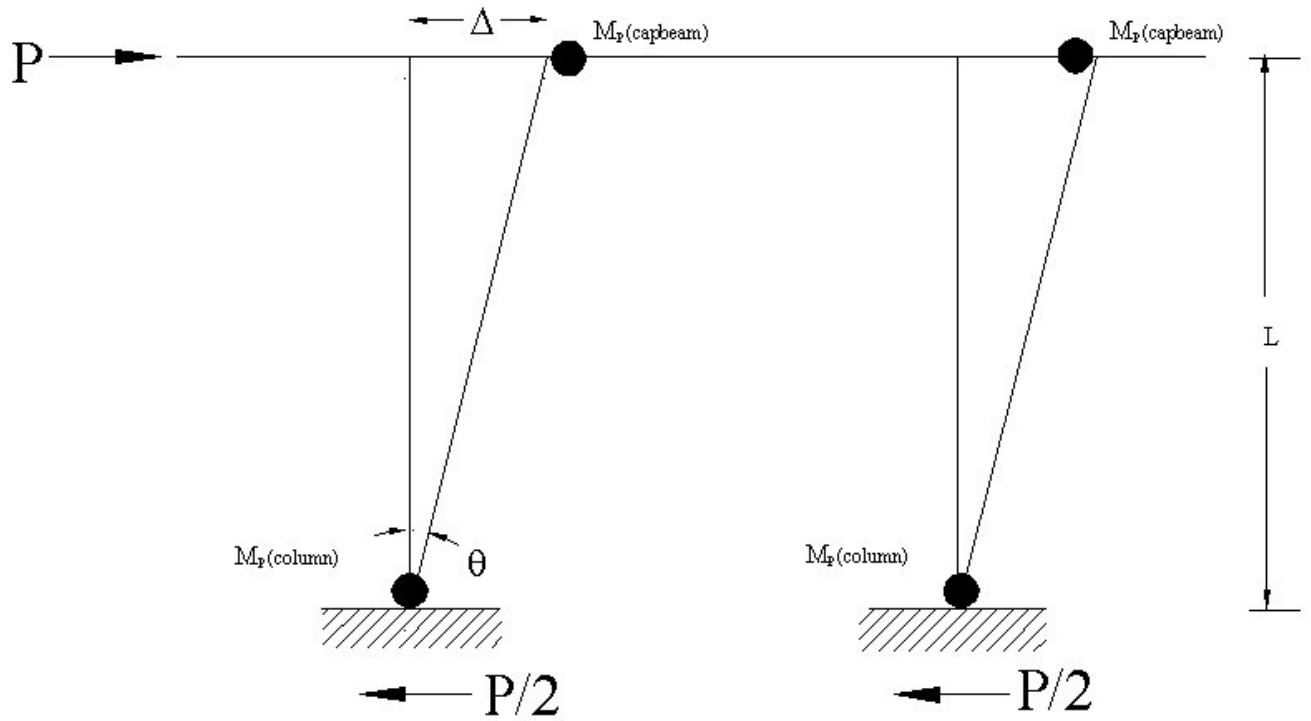


Figure 4.5 Bent plastic collapse mechanism under lateral inertial loading

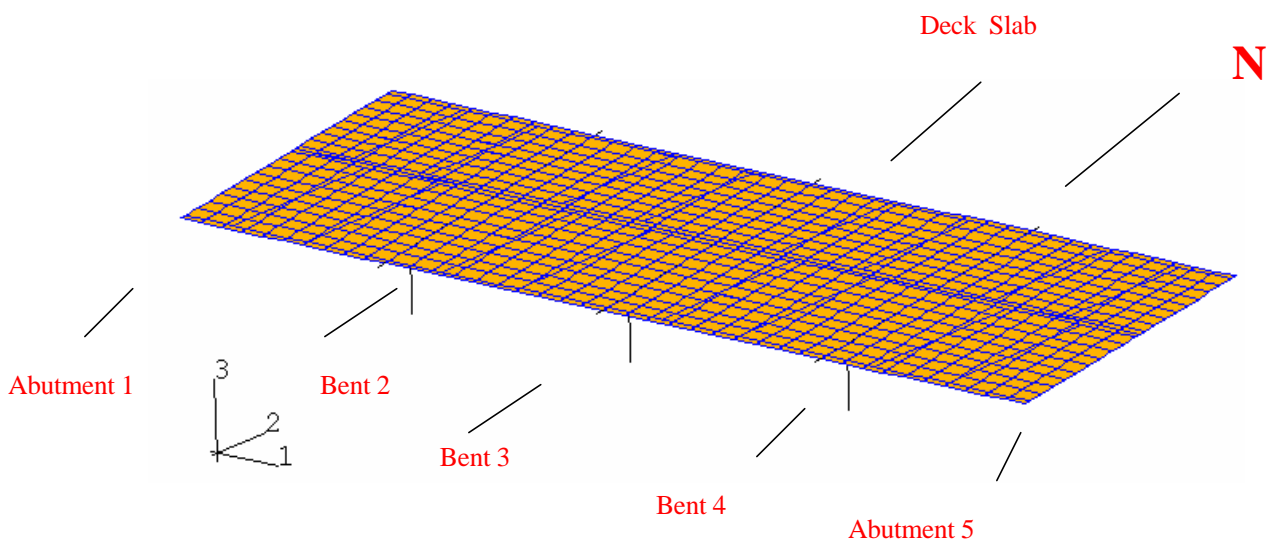


Figure 5.1 `Level 2 analysis model – isometric view

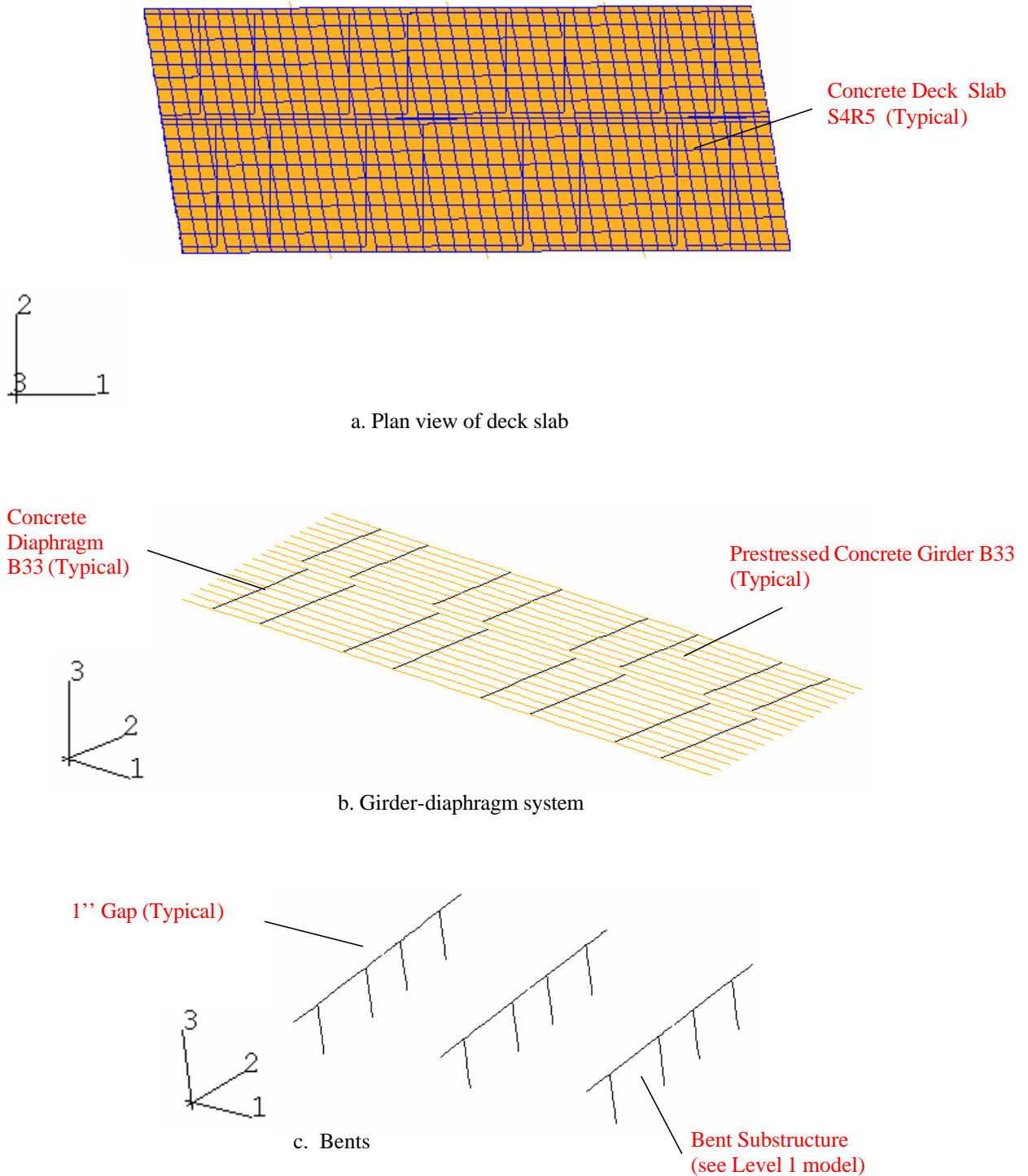
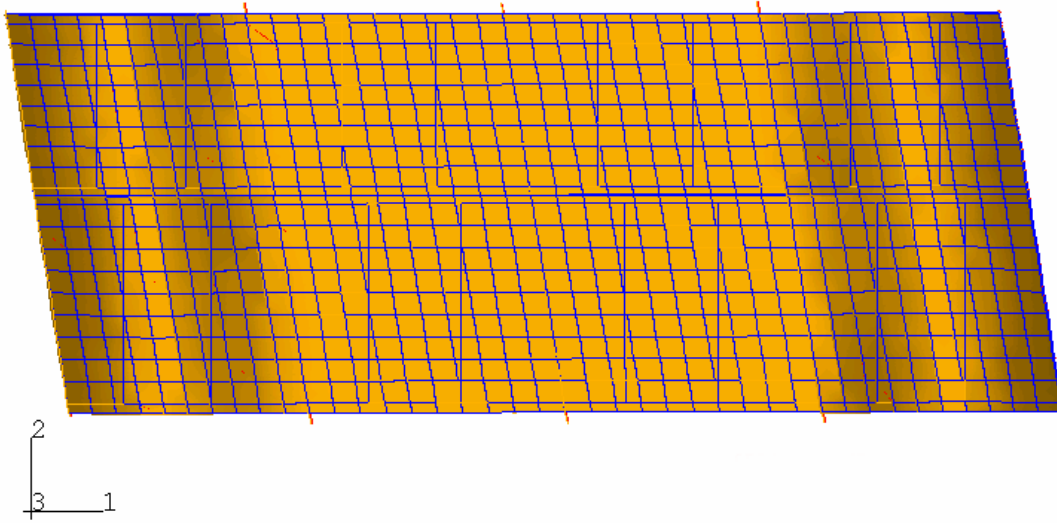
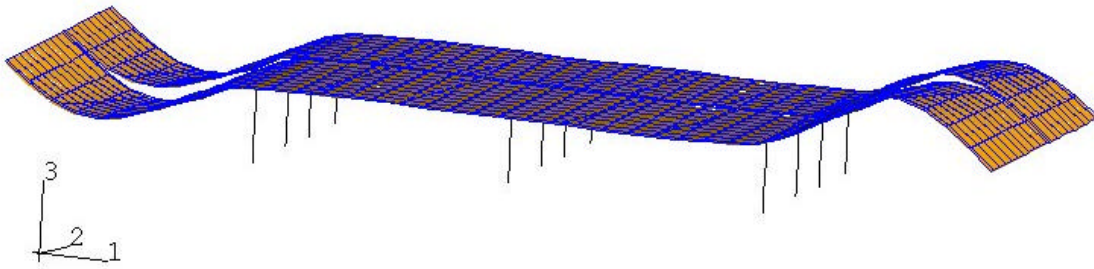


Figure 5.1 (Cont'd) Level 2 analysis model details

EIGENMODE A (1.29 Hz)

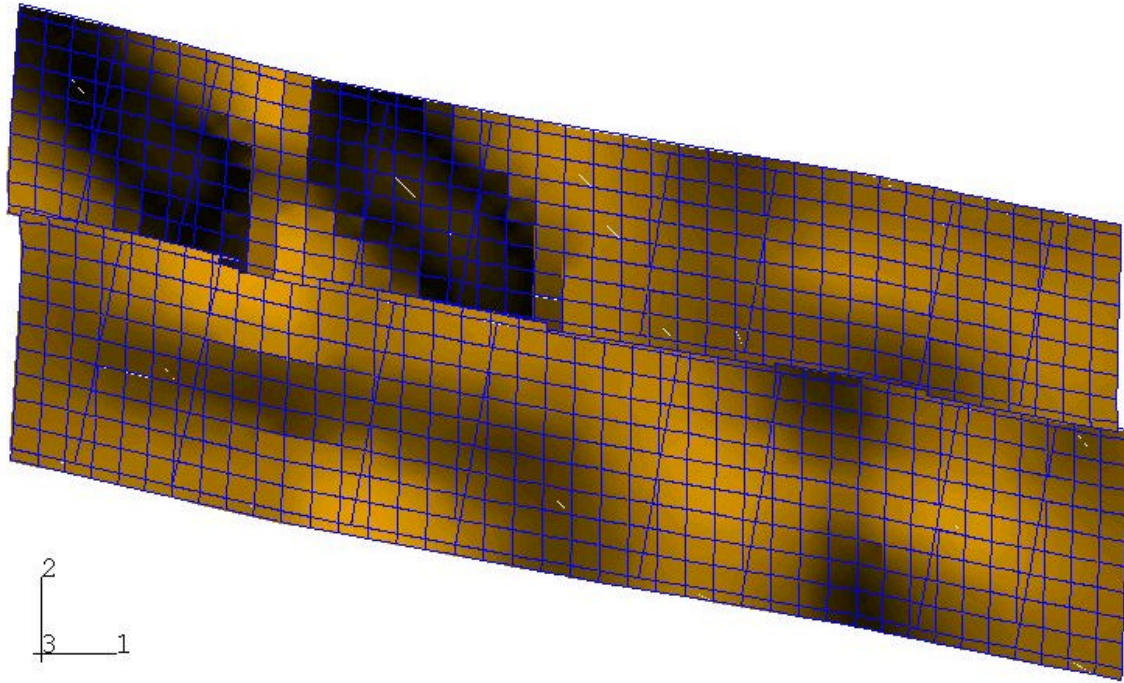


a. Plan view

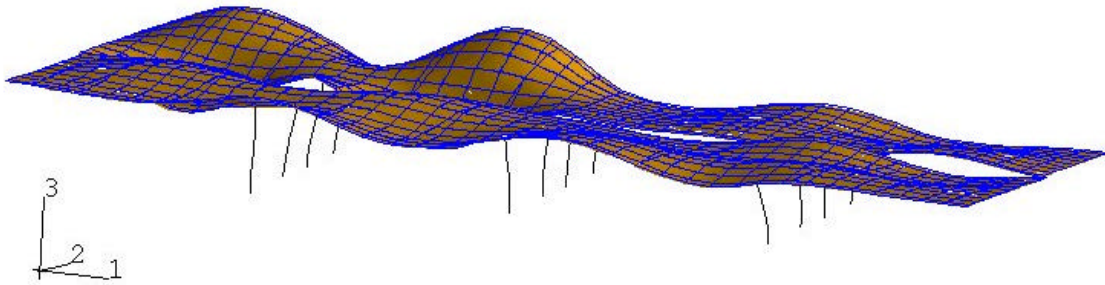


b. Isometric view

Figure 5.2 Characteristic modes of the Level 2 model
EIGENMODE B (2.96 Hz)



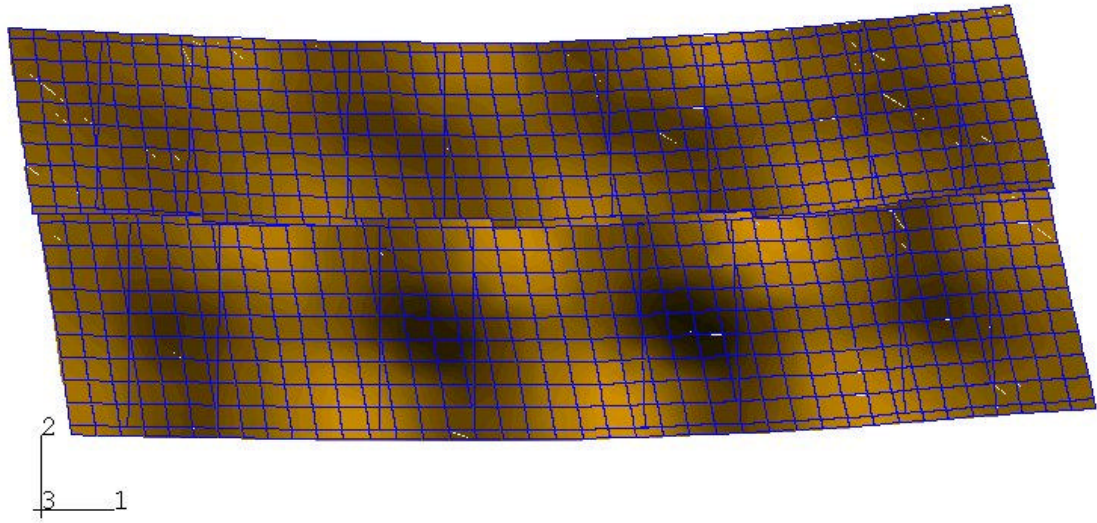
a. Plan view



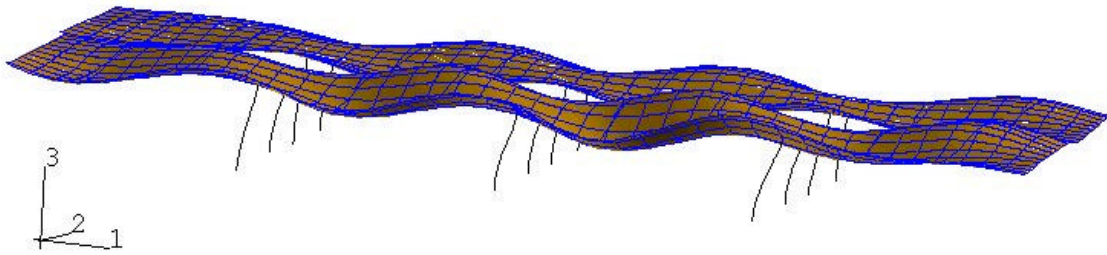
b. Isometric view

Figure 5.2 (cont'd) Characteristic modes of the Level 2 model

EIGENMODE C (3.63 Hz)



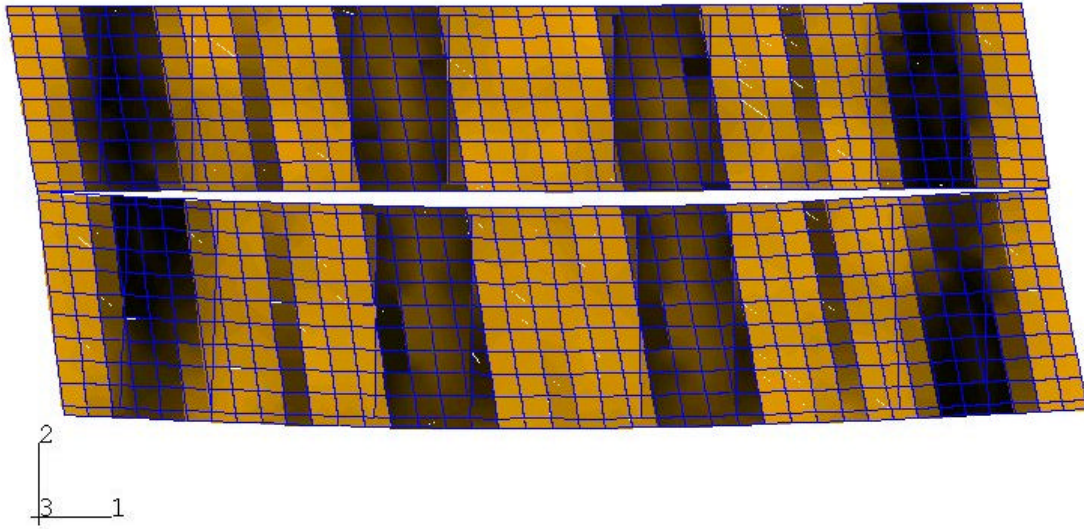
a. Plan view



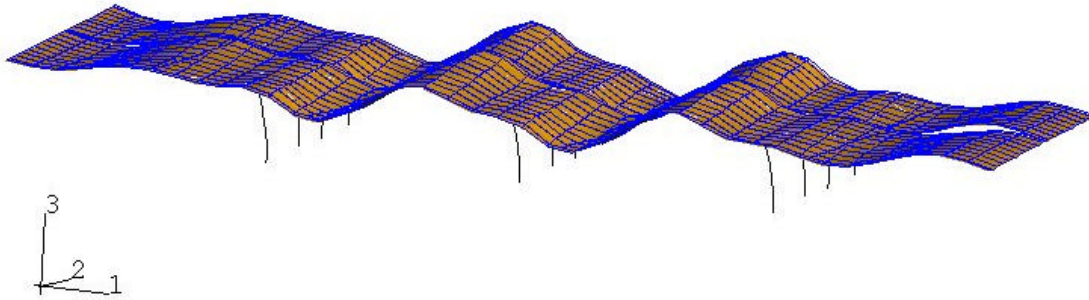
b. Isometric view

Figure 5.2 (cont'd) Characteristic modes of the Level 2 model

EIGENMODE D (5.19 Hz)



a. Plan view



b. Isometric view

Figure 5.2 (cont'd) Characteristic modes of the Level 2 model



Figure 5.3 Accelerometer array installation and vibration measurement





Figure 5.3 (cont'd) Accelerometer array installation and vibration measurement



Figure 5.3 (cont'd) Accelerometer array installation and vibration measurement

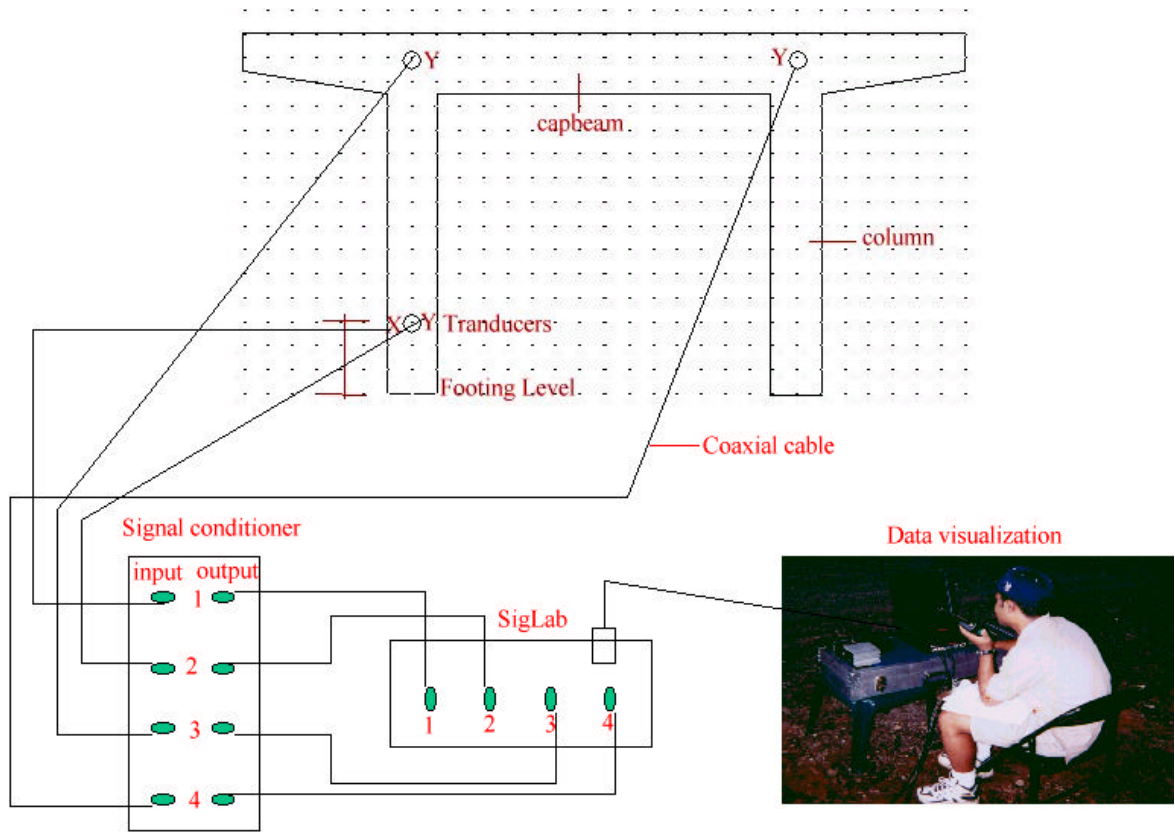


Figure 5.4 Schematic four-channel array configuration

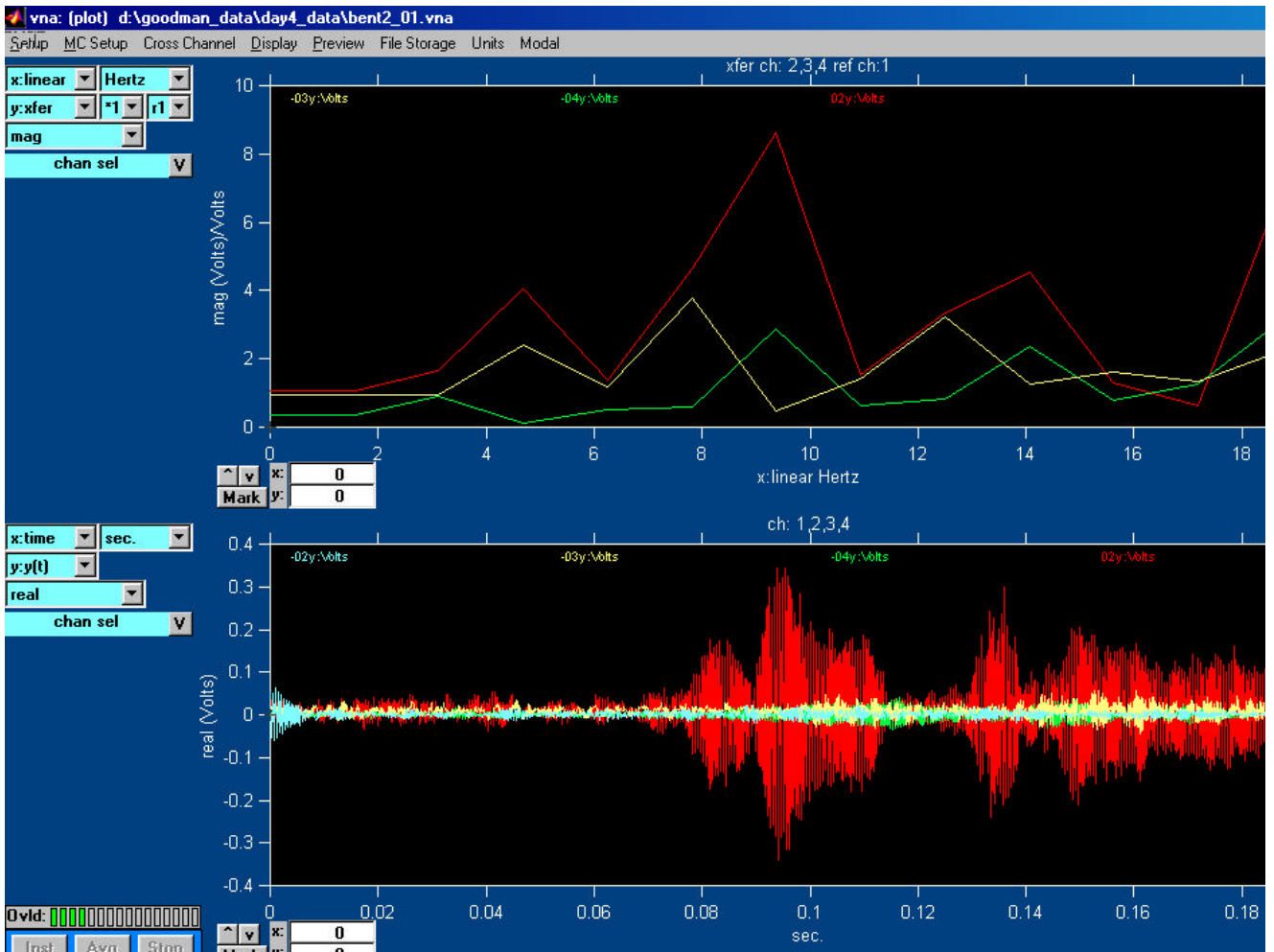


Figure 5.5 Sample record as presented by SigLab VNA and viewed in the field

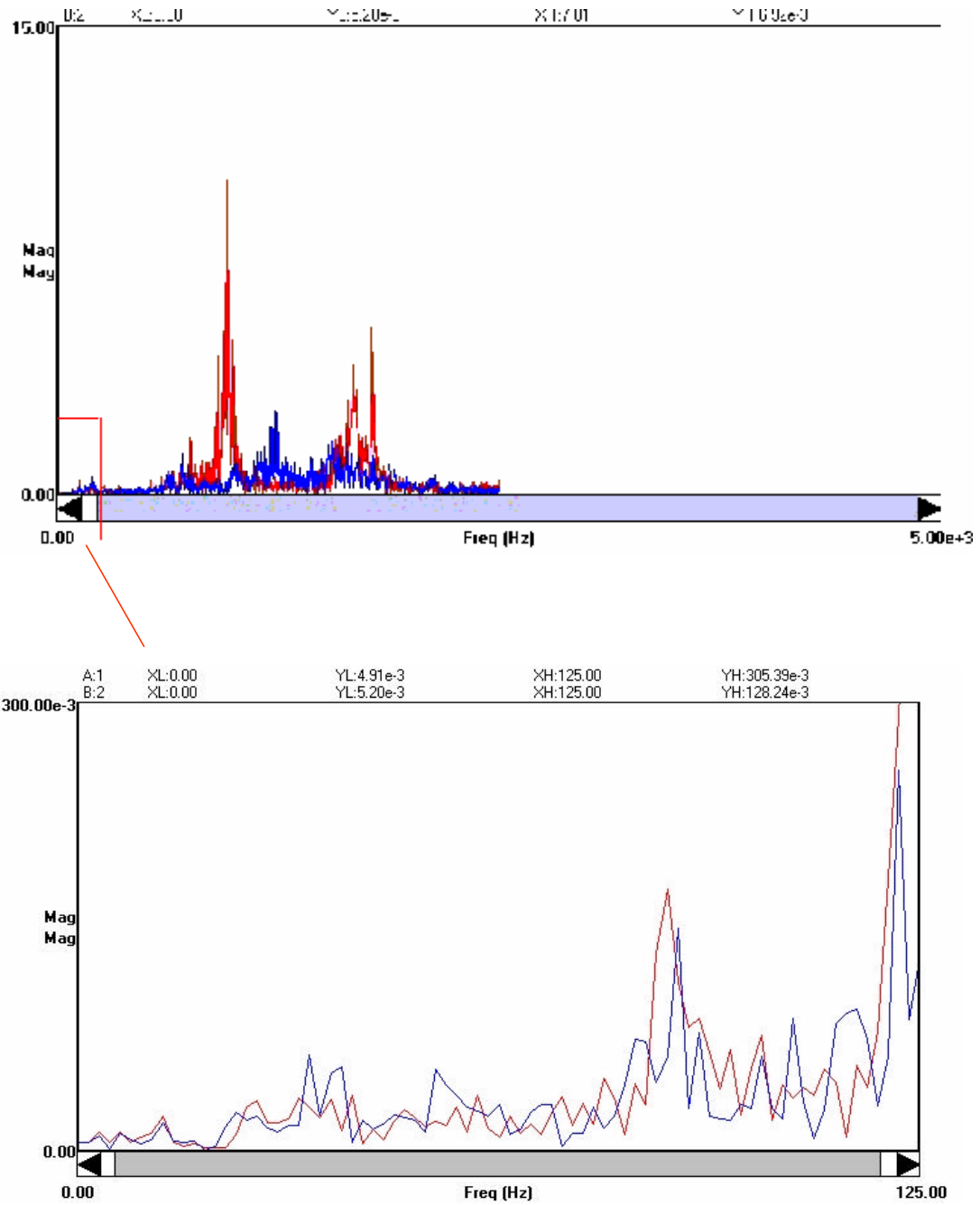


Figure 5.6 Sample records as presented by STAR Modal and viewed in the lab.

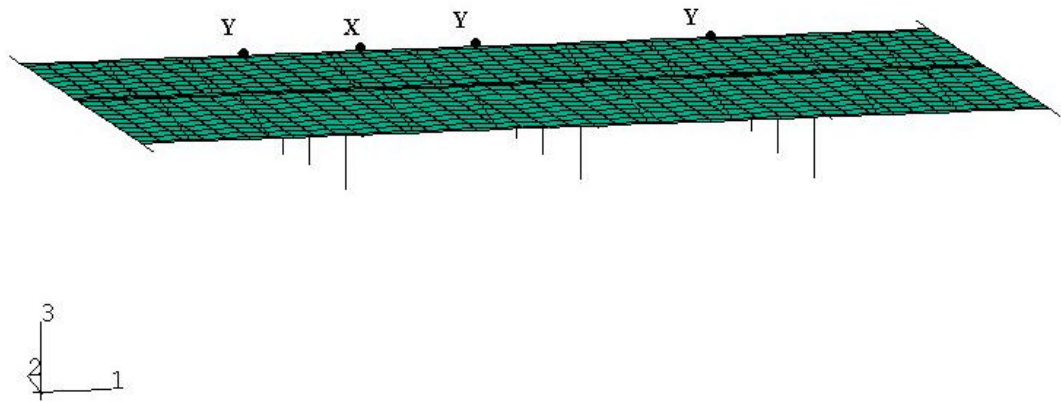
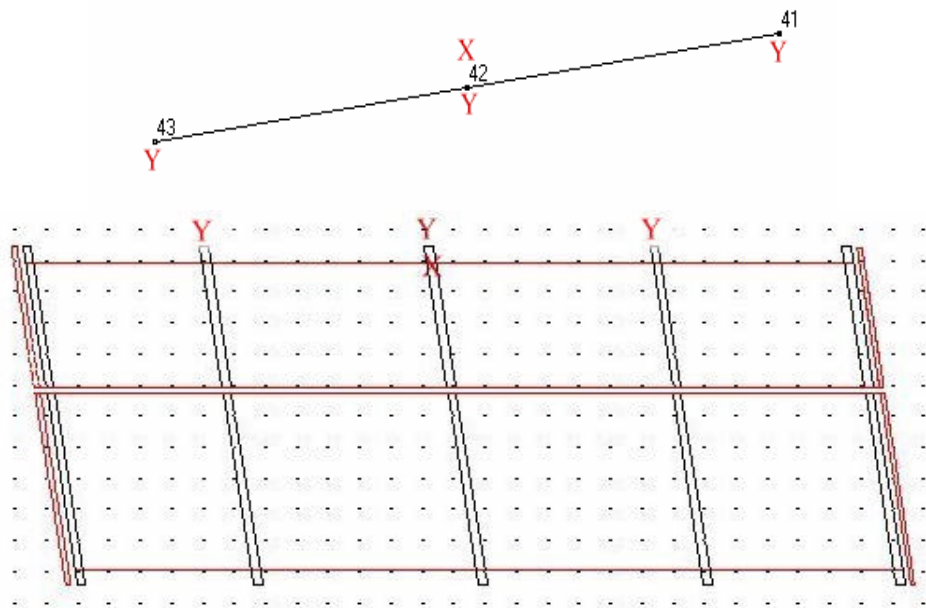
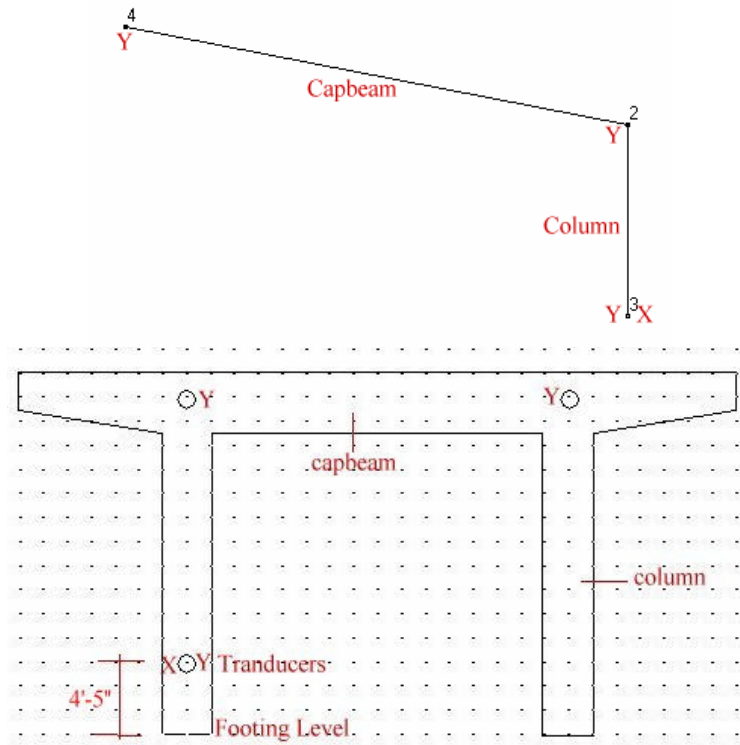


Figure 5.7 Transducer array configuration to identify transverse modes.

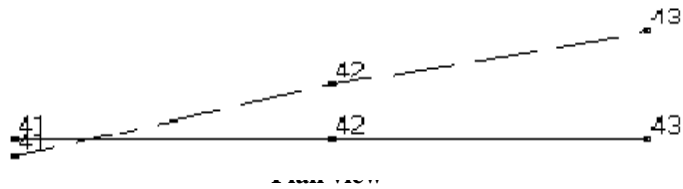


a. Configuration to identify transverse modes

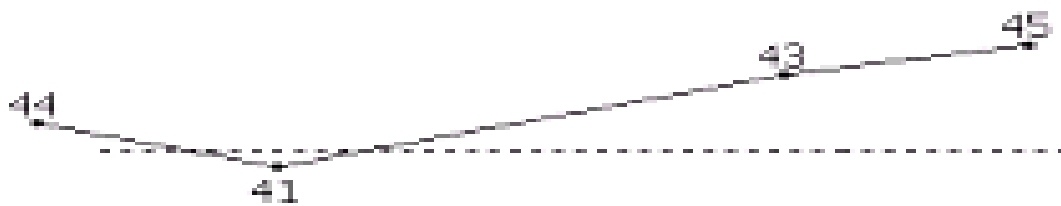


b. Configuration to identify longitudinal modes

Figure 5.8 Transducer array configurations

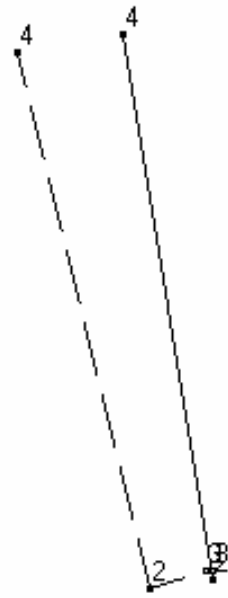


c. Mode B identified by STAR Modal (2.99 Hz)

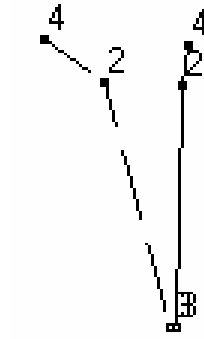


Plan view

d. Mode B identified by ME'Scope (3.12 Hz)



Plan view



Elevation view

e. Mode D identified by STAR Modal (5.24 Hz)

Figure 5.9 Results of modal system identification

SOUTHAVEN SOIL PROFILE

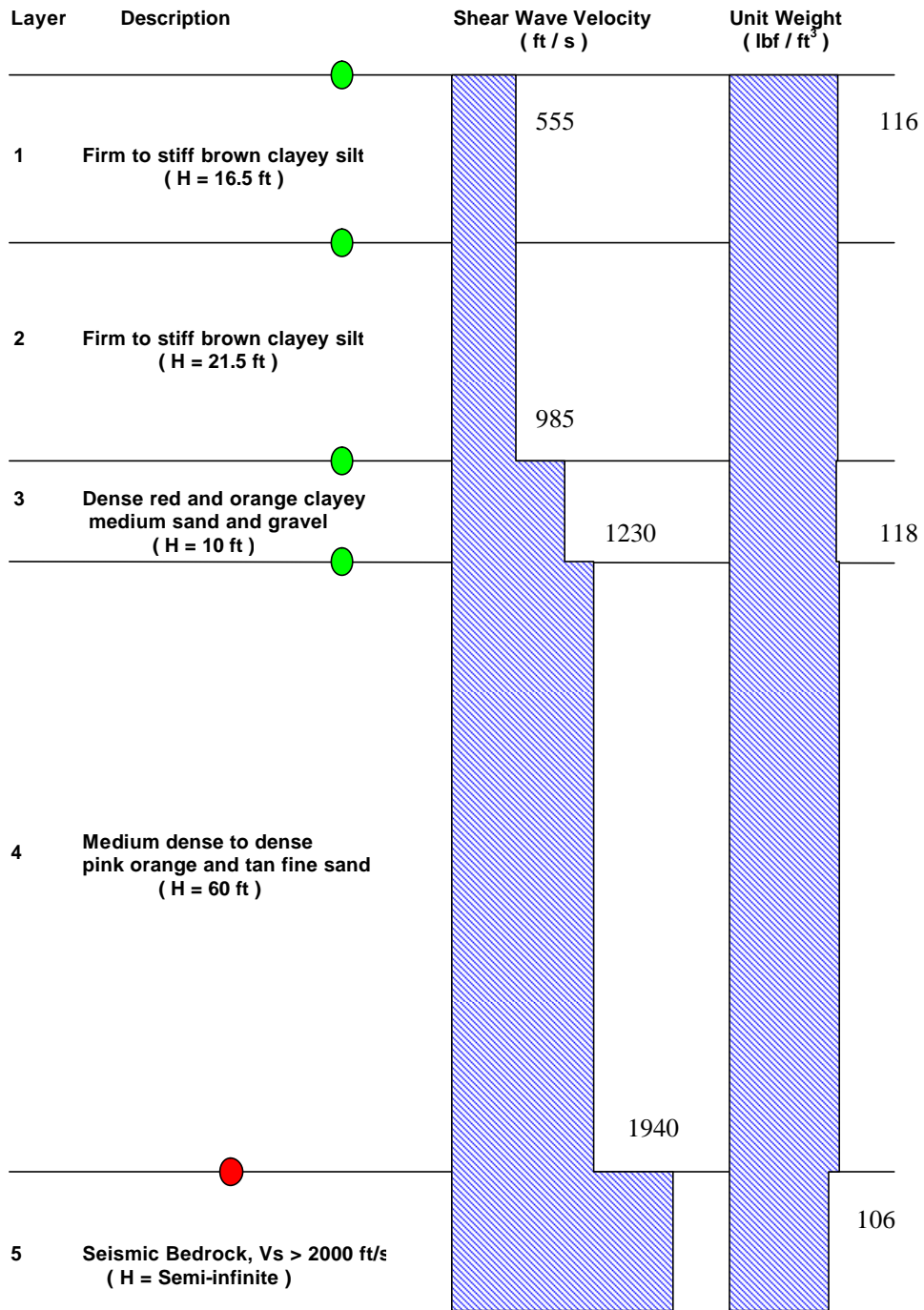


Figure 5.10 ProShake soil column model for generation of site-specific ground motions

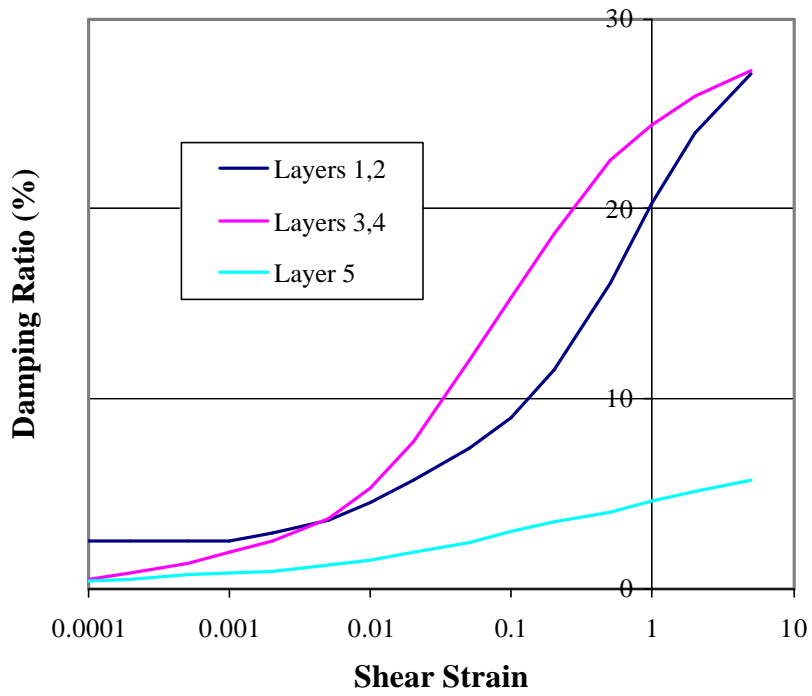
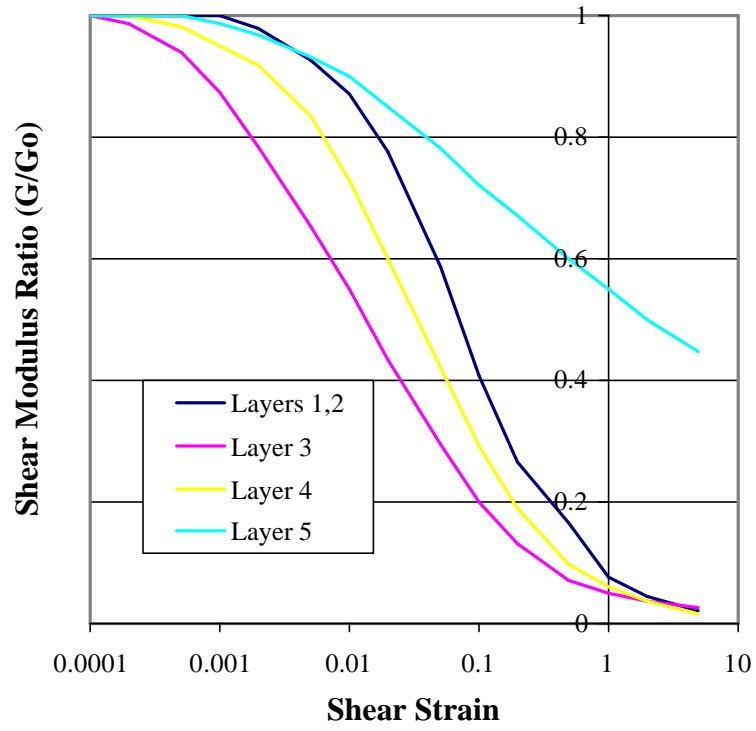


Figure 5.11 Soil degradation curves

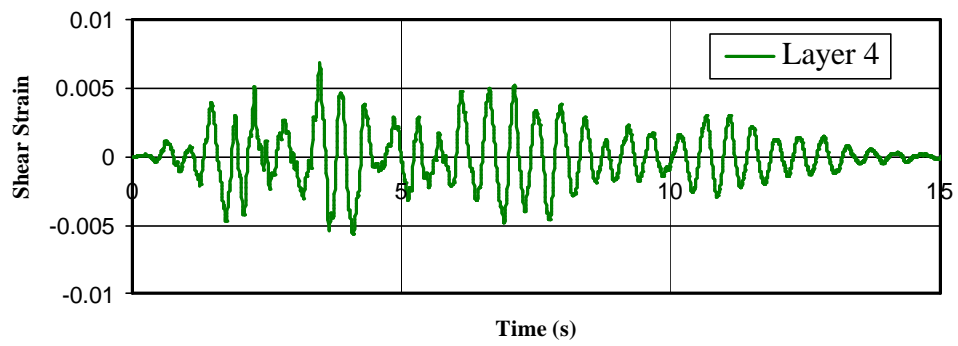
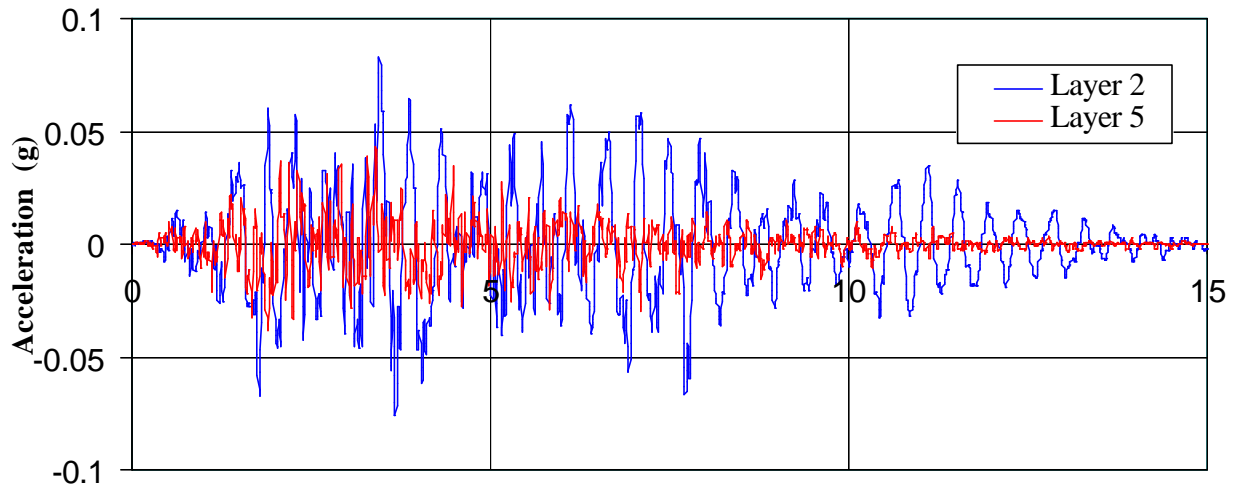
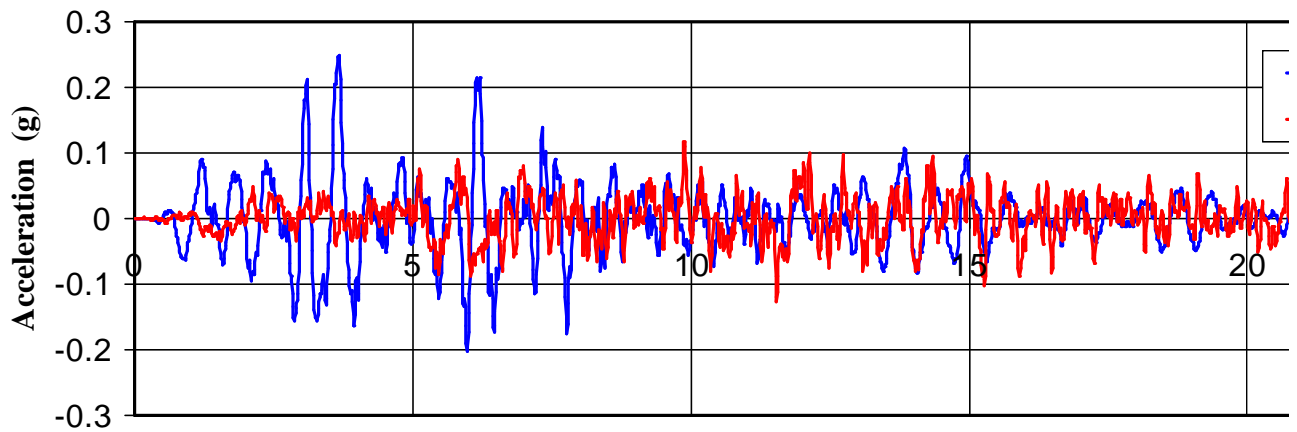


Figure 5.12 Predicted soil column acceleration and shear strain time histories ($M = 6$)



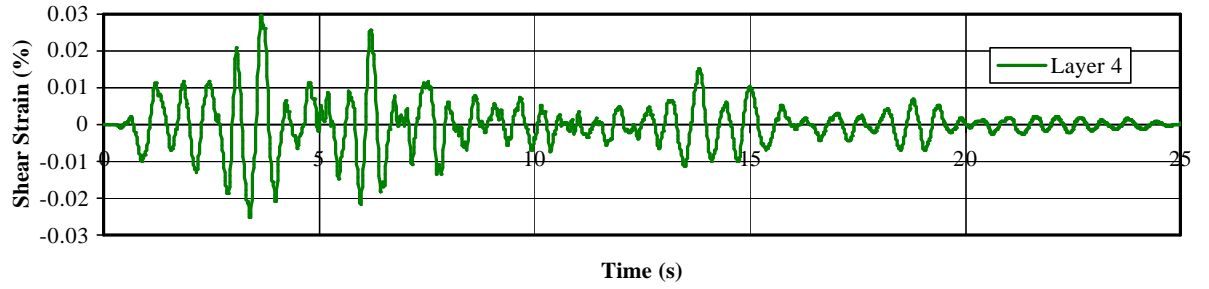


Figure 5.12 (cont'd) Predicted soil column acceleration and shear strain time histories ($M = 7$)

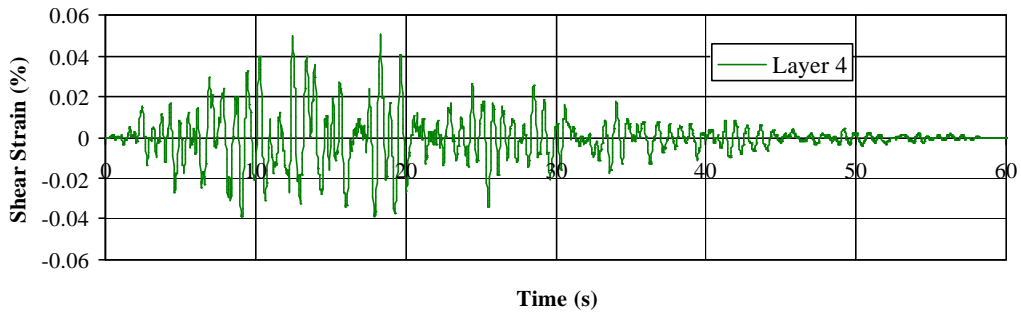
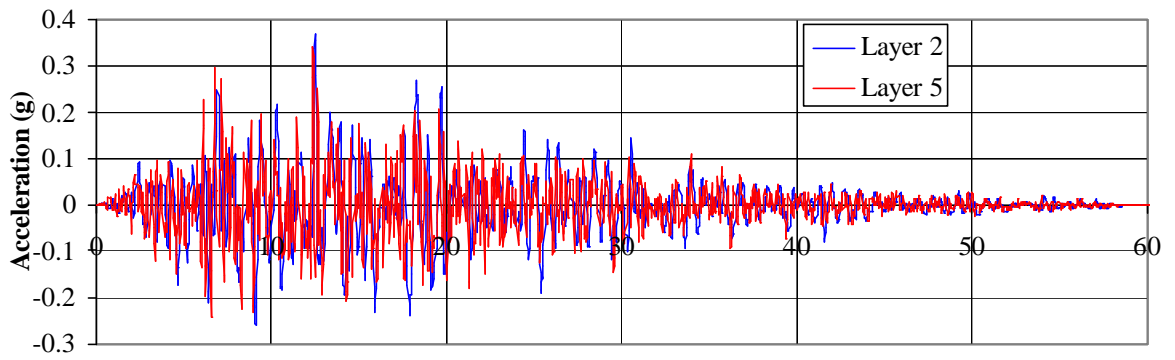
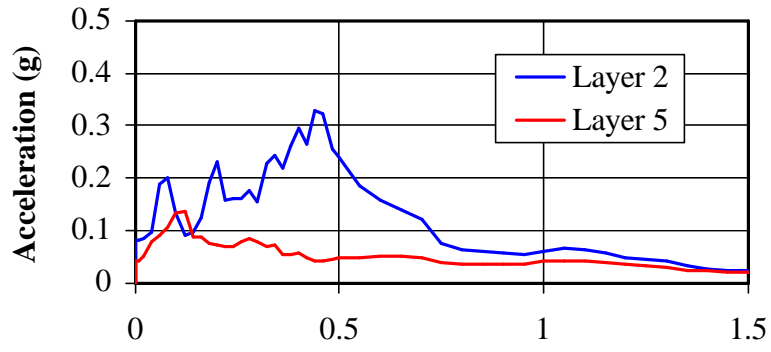
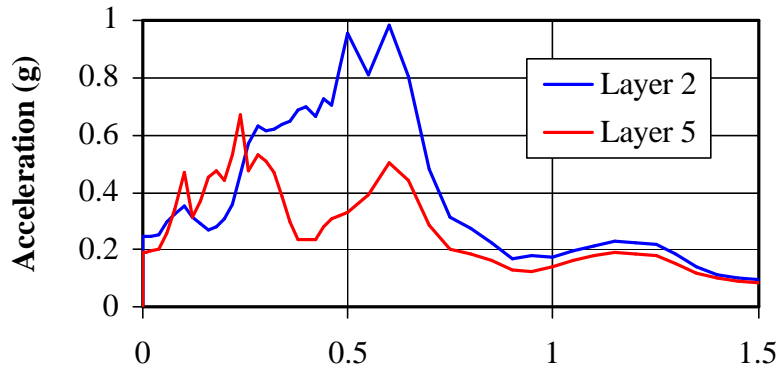


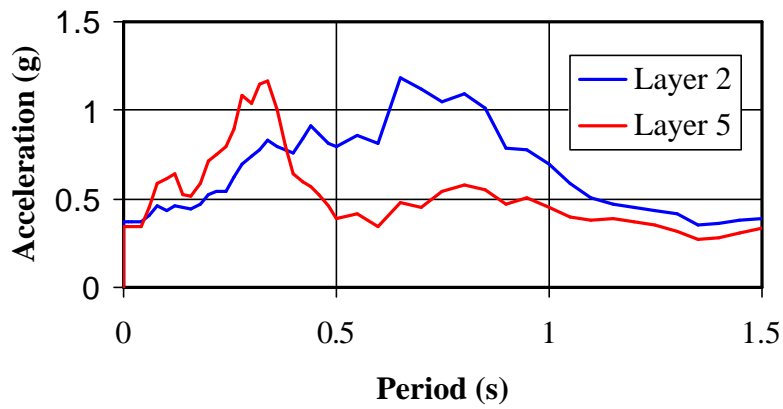
Figure 5.12 (cont'd) Predicted soil column acceleration and shear strain time histories ($M = 8$)



a. $M = 6$



b. $M = 7$



c. $M = 8$

Figure 5.13 Predicted soil column acceleration response spectra

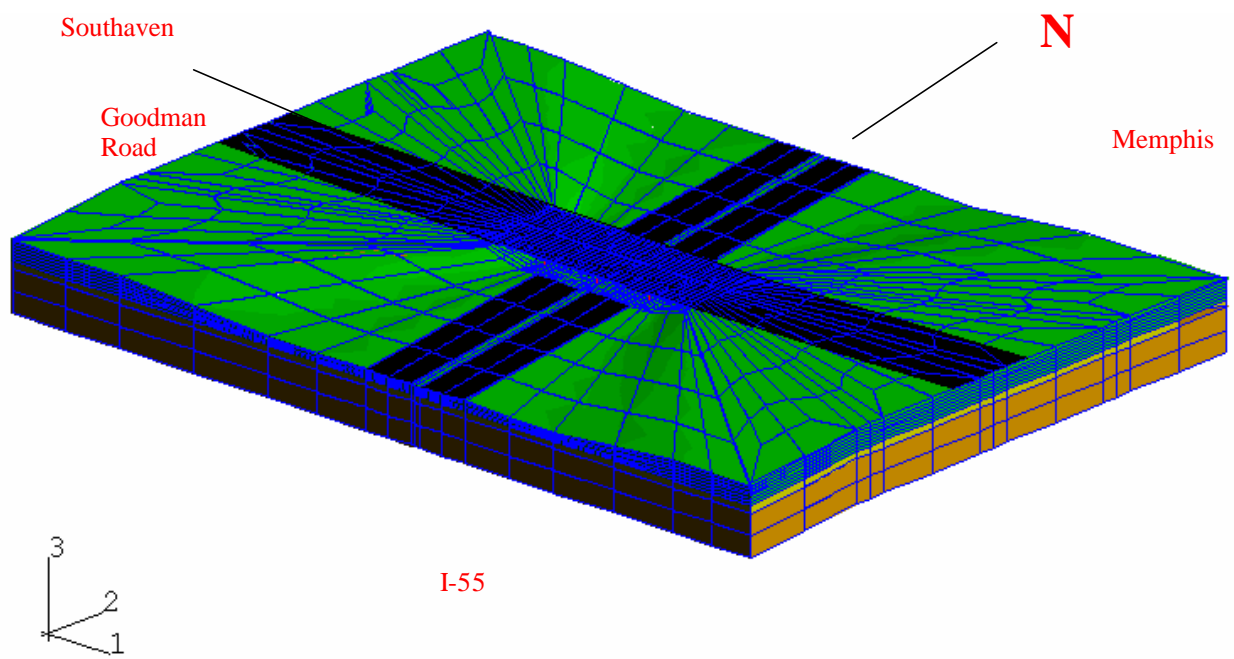


Figure 6.1 Level 3 analysis model: soil-structure system

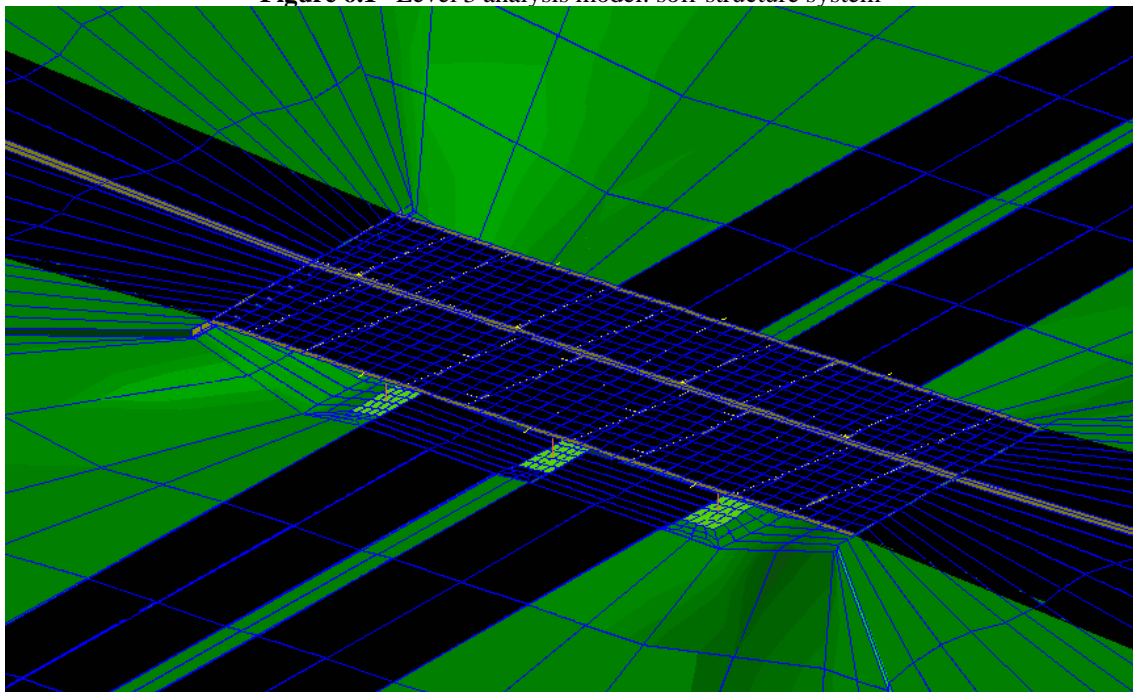
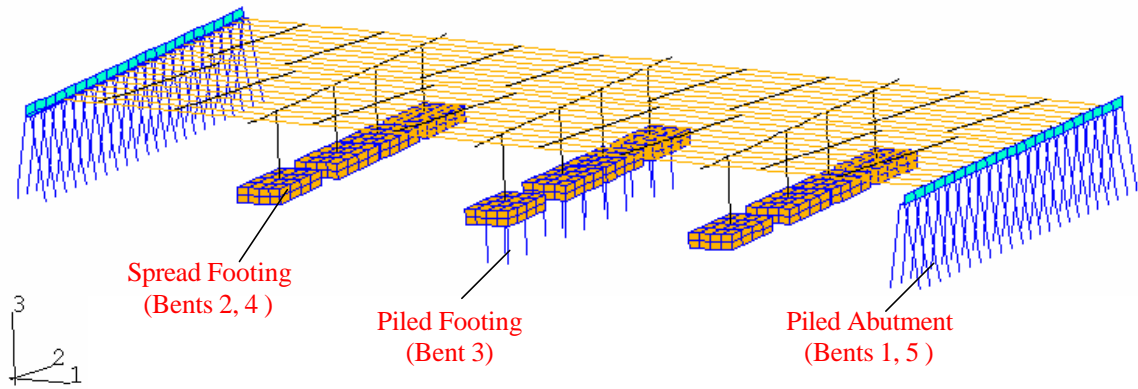
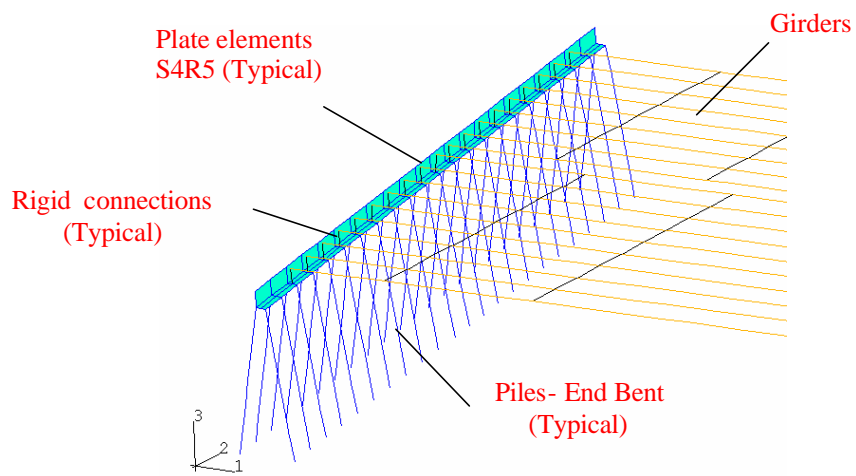


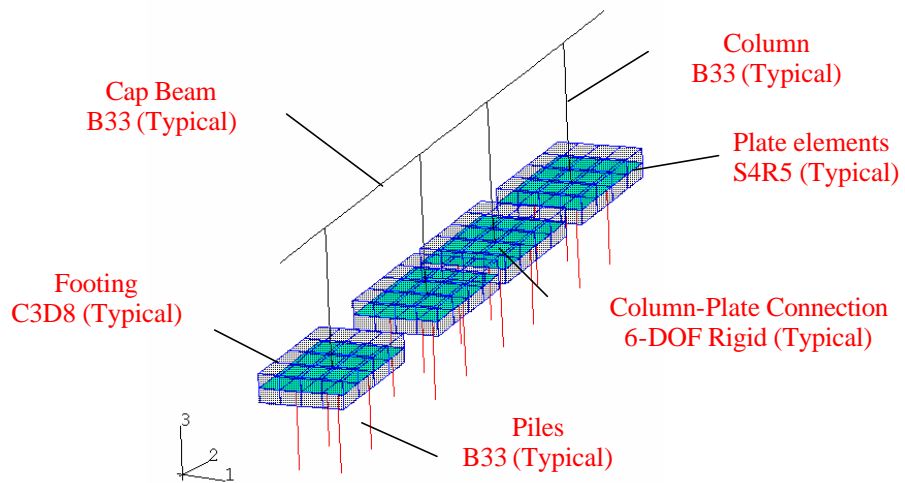
Figure 6.1 (cont'd) Level 3 analysis model: detail of soil-structure system



a. Bent substructures- isometric view

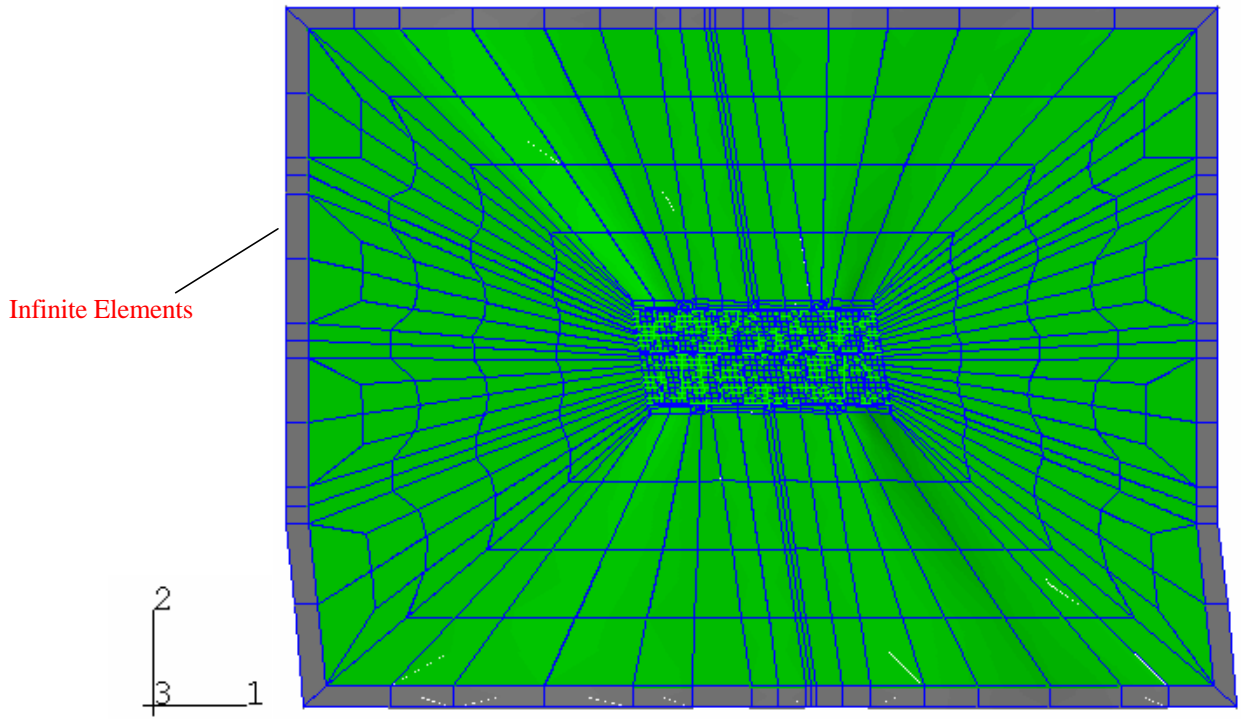


b. Detail of abutment-girder connection: Bents 1, 5

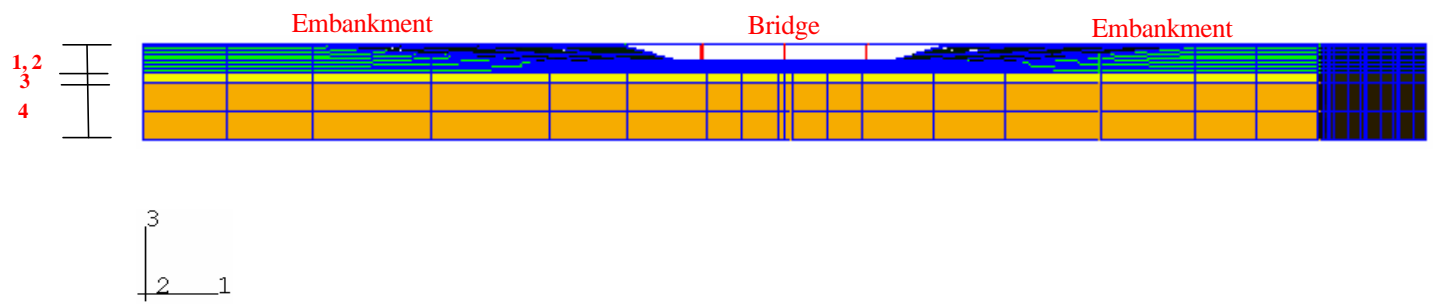


c. Detail of column-footing connection: Bent 3 (also Bents 2, 4 without piles)

Figure 6.1 (cont'd) Level 3 analysis model: detail of soil-structure system



b. Deck-bent-soil system: plan view

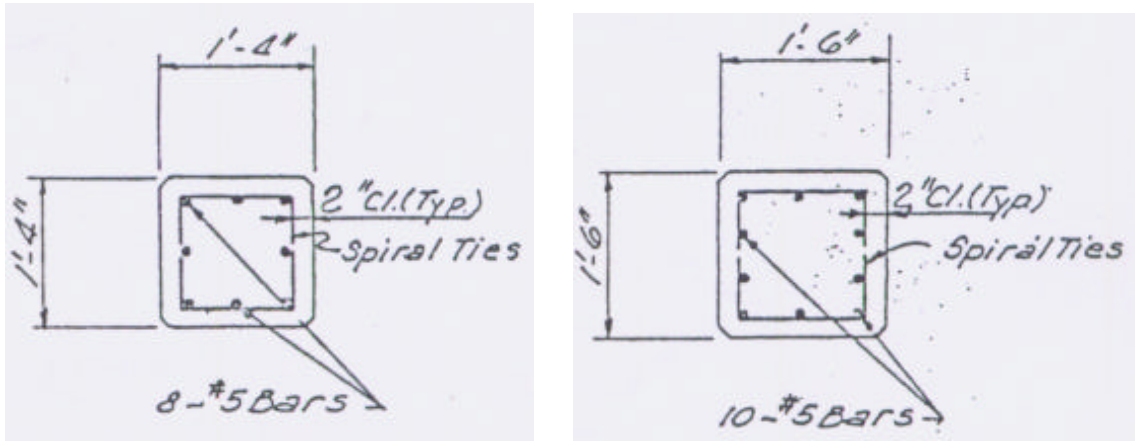


c. Deck-bent-soil system: side view

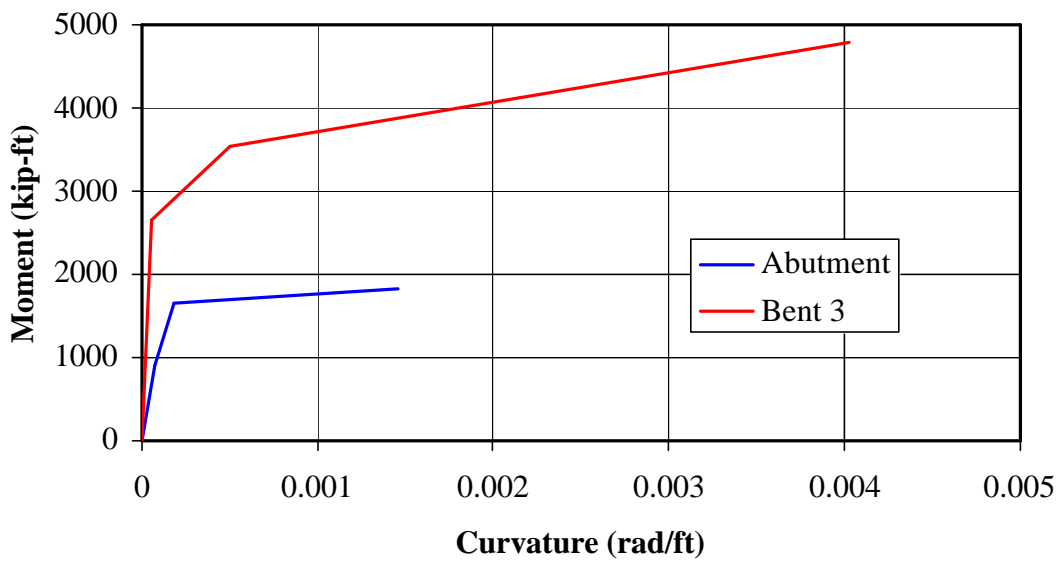
Figure 6.2 Level 3 analysis model: soil-structure system

Abutment (Bents 2, 4)

Bent 3 Footing



a. As-built drawings

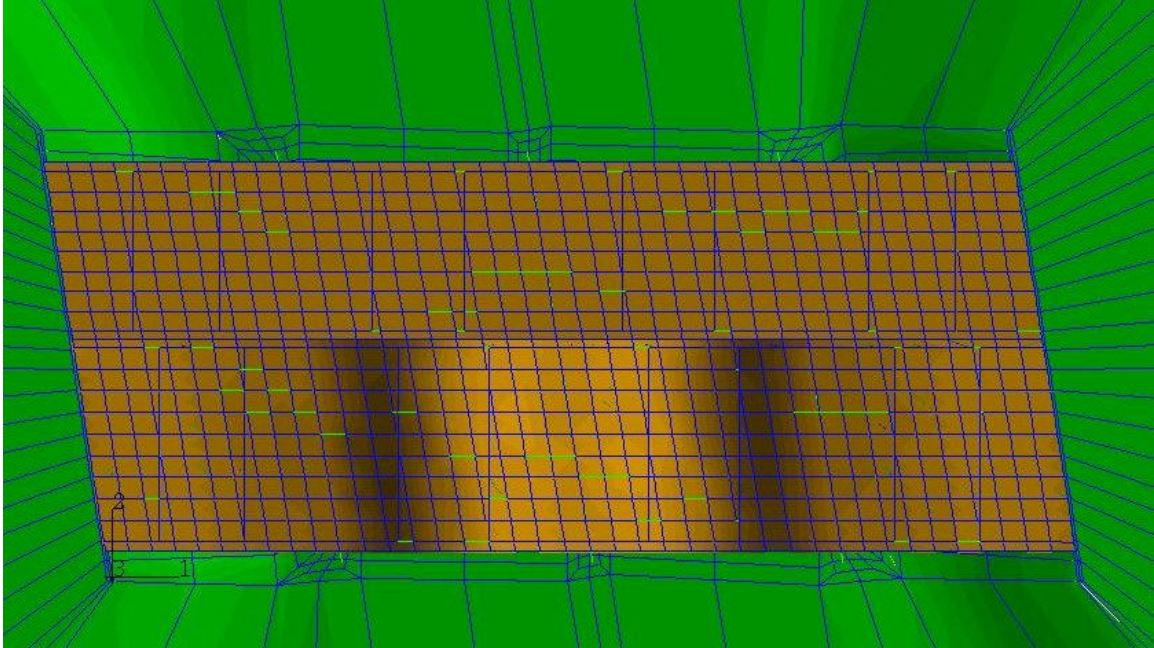


b. Backbone curves computed using IDARC2D

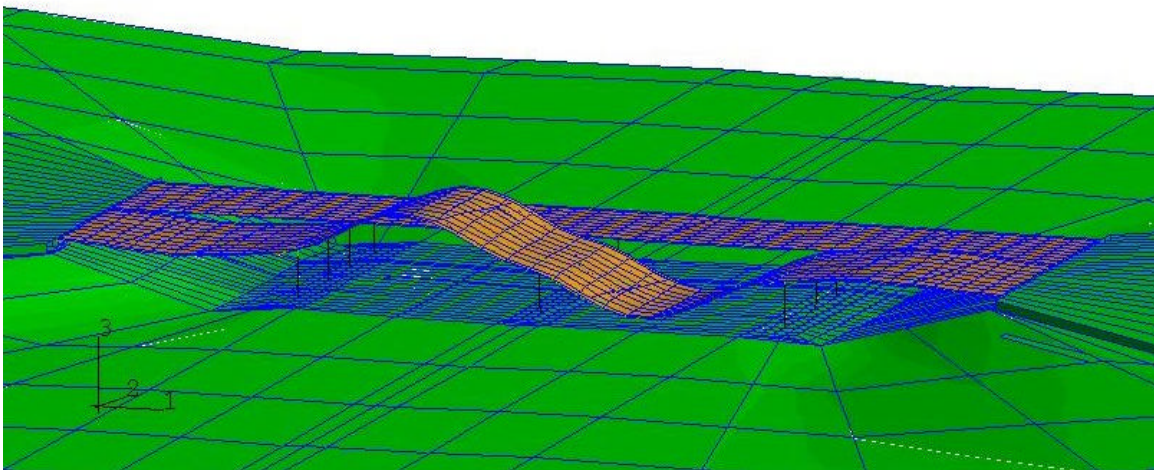
Figure 6.3 Section stiffness degradation and capacity estimates: piles



Figure 6.4 Condition of girder supports at time of field vibration test
EIGENMODE A (1.51 Hz)

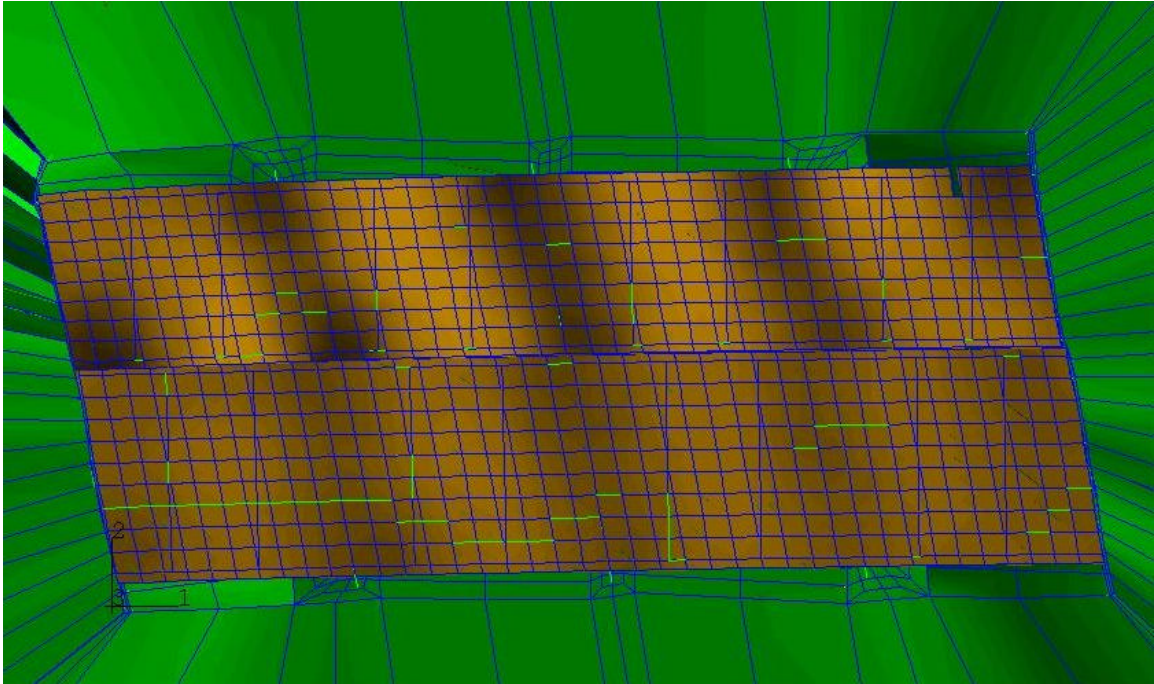


a. Plan view

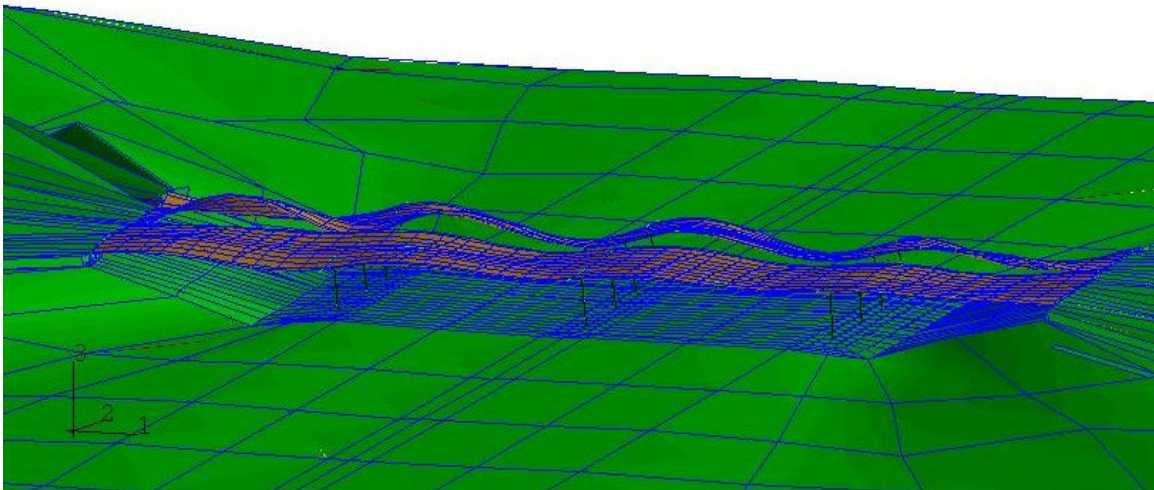


b. Isometric view

Figure 6.5 Characteristic modes of the Level 3 model
EIGENMODE B (3.11 Hz.)

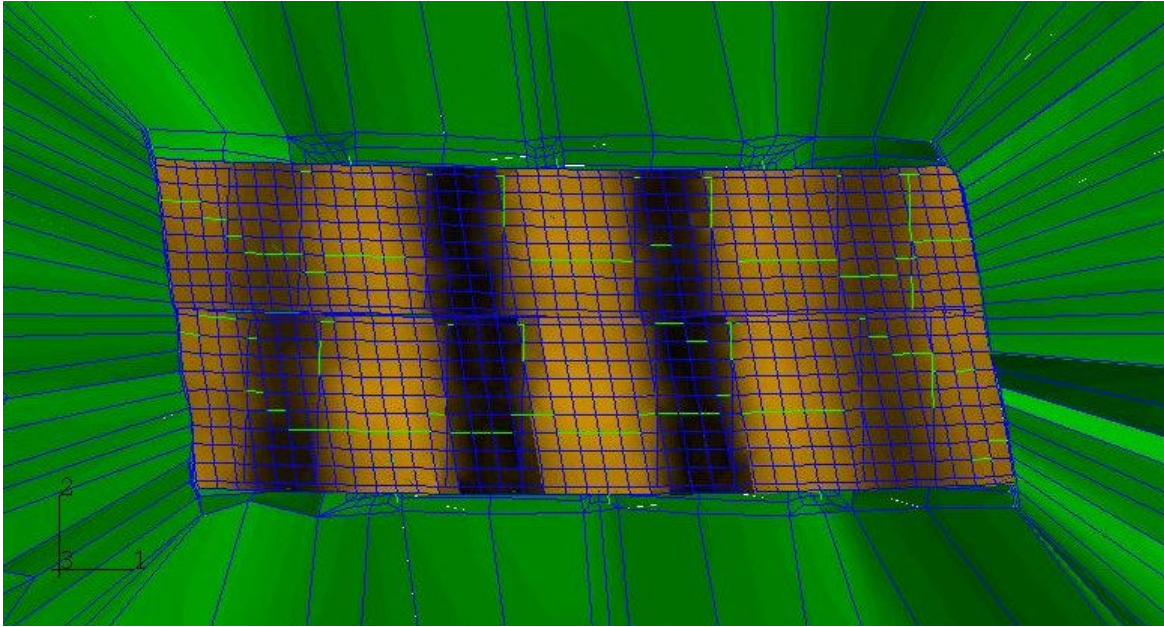


a. Plan view

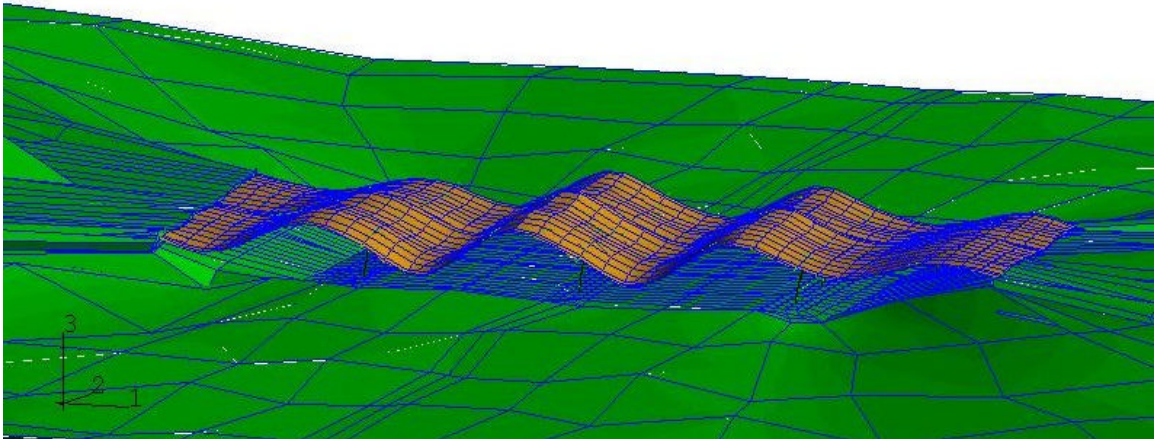


b. Isometric view

Figure 6.5 (cont'd) Characteristic modes of the Level 3 model
EIGENMODE C (3.81 Hz)

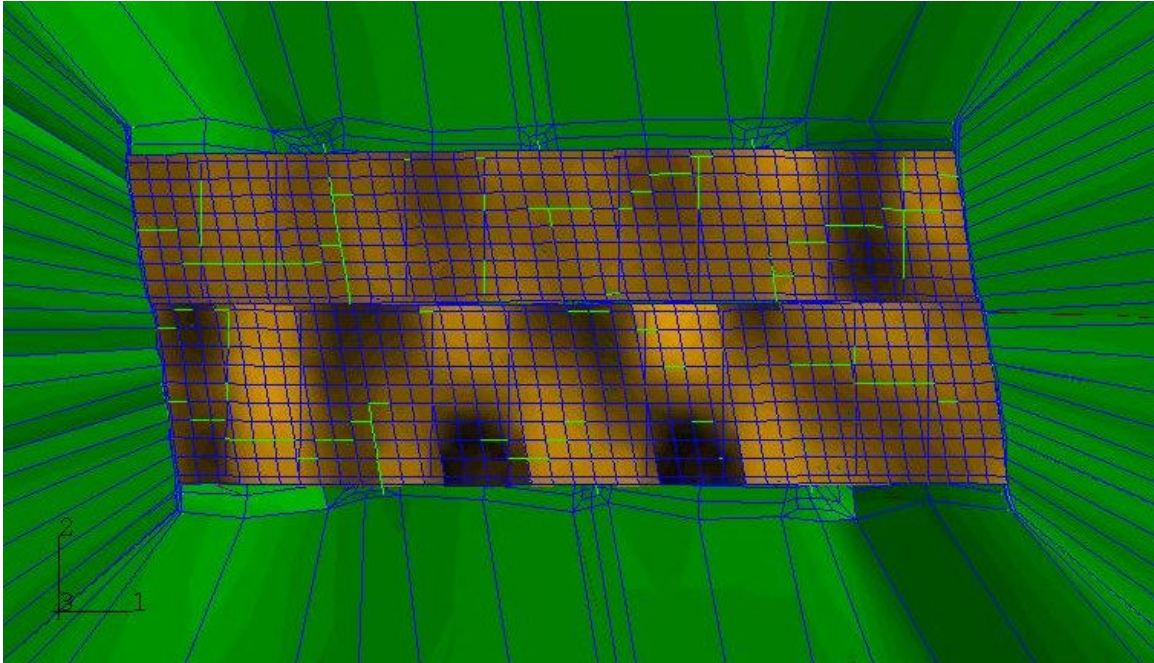


a. Plan view

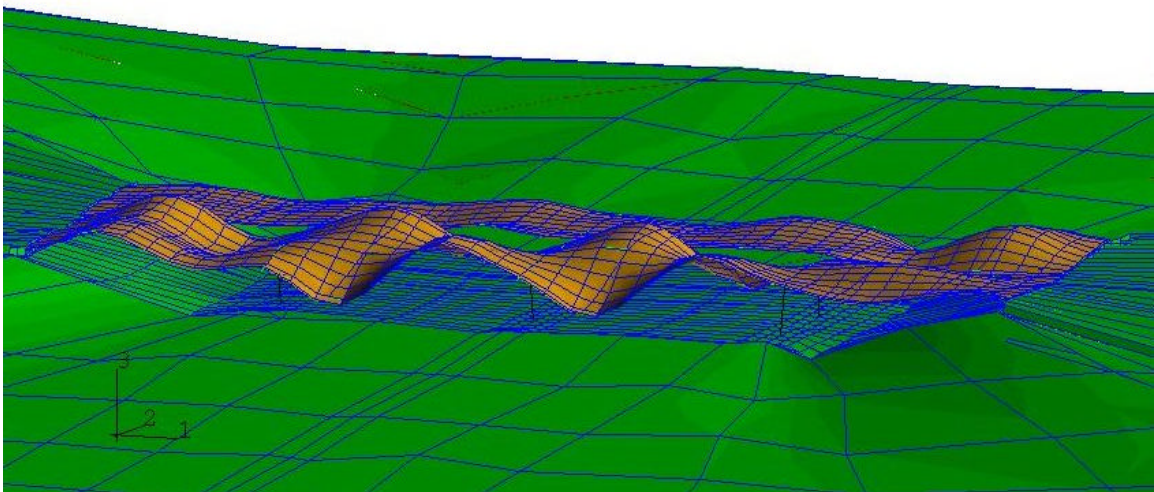


b. Isometric view

**Figure 6.5 (cont'd) Characteristic modes of the Level 3 model
EIGENMODE D (5.46 Hz.)**



a. Plan view



b. Isometric view

Figure 6.5 (cont'd) Characteristic modes of the Level 3 model

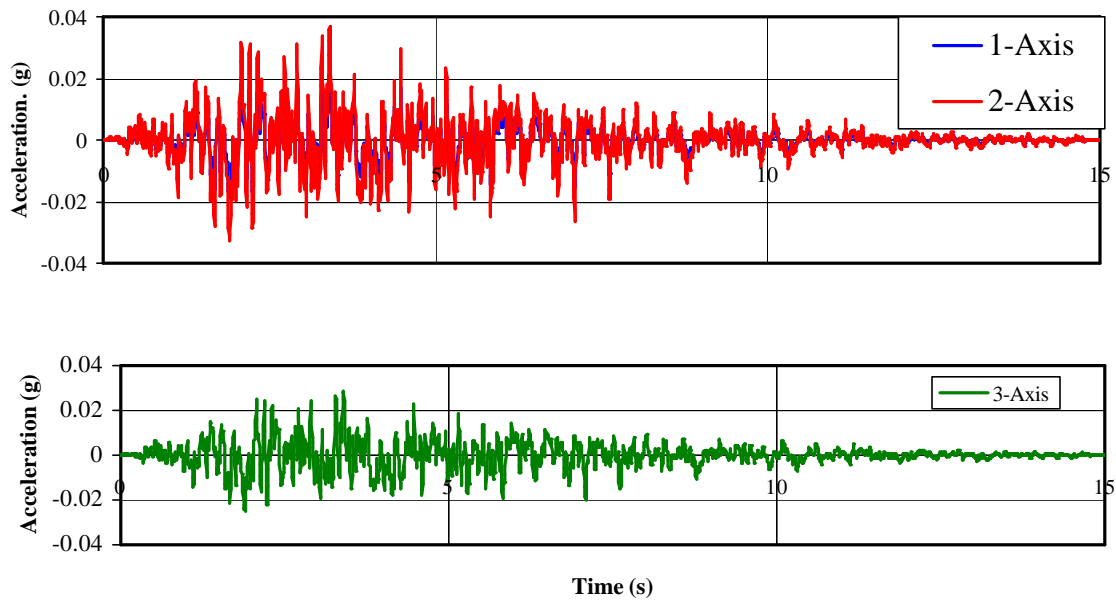


Figure 6.6 Input component time histories (M = 6)

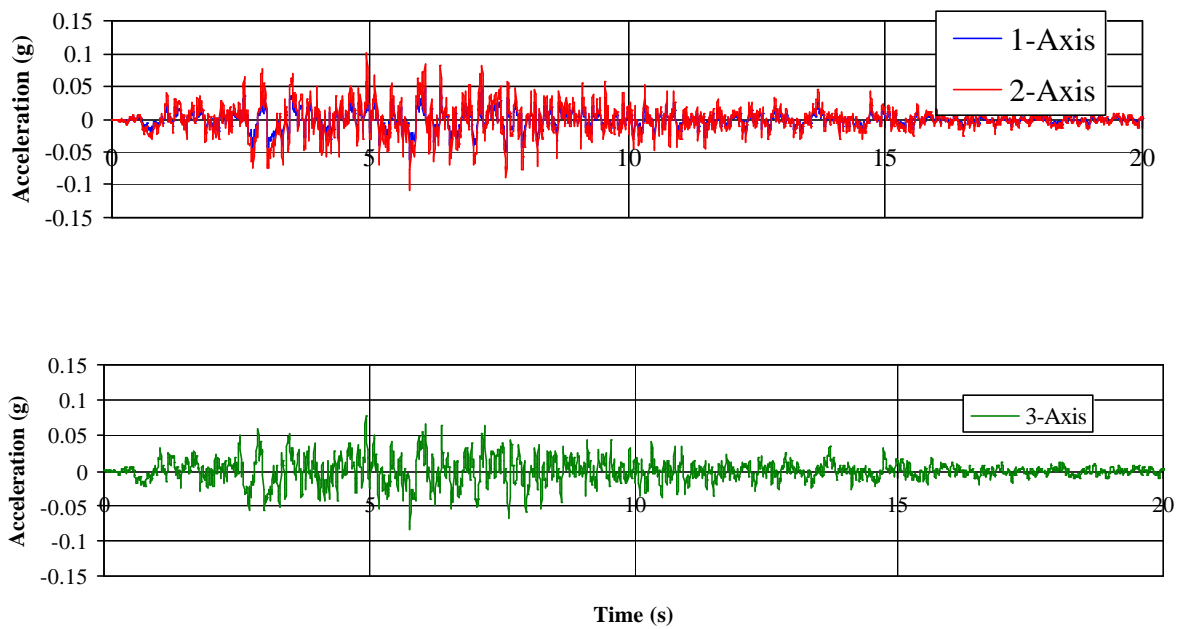


Figure 6.6 (cont'd) Component input time histories (M = 7)

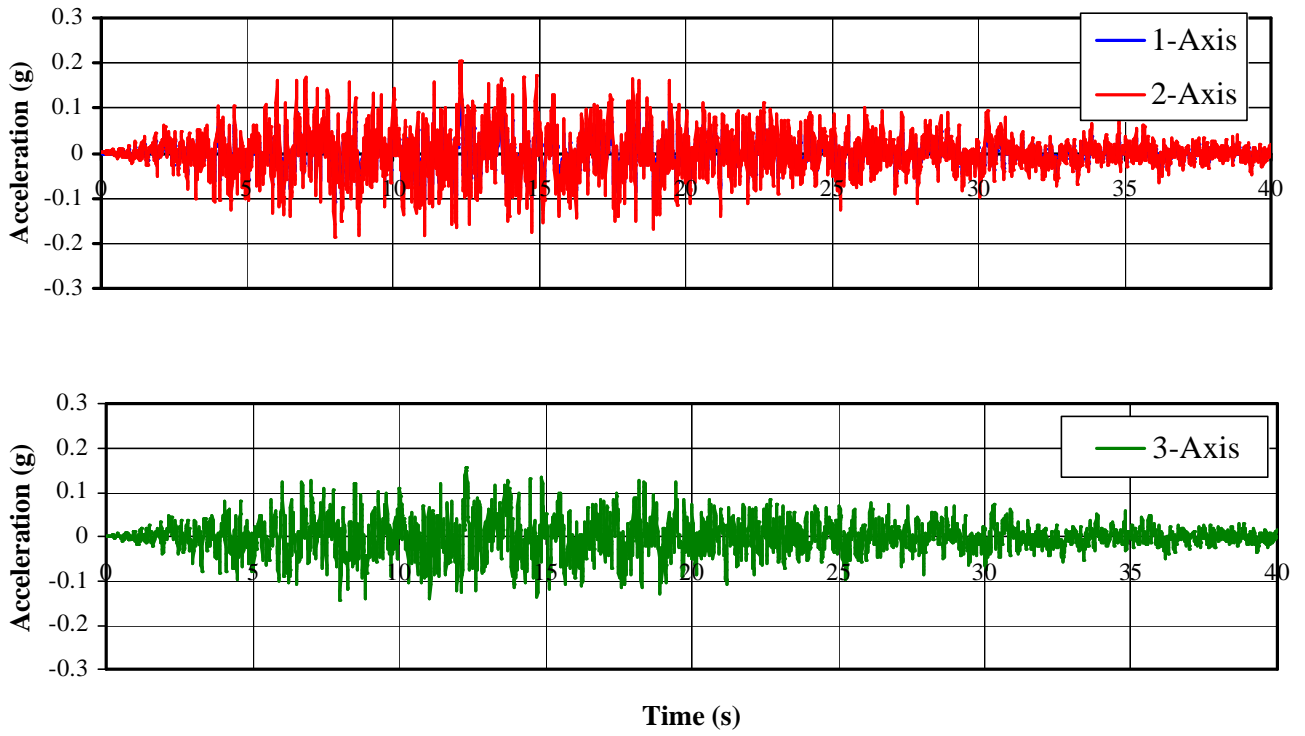
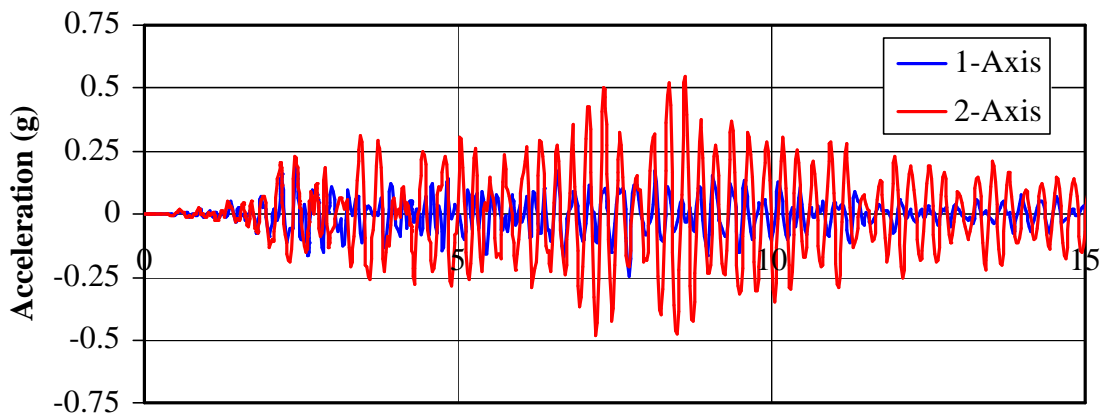
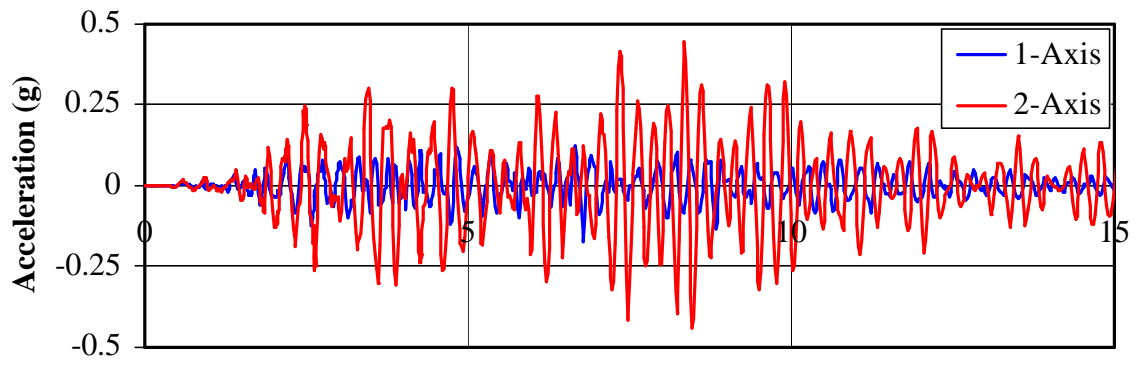


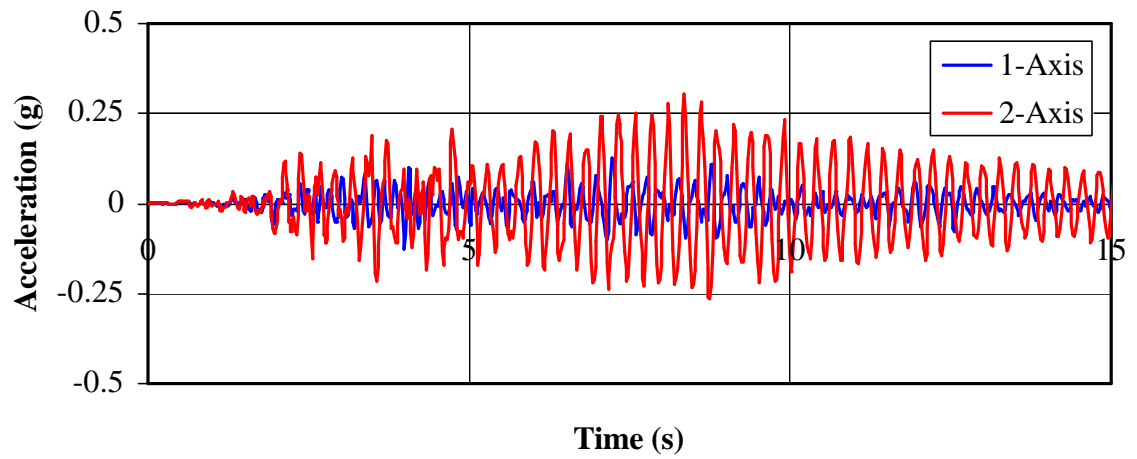
Figure 6.6 (cont'd) Component input time histories (M = 8)



a. Deck

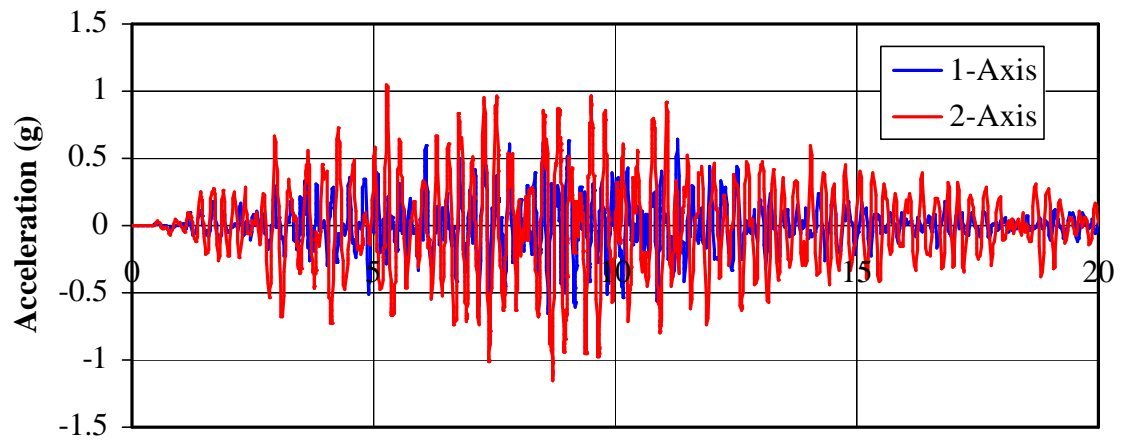


b. Top of column

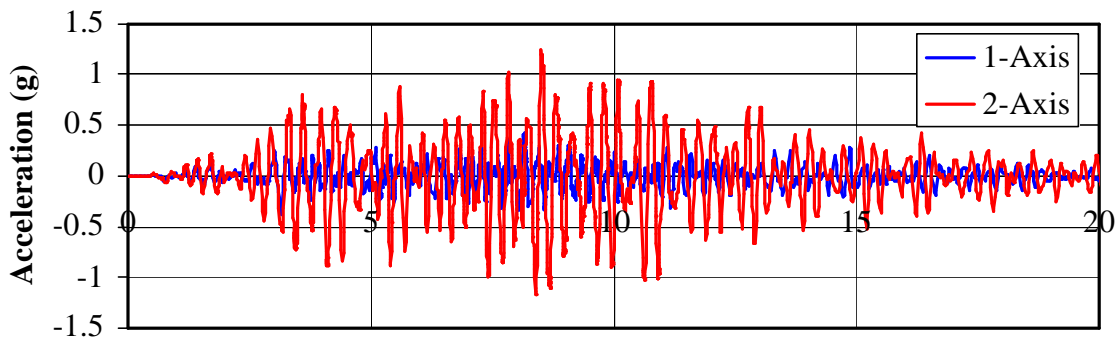


c. Footing

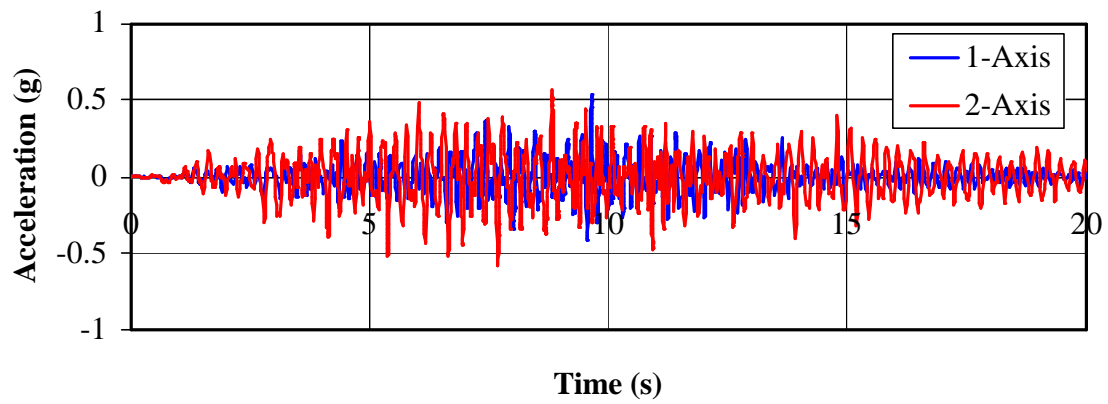
Figure 6.7 Response time histories at Bent 3 ($M = 6$)



a. Deck

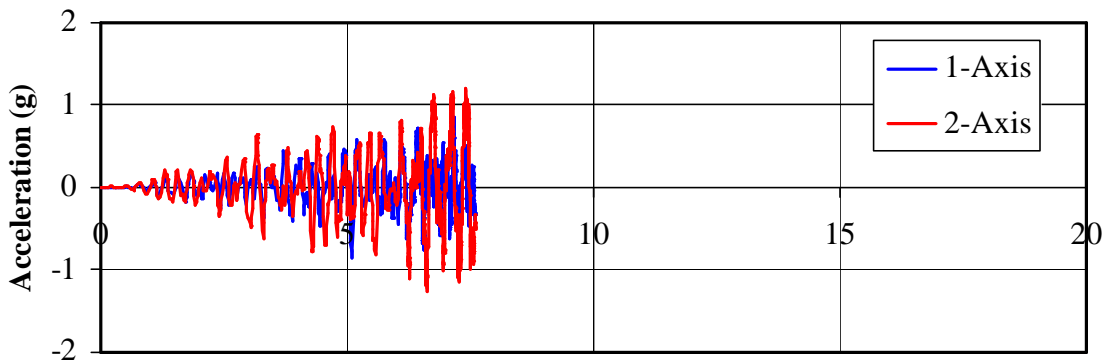


b. Top of column

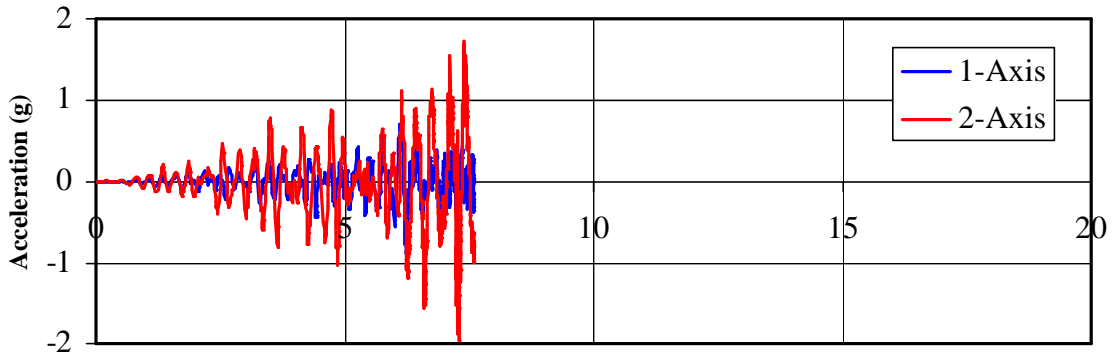


c. Footing

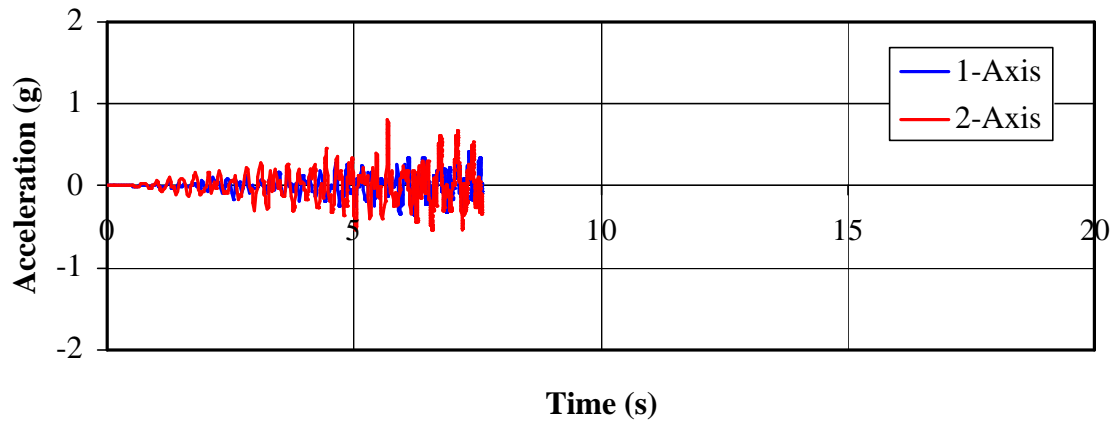
Figure 6.7 (cont'd) Response time histories at Bent 3 (M = 7)



a. Deck

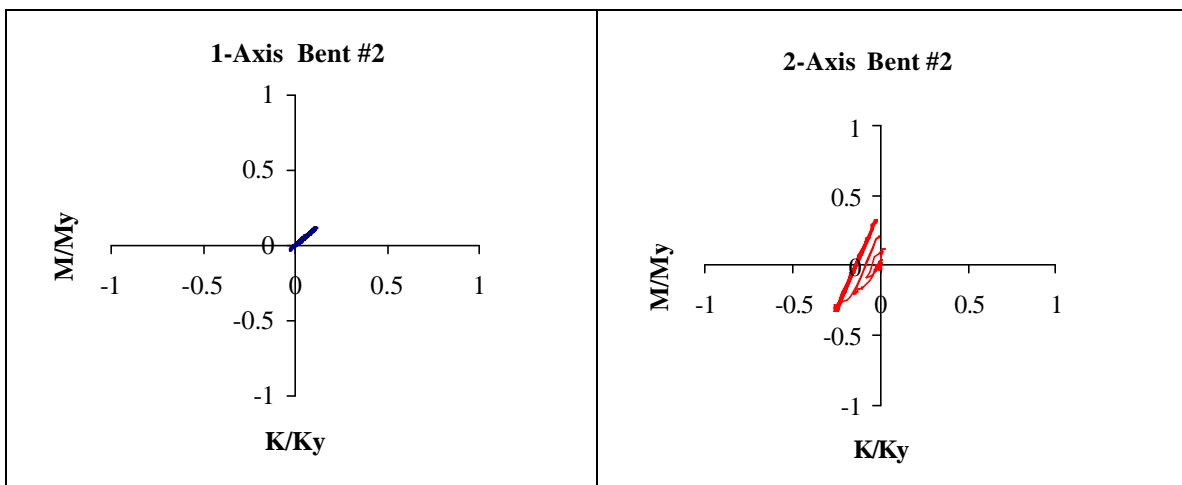


b. Top of column



c. Footing

Figure 6.7 (cont'd) Response time histories at Bent 3 (M = 8)



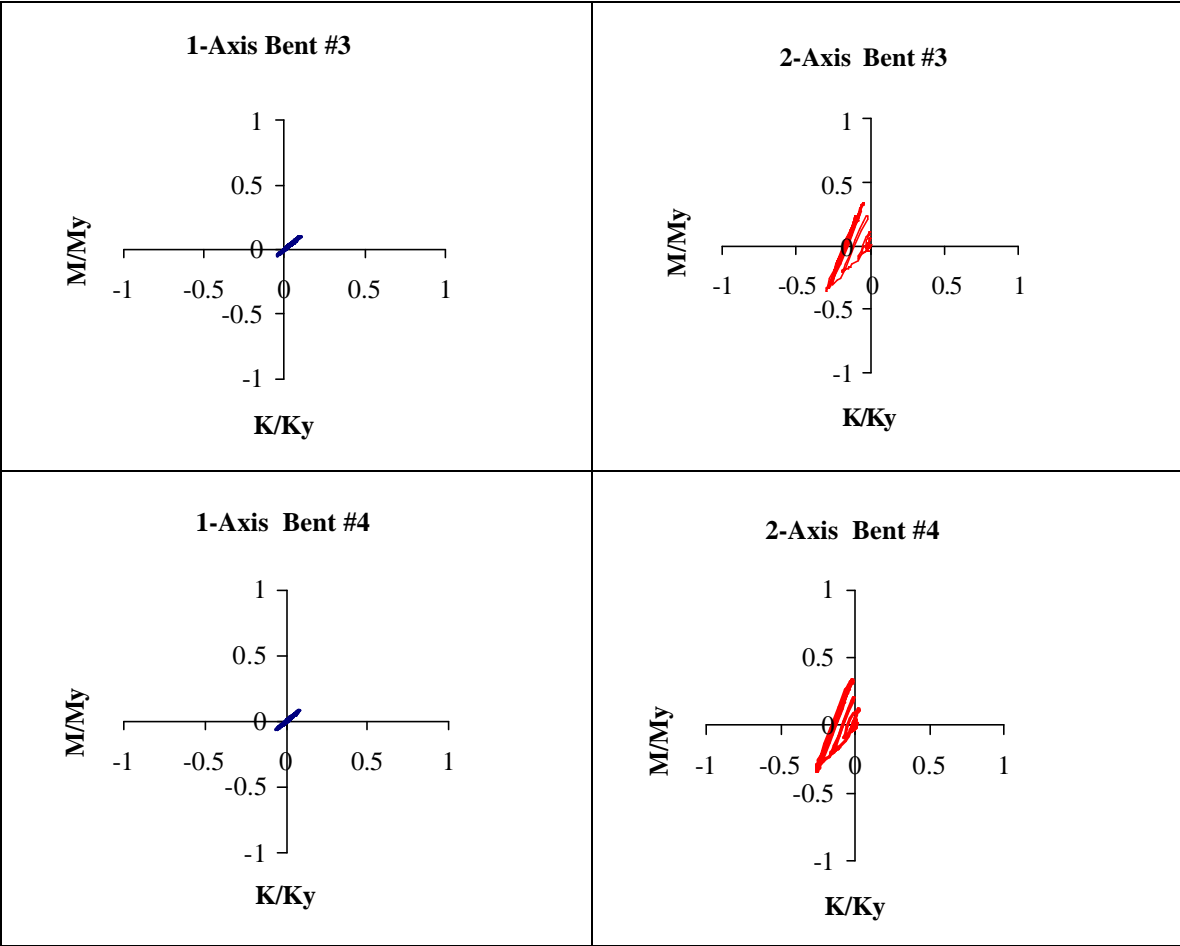
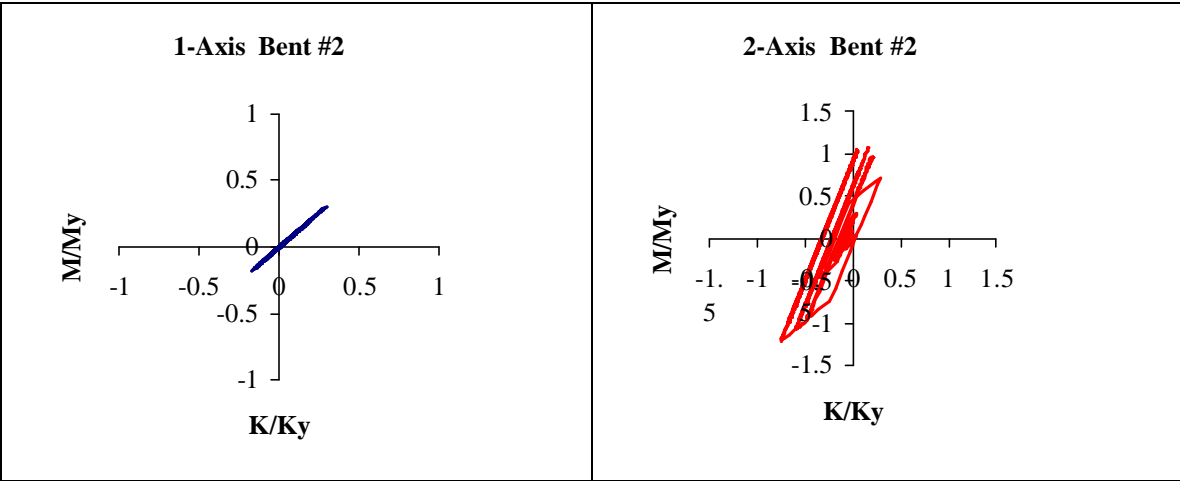


Figure 6.8 Section hysteresis: top of column (M = 6)



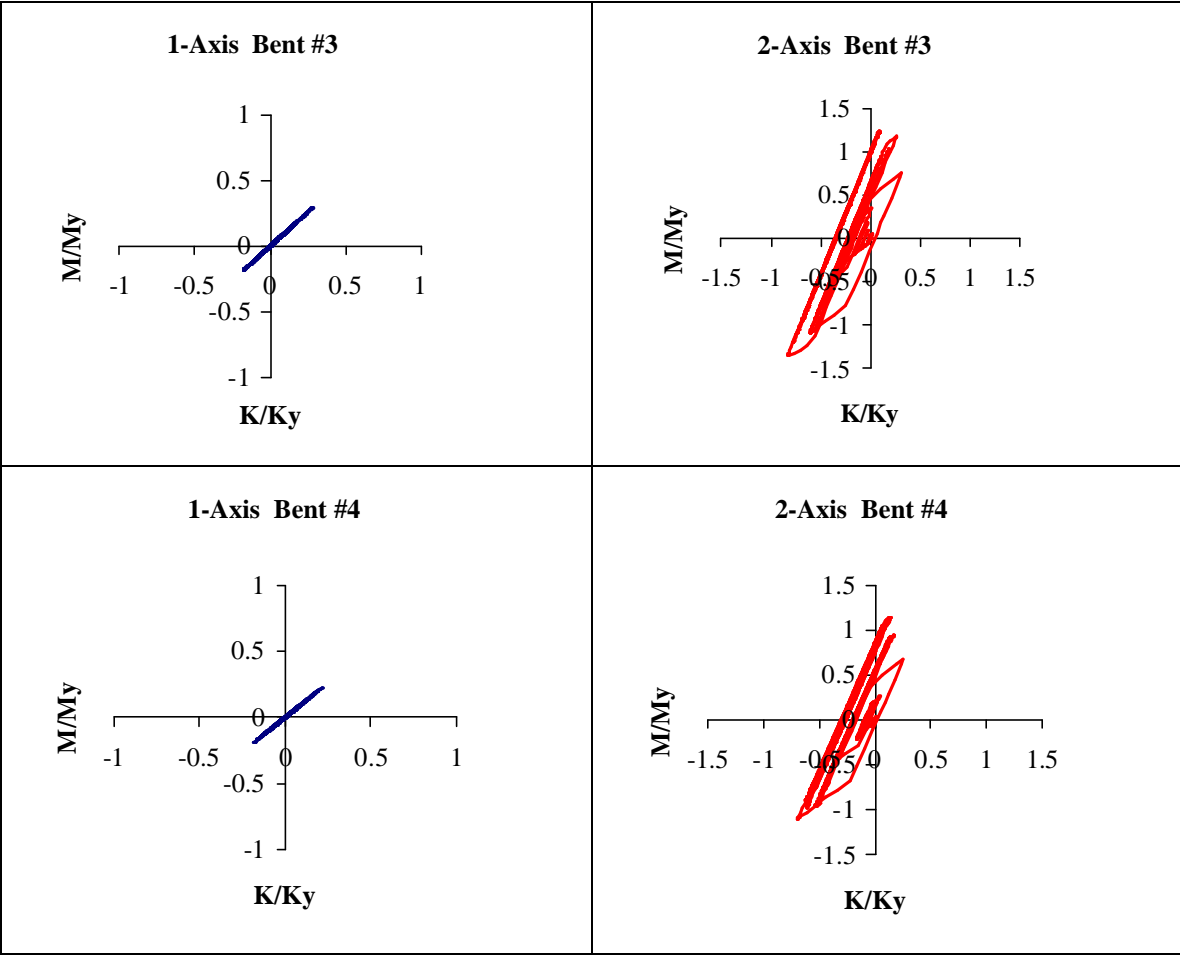
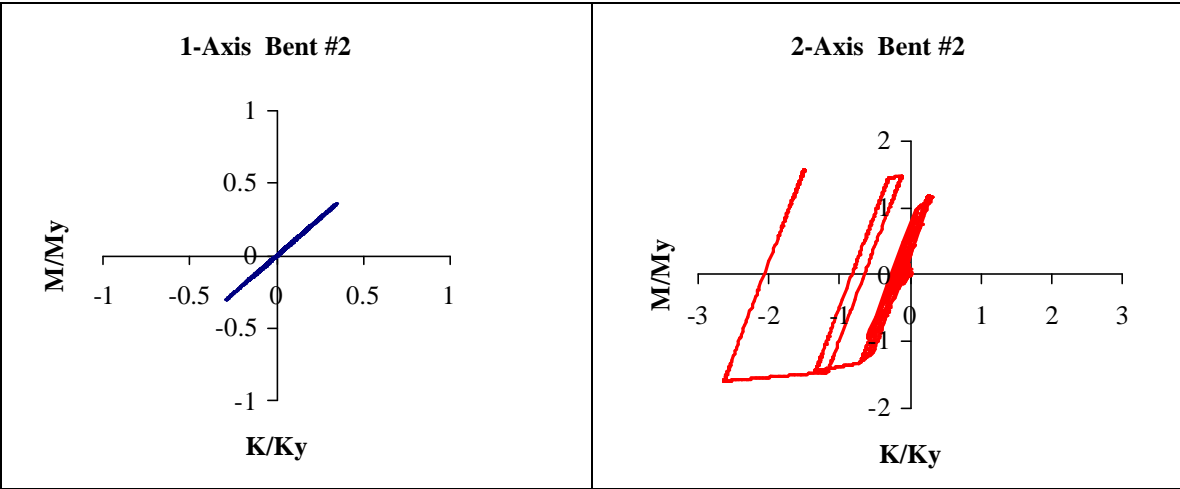


Figure 6.8 (cont'd) Section hysteresis: top of column (M = 7)



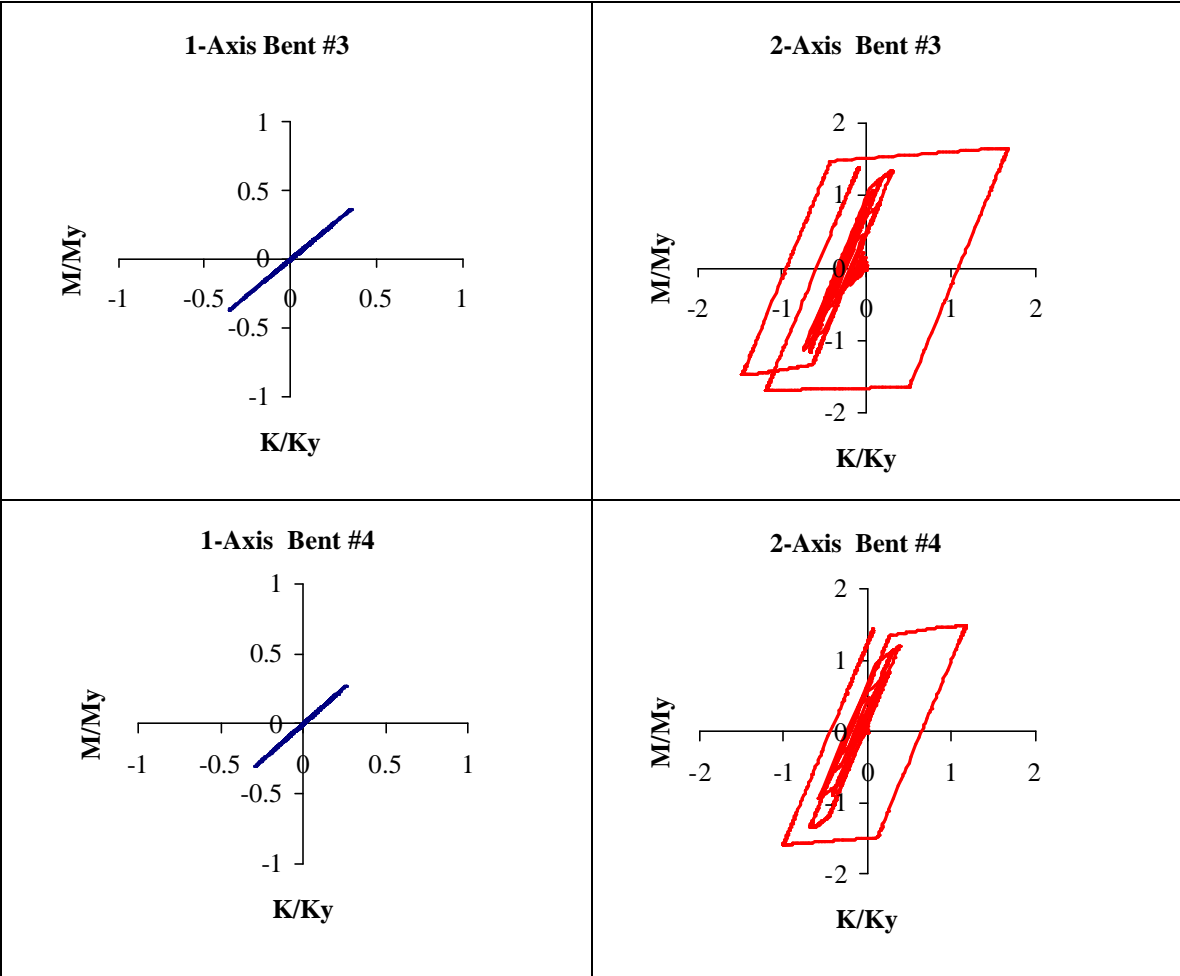
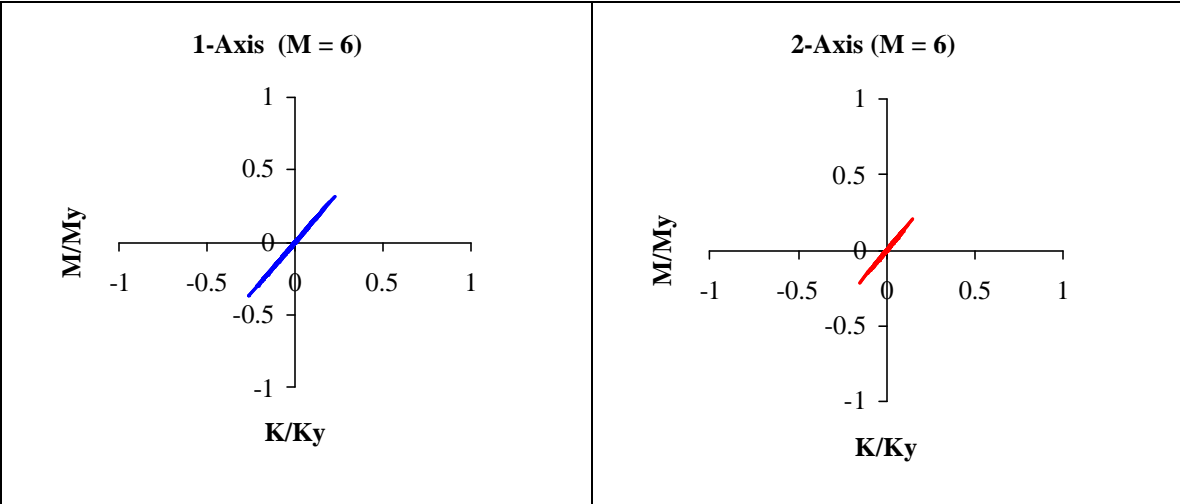


Figure 6.8 (cont'd) Section hysteresis: top of column (M = 8)



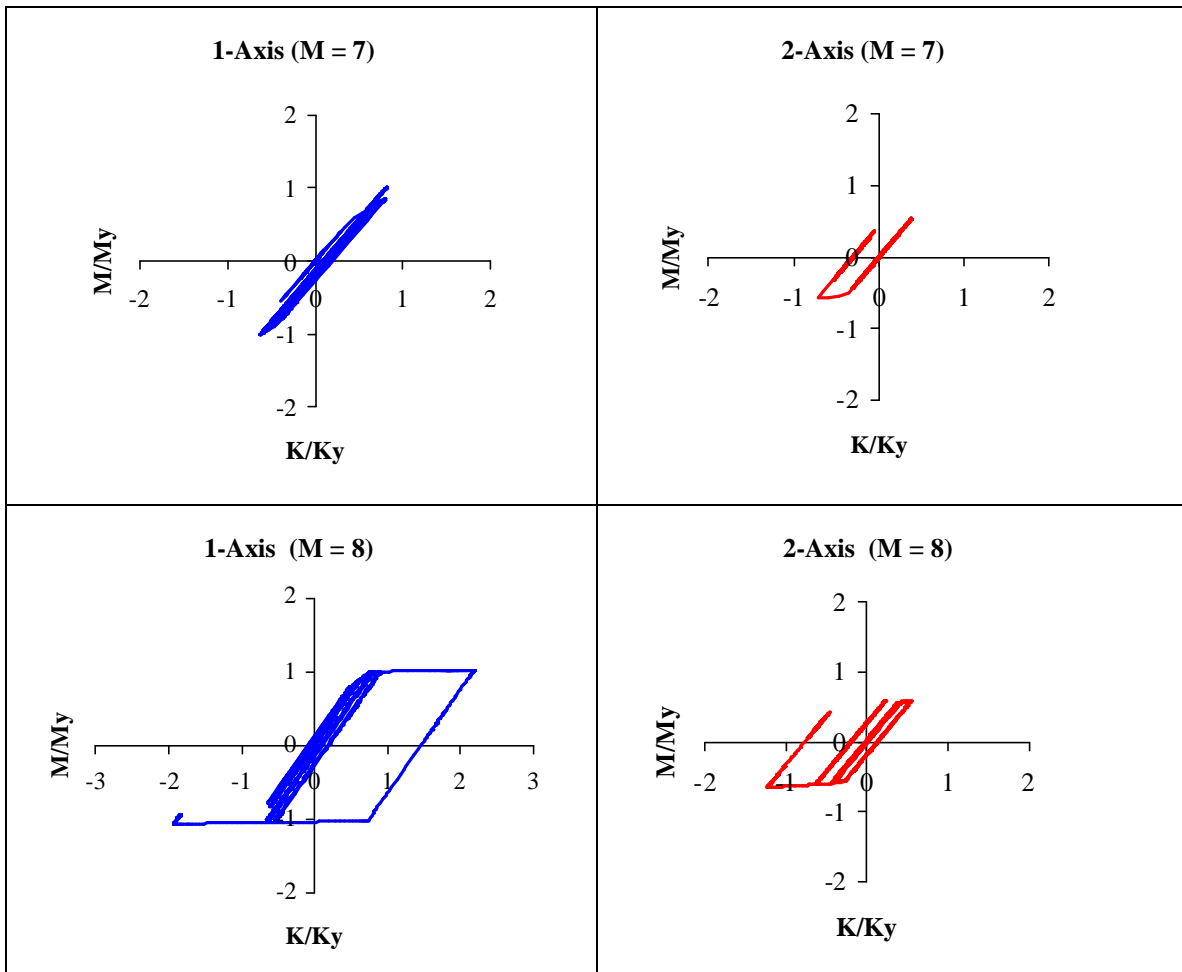
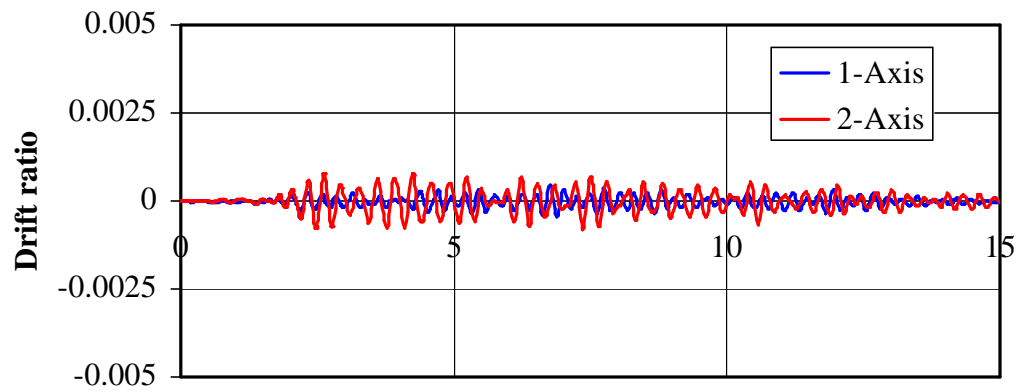
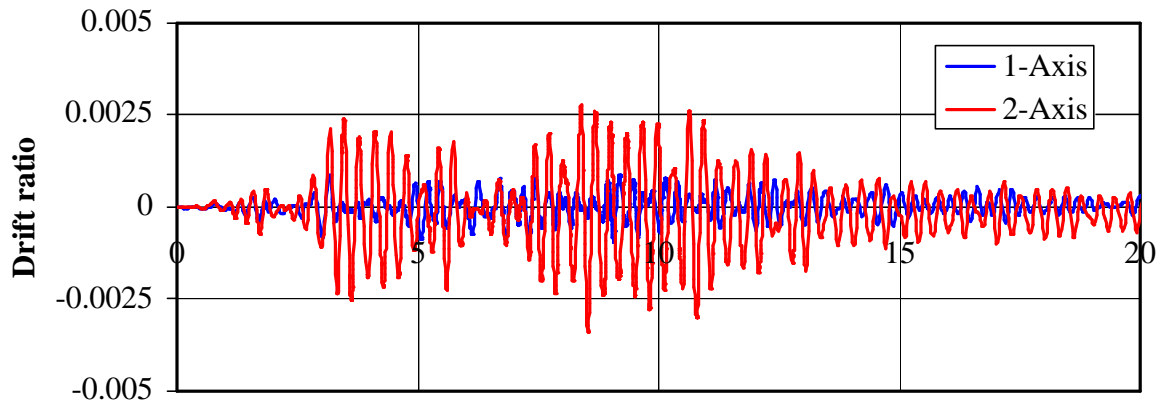


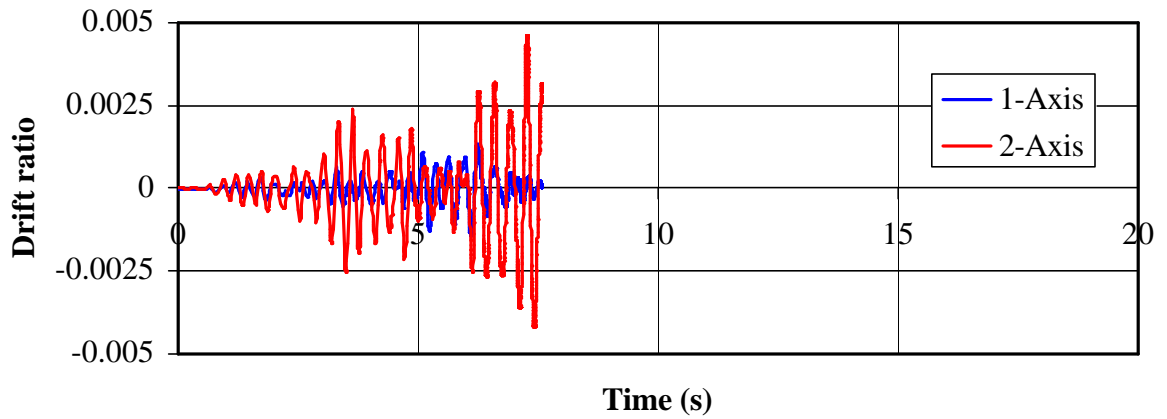
Figure 6.9 Section hysteresis: top of abutment pile ($M = 6, 7, 8$)



a. $M = 6$

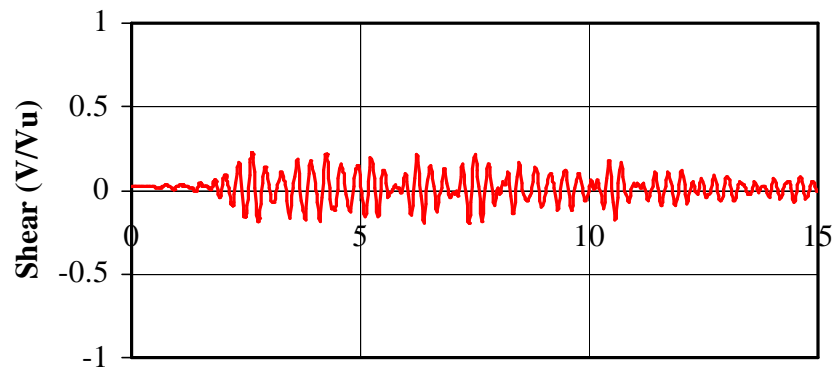


b. $M = 7$

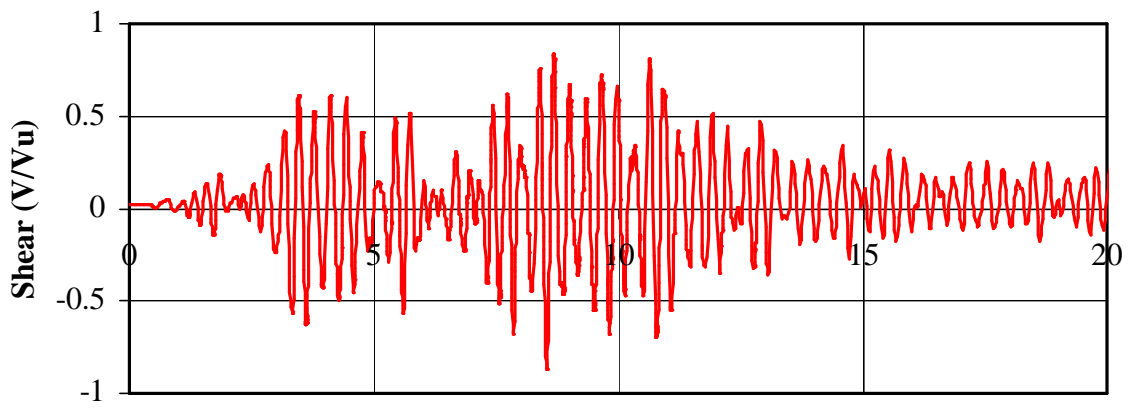


c. $M = 8$

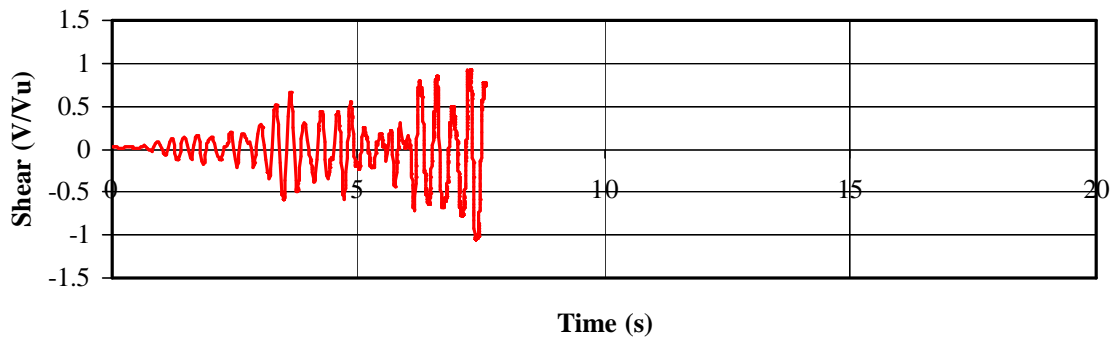
Figure 6.10 Response time histories at Bent 3: drift ratio



a. $M = 6$



b. $M = 7$



c. $M = 8$

Figure 6.11 Response time histories at Bent 3: transverse shear

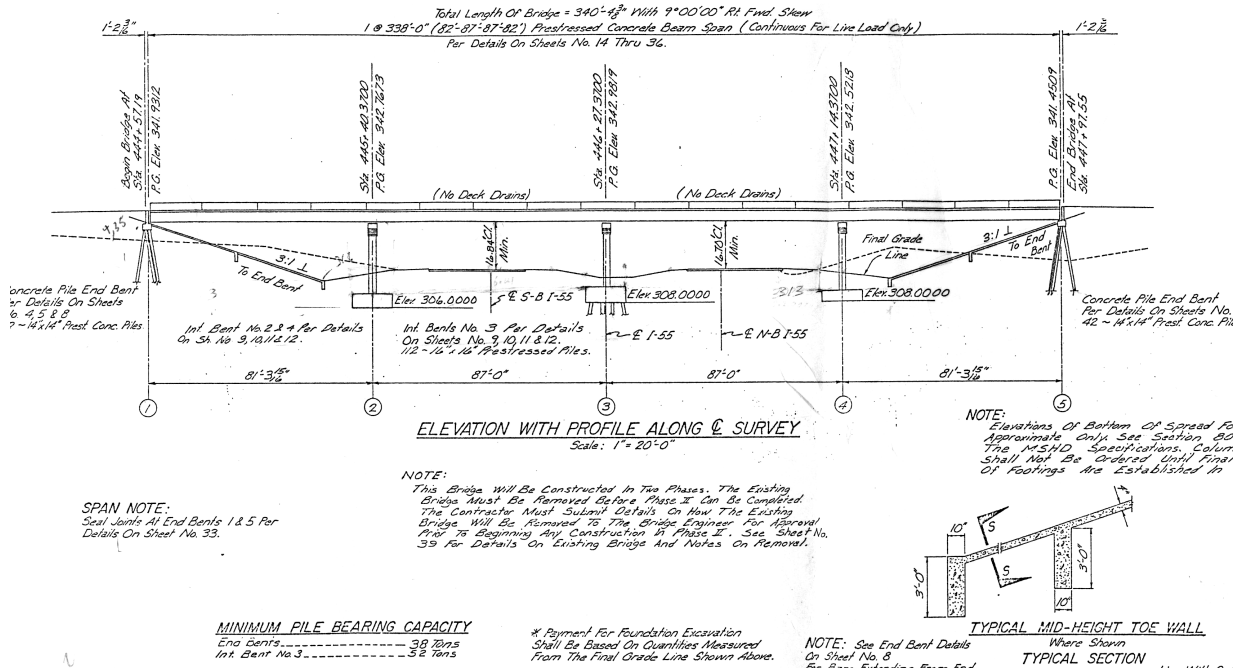


Figure A.1 Bridge elevation showing primary substructure elements

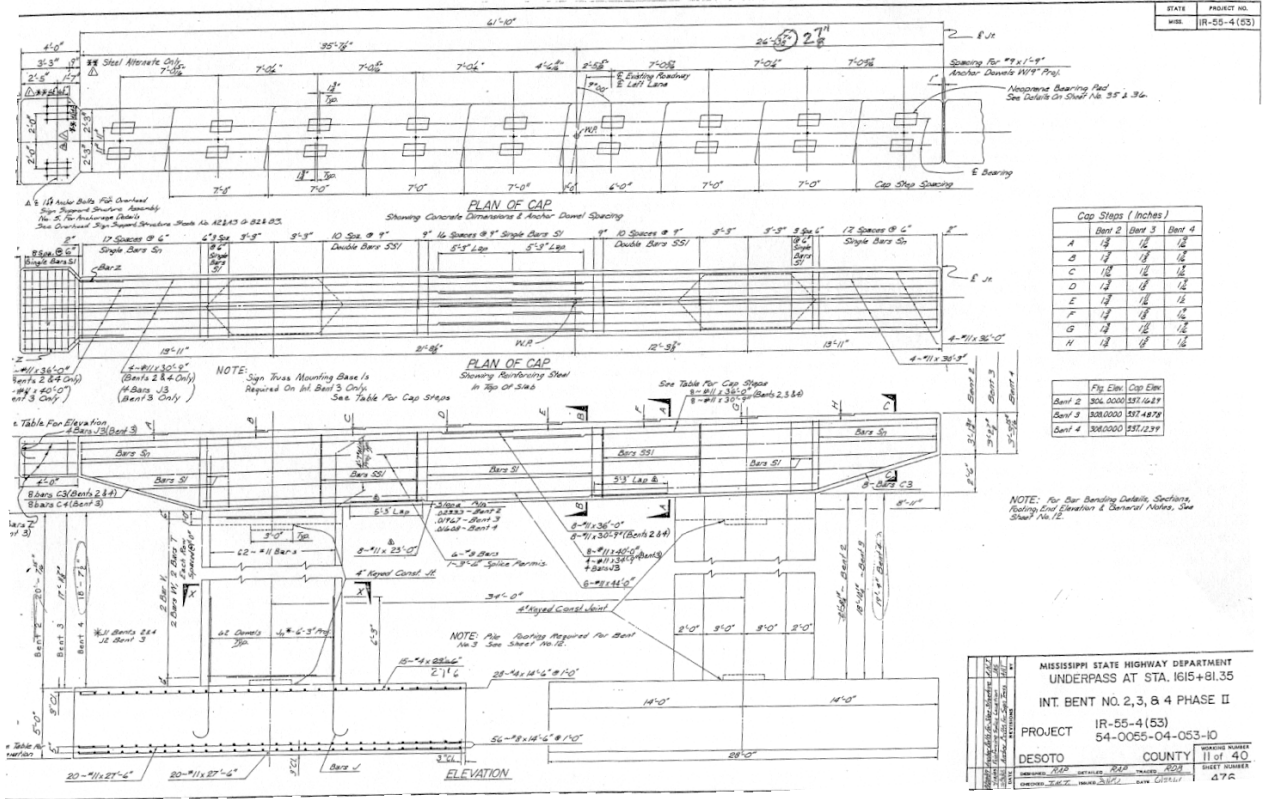


Figure A.3 Interior bent (typical) - elevation view

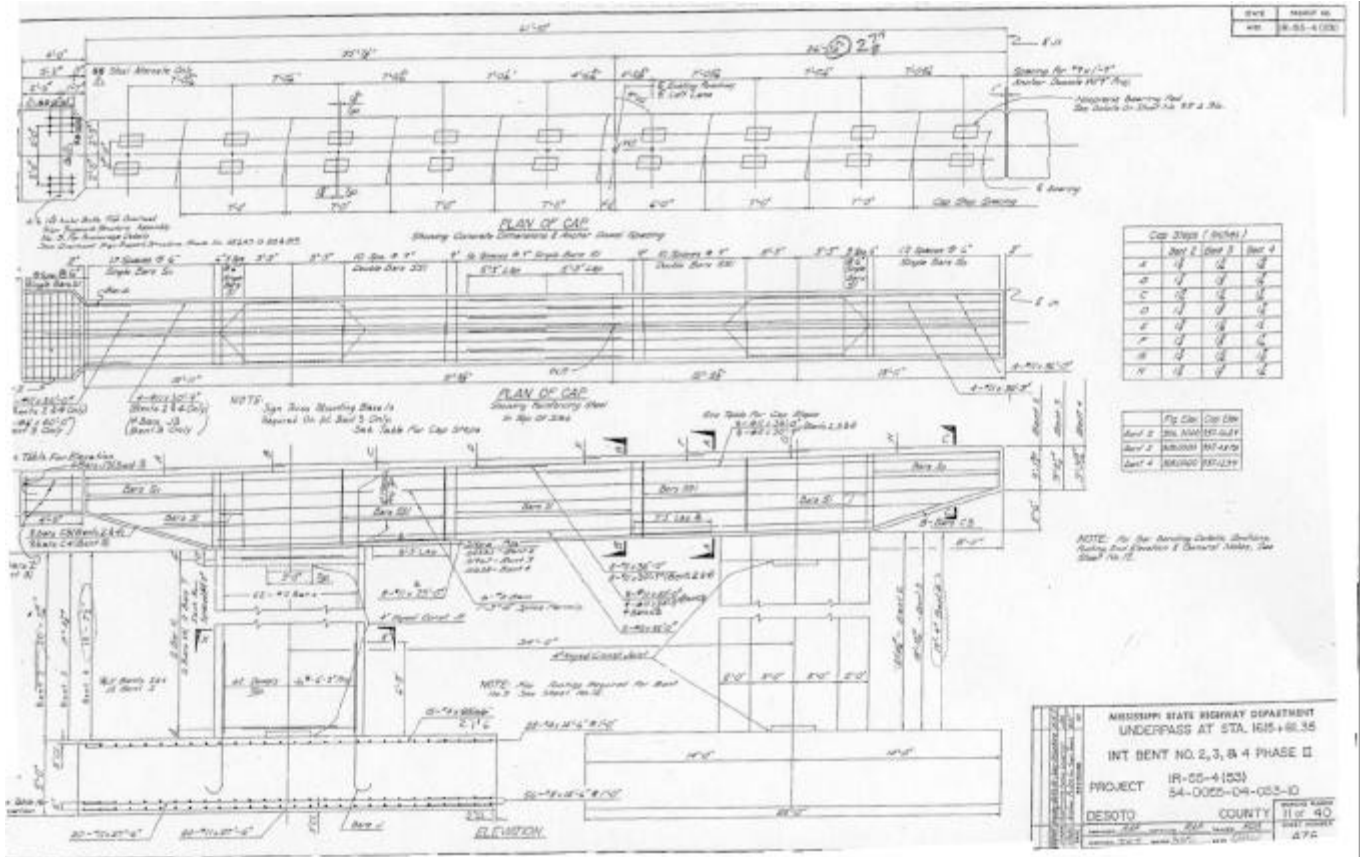


Figure A.3 (cont'd) Interior bent (typical) - elevation view

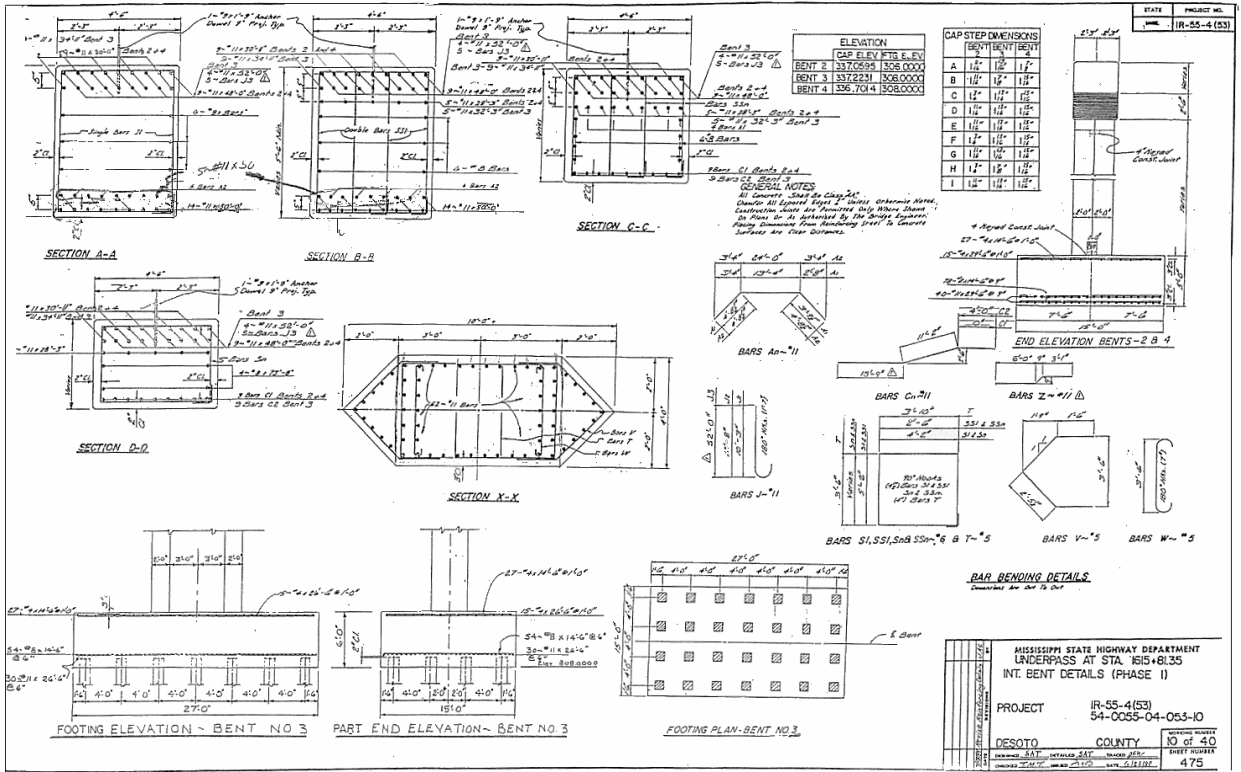


Figure A.3 (Cont'd) Interior bent (typical)- section views

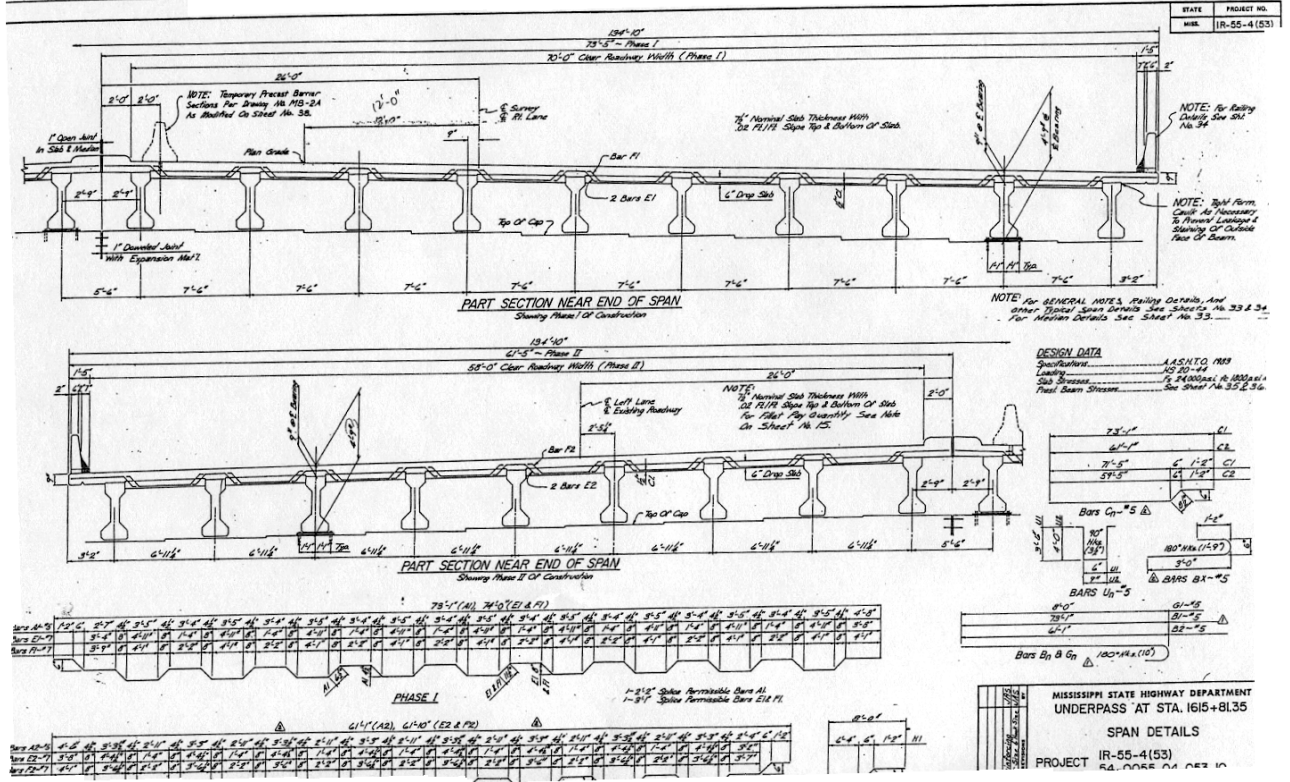


Figure A.4 Deck superstructure (typical)- section views

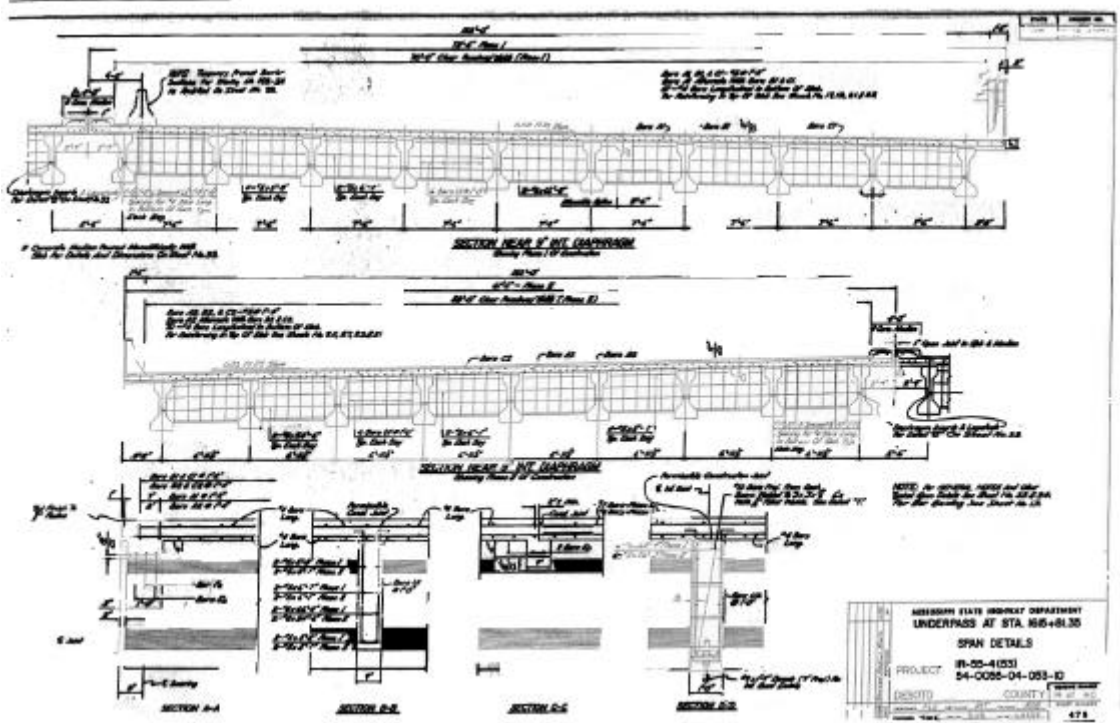
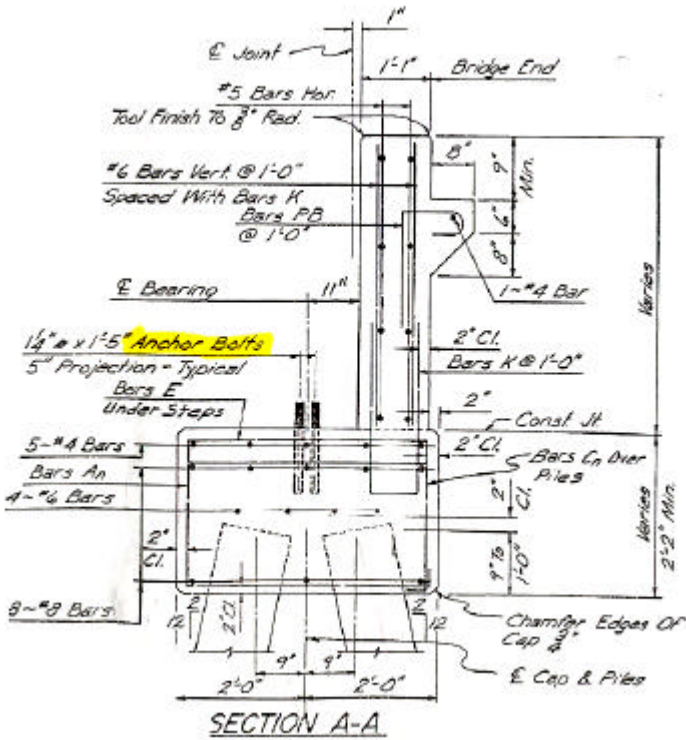
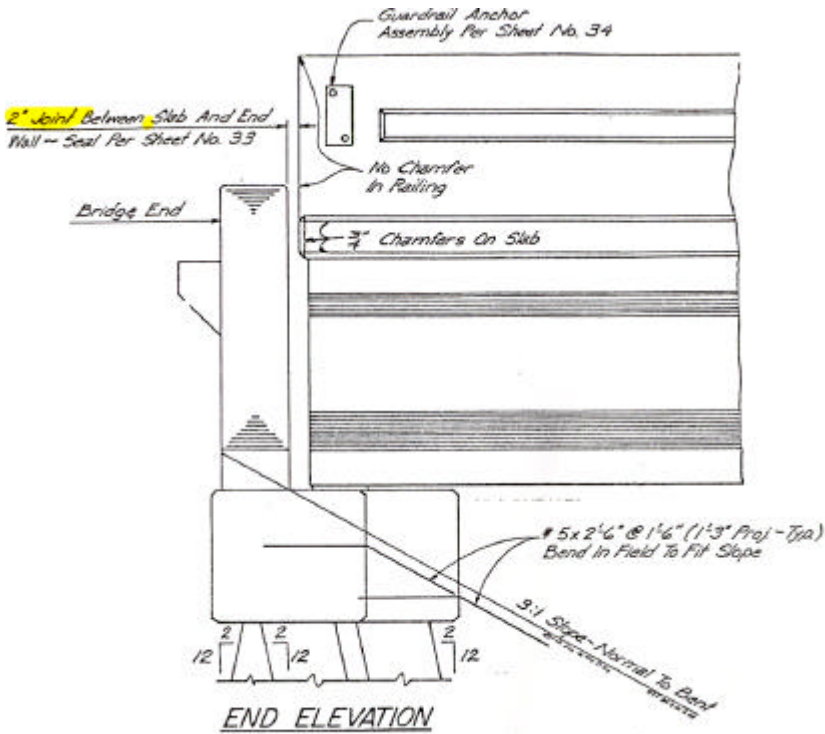


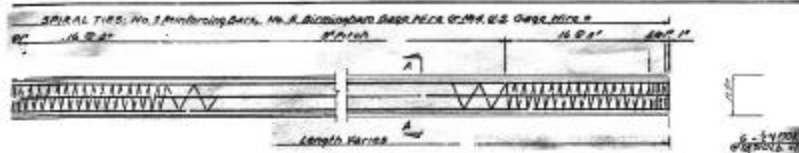
Figure A.4 (cont'd) Deck superstructure (typical)- section views



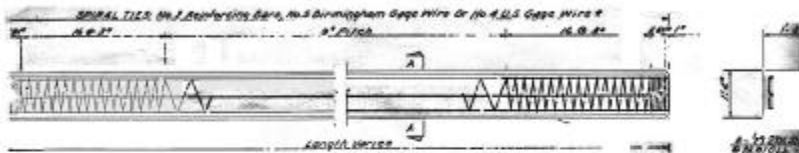
GENERAL NOTES:

All Concrete In End Bents Shall Be **Class AA**.
Chamfer All Edges $\frac{3}{4}$ " Unless Otherwise Noted.
End Wall Above Construction Joint At Top Of Cap
Shall Not Be Constructed Until End Span Is
In Place And Forms Removed.
Piles For End Bents Shall Not Be Driven Until Bridge
End Fill Has Been Constructed To Grade.
No Payment Will Be Allowed For Excavation Incidental
To Construction Of End Bent Caps.

Figure A.5 Abutment details (typical)



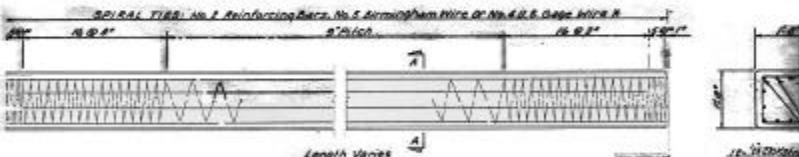
14'x14" PRESTRESSED CONCRETE PILE



16'x16" PRESTRESSED CONCRETE PILE



18'x18" PRESTRESSED CONCRETE PILE



20'x20" PRESTRESSED CONCRETE PILE



MAXIMUM LENGTH "L"			
PILE SIZE	THREE POINT	TWO POINT	ONE POINT
14'x14"	27'0"	27'0"	27'0"
16'x16"	30'0"	30'0"	30'0"
18'x18"	33'0"	33'0"	33'0"
20'x20"	36'0"	36'0"	36'0"

1. The piles shall be marked plainly with a band of paint to indicate proper pickup points for attaching handling lines.
 2. The piles shall be marked with a resistor paint.
 3. The piles shall be marked with a resistor paint.
 4. The piles shall be marked with a resistor paint.
 5. The piles shall be marked with a resistor paint.
 6. The piles shall be marked with a resistor paint.
 7. The piles shall be marked with a resistor paint.
 8. The piles shall be marked with a resistor paint.
 9. The piles shall be marked with a resistor paint.
 10. The piles shall be marked with a resistor paint.

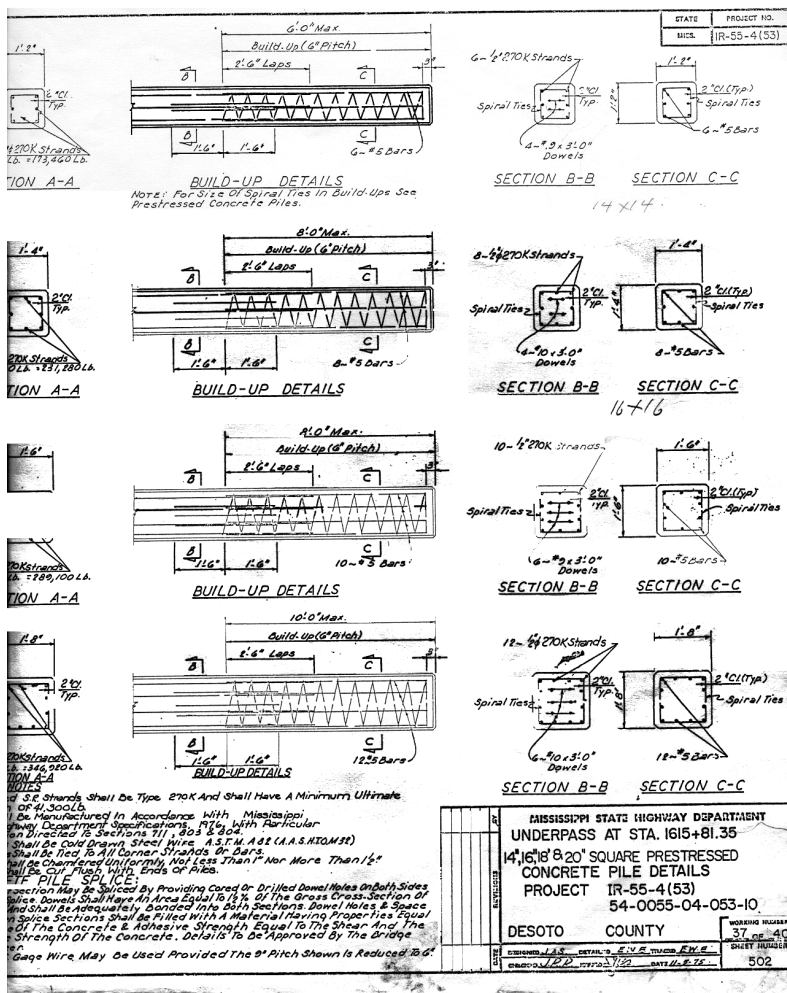
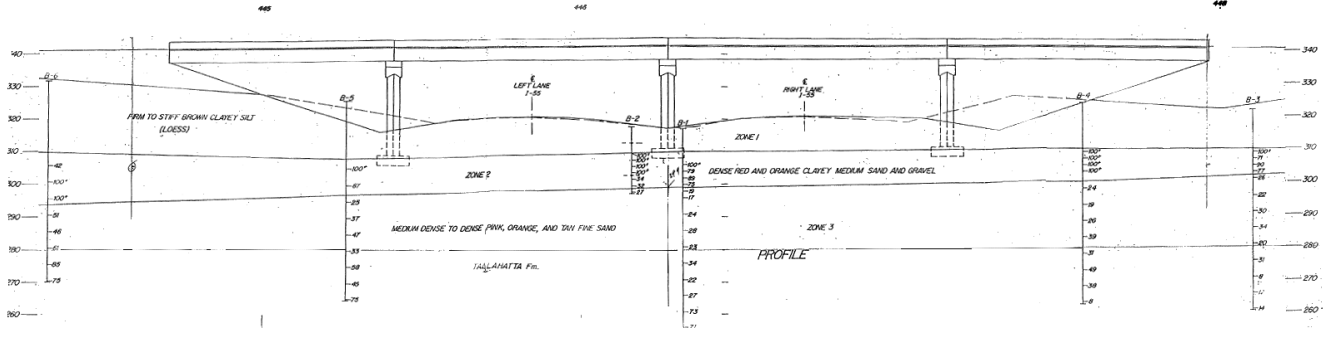


Figure A.6 Pile details (typical)



a. Plan showing boring locations



b. Elevation composite showing blow counts profile

Figure B.1 Soil profile composite from soil boring data

LOG OF BORING NO. 87-17
54-0055-04-053-10

LOCATION: Sta. 446+33:18" R.L. Survey Hwy. 302

DEPTH, FT.	SAMPLES	DESCRIPTION OF MATERIAL	BLOWS PER FT. UNIT GRY. RESIST. LB. SQ. FT.	COHESION, KIP/ SQ. FT.				ELEVATION, FT.
				1	2	3	4	
		SURFACE ELEV. 331.6						
10		Hard Brown dry Silty Clay (Loess)	100	0	0		321.6	
		012' Firm Brown Silt & Clay (Damp)	96					
			102					
			100					
20		020' Hard Brown & Gray Clay w/ Gravel	108				311.6	
		025' Dense Orange & Gray Sandy Clay w/Gravel	42					
30		030' Very Dense Orange Coarse Sand	100				301.6	
			100					
40		030' Medium Dense Orange, Gray, & Pink Fine Sand (Tallahassee Fm.)	51				291.6	
			46					
50			61				281.6	
			85					
60		060' Dense Orange, Tan & Gray Sand with Soft Clay	75				271.6	

COMPLETION DEPTH 61.5' DEPTH TO WATER IN BORING: NOT DETERMINED
DATE: 1-15-07 DATE:

SI: Spitz Spoon T: Shelby Tube PLATE 18

LOG OF BORING NO. 87-17-1224-1
54-0055-04-053-10

LOCATION: Sta. 446+32:17" Lt. C.L. Survey Hwy. 302

DEPTH, FT.	SAMPLES	DESCRIPTION OF MATERIAL	BLOWS PER FT. UNIT GRY. RESIST. LB. SQ. FT.	COHESION, KIP/ SQ. FT.			ELEVATION, FT.
				1	2	3	
		SURFACE ELEV. 316.9					
		7' Firm Brown Silt					
10		At 4' Stiff Brown Sandy Cl w/Gravel	116				306.9
		At 7' Very Dense Red & Tan Clayey Sand w/Gravel	100				
			79				
			89				
20		At 14' Dense Red Very Coarse Sand and Clay Gravel	117				256.9
		At 18' Loose Med Fine Sand (Tallahassee Fm.)	24				
		At 25' Pink Fine Sand	28				
30		At 30' Medium Dense Orange & Gray Fine Sand	23				276.9
			28				
40			34				276.9
			22				
50			27				266.9
			73				
60		At 55' Dense Yellow Fine Sand	71				256.9
		At 60' Dense Gray Fine Sand w/thin Clay					

COMPLETION DEPTH 0' DEPTH TO WATER IN BORING: NOT DETERMINED
DATE: DATE:

SI: Spitz Spoon T: Shelby Tube PLATE 21

LOG OF BORING NO. 87-17-1224-4
54-0055-04-053-10

TYPE: Rotary Wash LOCATION: Sta. 447+57.10' Rt. CL Survey Hwy. 307

DEPTH, FT.	SAMPLES	DESCRIPTION OF MATERIAL	UNITS PER WEIGHT UNITS PER VOLUME	COHESION, KIP/SQ FT				ELEVATION, FT.
				PLASTIC LIMIT		LIQUID LIMIT		
				1	2	3	4	
		SURFACE ELEV: 324.2						
	T	At 5' Hard Red and Gray Clay	92					
10'	T		103					314.2
	S	At 14' Hard Red Clay w/Gravel	100					
	S	At 18' Gravel	100					
20'	S	At 18' Very Loose Red Fine Sand w/Gravel	100					304.2
	S	At 24' Medium Dense Orange & Gray Sand (Tallahatta Fm.)	24					
30'	S	At 30' Red and Gray	19					294.2
	S	At 35' Orange and Gray	26					
40'	S		39					284.2
	S		31					
50'	S		49					274.7
	S		38					
60'	S	At 60' Loose Orange & Gray Fine Sa	8					264.2

COMPLETION DEPTH 61.5' DEPTH TO WATER IN BORING: 50' DATE: 1/14/87

1: Split Spoon 2: Shelby Tube PLATE 22

Figure B.2 Boring logs